UCRL- 15521 Volume 2
S/C 9462309

HEAT-TRANSFER CHARACTERISTICS OF FLOWING AND STATIONARY PARTICLE-BED-TYPE FUSION-REACTOR BLANKETS
Volume 2

Russell E. Nietert
S. I. Abdel-Khalik
University of Wisconsin

February 1983

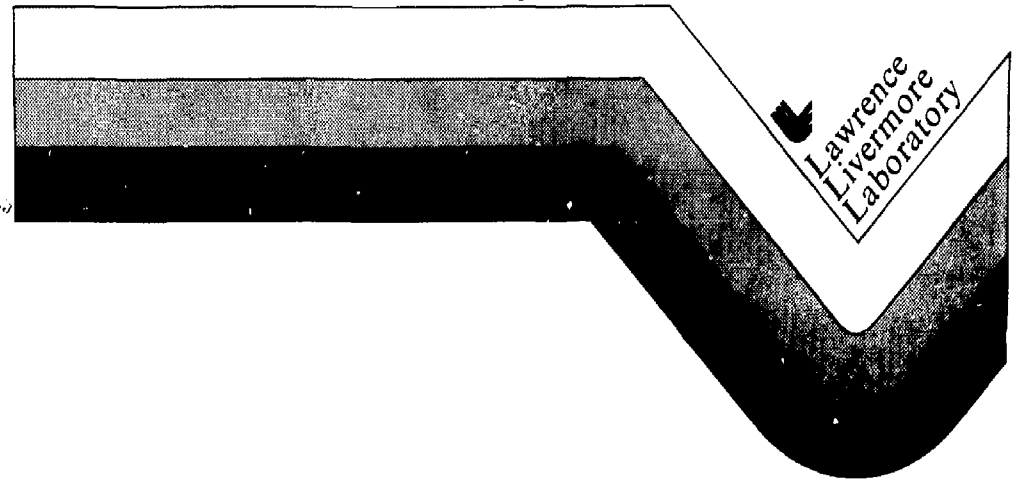

HEAT-TRANSFER CHARACTERISTICS OF FLOWING AND STATIONARY PARTICLE-BED-TYPE FUSION-REACTOR BLANKETS

by

UCRL--15521-Vol.2

DE83 000322

RUSSELL E. NIETERT

A thesis submitted in partial fulfillment of the requirements for the degree of

DOCTOR OF PHILOSOPHY

(Nuclear Engineering)

at the

UNIVERSITY OF WISCONSIN--MADISON

1982

DEDICATION

To the three most important people in my life. First to my father, who in encouraging me to address my different curiosities helped me develop the qualities necessary to pursue this experimental investigation. Second to my mother, who always treated me like someone special, and finally to my wife, whose patience and support I could not have done without.

HEAT TRANSFER CHARACTERISTICS OF FLOWING AND STATIONARY PARTICLE BED TYPE FUSION REACTOR BLANKETS

Russell E. Nietert

Under the supervision of Professor S. I. Abdel-Khalik

ABSTRACT

The heat-transfer characteristics of flowing and stationary packed-particle beds have recently become of interest in connection with conceptual designs of fusion-reactor blankets. A detailed literature survey has shown that the processes taking place in such beds are not fully understood despite their widespread use in the chemical industry and other engineering disciplines for more than five decades. In this study, two experimental investigations were pursued.

In the first, a heat-transfer loop was constructed through which glass microspheres were allowed to flow by gravity at controlled rates through an electrically heated stainless steel tubular test section. The falling bed was treated as a pseudofluid and extensive data for the local convective heat-transfer coefficient and Nusselt number were obtained for the thermal-entrance region of heated tubes. Comparisons were made with theoretical predictions based upon a fully developed flat-velocity-profile assumption. Several predictions of the static

effective thermal conductivity obtained from the literature applied to flowing beds were utilized in this regard. Experiments were conducted for various particle sizes, flow channel diameters, and particle flow rates.

In the second, an annular packed bed was constructed in which heat was applied through the outer wall by electric heating of a stainless steel tube. Cooling occurred at the inner wall of the annular bed by flowing air through the central tube. A second air stream was allowed to flow through the voids of the packed bed. An error-minimization technique was utilized in order to obtain the two-dimensional one-parameter effective conductivity for the bed by comparing the experimental and theoretically predicted temperature profiles. Experiments were conducted for various modified Reynolds numbers less than ten.

The information obtained in this study are necessary for the design of flowing-bed-type fusion reactor blankets which serve the dual purposes of heat transport and tritium breeding as well as for stationary-bed-type blankets where the purge gas acts only as the heat-transport medium.

Approved

S. Abdel-Khalik

12/16/82

PREFACE

This thesis consists of three parts: i) problem definition; ii) literature survey; and iii) experimental results. In Chapter 1, the problem is defined and the detailed research program is outlined. An in-depth literature survey is presented in the following three chapters. Methods used in analysis and correlation of experimental data for stationary packed particle bed heat transfer are reviewed in Chapter 2. Various theoretical and semi-empirical models that have been proposed to predict stationary packed bed behavior are presented in Chapter 3. Previous work on falling particle bed heat transfer is discussed in Chapter 4. The falling particle bed experiments are discussed in Chapter 5. Finally, the stationary annular packed particle bed experiments are discussed in Chapter 6.

ACKNOWLEDGEMENTS

In any Ph.D. research program, invaluable aid is obtained from various sources. I would like to thank the many individuals that have directly helped me. Professor S. I. Abdel-Khalik guided my research and allowed me many freedoms in so doing. Various students spent numerous hours collecting data for the two experimental apparatuses I have built to carry out this study; they are J. K. Kapitz, J. D. Mantyh, and R. A. Decker. H. H. Miller of the Instrumentation Systems Center and the individuals of the University of Wisconsin Nuclear Reactor Laboratory, especially S. M. Matusewic and R. C. Walsh, have helped immensely with the more intricate points of design and machining. My fellow students often provided help and suggestions during the course of this investigation. In particular, I would like to mention R. J. Kohrt, D. K. Felde, D. D. Paul, H. S. Kim, I. K. Palk, W. P. Chang, and R. M. Summers. J. E. Keller provided support in preparing this text in which T. G. Janssen spent many hours typing. Finally, support for this research was provided by the University of Wisconsin Graduate School, the Electric Power Research Institute, the Wisconsin Electric Utilities Research Foundation, and the Lawrence Livermore National Laboratory.

TABLE OF CONTENTS

LIST OF TABLES

LIST OF FIGURES

CHAPTER 1

INTRODUCTION

Packed particle beds have been a subject of interest for over five decades. The chemical industry has made extensive use of such systems in order to carry out catalytic reactions. The productivity of catalytic converters depends heavily upon the ability to efficiently remove the heat produced in the reaction. The temperature in the bed must generally be prescribed to within narrow limits; a knowledge of the heat transfer in the packed bed is thus necessary in order to maintain the temperature in the desired range and to avoid local sintering of the particles. In the latter case, the cooling characteristics may be drastically altered and the reaction process may cease.

More recently, packed particle beds made of various forms of lithium compounds have been proposed for use as fusion reactor blankets. In these conceptual design proposals, the particles in the bed serve as the tritium breeder and sometimes also as the heat transport medium. Knowledge of the heat transfer characteristics of these systems is necessary since realistic estimates of the temperature distribution within the blanket structure are of utmost importance. Knowledge of the temperature distribution is needed in order to estimate the stress levels within the blanket. In addition, the heat transfer characteristics have a direct impact on the design of the tritium recovery system inasmuch as the diffusion coefficient is a strong function of temperature.

Analysis of the performance of these blankets, associated power cycles, and tritium recovery equipment has been hampered by lack of heat transfer data and by their dependence on the different design and operational parameters. Lack of heat transfer data sometimes forced the use of crude approximations in order to design these conceptual fusion reactors. Any calculations based upon these data can therefore only be treated as first order estimates. To this end, this investigation has been undertaken in order to provide the needed heat transfer data.

In particular, two blanket designs have provided the motivation for this study. The first, proposed by the Lawrence Livermore National Laboratory (LLNL), incorporates a stationary packed particle bed where tritium is bred and most of the fusion neutrons' energy is deposited. The second blanket design, proposed by the University of Wisconsin, incorporates a falling particle bed that serves as the heat transport medium and tritium breeder.

These two blanket designs will be briefly reviewed in Section 1.1. The objectives of this research program are summarized in Section 1.2.

1.1 Reactor Design Studies

The Magnetic Fusion Engineering Division (MFE) at the Lawrence Livermore National Laboratory (LLNL) has completed a conceptual design of a Tandem Mirror Reactor (TMR) utilizing a stationary particle bed blanket (Carlson et al. (1979)). The TMR blanket consists of several rows of tubes called "pods" arranged in an

annular ring about the central cell as shown in Figure 1.1-1. The diameter of these pods increases with distance away from the center line of the machine so that the largest amount of breeding material may be incorporated. Groups of either six or ten pods are organized into small subassemblies that allow for simple remote maintenance; pods are removed by a moving service car operating down the bore of the reactor. A cross section of the blanket and shield is presented in Figure 1.1-2. The shield consists of poured lead concrete inside a steel case. The helium coolant flows through inlet and exit tubes passing through the outer shield.

A cutaway view of a blanket pod can be seen in Figure 1.1-3. Helium at 350°C enters the pod near its center and flows outward through the shell of the pod. At the ends, the coolant reverses its direction and flows back to the central plenum through several tubes where it exits at 550°C. The space inside of the pod's shell, but outside of the coolant return tubes, is filled with granules of lithium oxide. A small purging flow of helium at the same pressure as the main coolant, 60 atm, removes the tritium from the packed bed. Tritium is expected to be easily extracted so long as the particles are between 10 and 100 μm in diameter. Such particle sizes and the corresponding modified Reynolds numbers (which are based upon the particle diameter) are considerably smaller than those generally discussed in the chemical engineering literature.

The SOLASE laser fusion reactor designed by the University of Wisconsin utilizes a gravity flowing particle bed blanket (Conn et al, 1977). The SOLASE blanket consists of a spherical shell made entirely of graphite with honeycomb-type construction. Lithium oxide particles between 100 and 200 μm in diameter flow under the influence of gravity through these honeycomb-like channels. The particles thus serve as both tritium breeder and heat transport medium. A schematic diagram of the SOLASE cavity is given in Figure 1.1-4.

The blanket is made of several sections; a cutaway view of one of these sectons is presented in Figure 1.1-5. Lithium oxide particles enter the top of the blanket at 400^{o}C and flow through one of six zones arranged as concentric spherical shells. The average particle velocity in the inner five zones is arranged by flow control baffles to attain a uniform exit temperature of 600^{o}C. This is done to match the local heat generation due to neutron deposition which decreases radially away from the first wall. The outer zone which contains 2% of the total flow rate is used for tritium extraction. The exit temperature of this zone was chosen as 850^{o}C, compatible with tritium extraction. Tritium extraction from the relatively large particles is expected to be feasible so long as they are porous.

One of the main advantages of the flowing particle bed blanket is its ability to "decouple" the first wall and blanket coolant temperatures as a result of the relatively low heat transfer

The SOLASE laser fusion reactor designed by the University of Wisconsin utilizes a gravity flowing particle bed blanket (Conn et al. 1977). The SOLASE blanket consists of a spherical shell made entirely of graphite with honeycomb-type construction. Lithium oxide particles between 100 and 200 μm in diameter flow under the influence of gravity through these honeycomb-like channels. The particles thus serve as both tritium breeder and heat transport medium. A schematic diagram of the SOLASE cavity is given in Figure 1.1-4.

The blanket is made of several sections; a cutaway view of one of these sectons is presented in Figure 1.1-5. Lithium oxide particles enter the top of the blanket at 400^{o}C and flow through one of six zones arranged as concentric spherical shells. The average particle velocity in the inner five zones is arranged by flow control baffles to attain a uniform exit temperature of 600^{o}C. This is done to match the local heat generation due to neutron deposition which decreases radially away from the first wall. The outer zone which contains 2% of the total flow rate is used for tritium extraction. The exit temperature of this zone was chosen as 850^{o}C, compatible with tritium extraction. Tritium extraction from the relatively large particles is expected to be feasible so long as they are porous.

One of the main advantages of the flowing particle bed blanket is its ability to "decouple" the first wall and blanket coolant temperatures as a result of the relatively low heat transfer

coefficient obtained (~ 2000 W/m^{2}K). The first wall can therefore be operated at temperatures significantly lower than the blanket breeder and coolant; this is important from a radiation damage viewpoint. Meanwhile, the temperature of the coolant is chosen on the basis of power cycle efficiency requirements. Such gravity-flowing particle bed systems have generally not been discussed in the literature.

1.2 Research Program Objectives

As will be discussed in the next few chapters, the heat transfer data required for the design of the two types of particle bed blankets presented in the previous section are not available in the literature. Thus. this experimental investigation has been undertaken to examine the heat transfer characteristics of stationary and flowing particle bed type fusion reactor blankets.

All of the predictive models and many of the experiments which have been presented for stationary packed beds correlate only the contributions to heat transfer when the gas in the voids is stationary. The turbulent contribution to heat transfer due to gas flow is then left to be determined by experiment; most of these experiments utilize particles larger than the range of interest for blanket designs such as that for TMR. In all cases, the modified Reynolds number for each experiment was greater than 10, the upper limit of the range of interest here.

In order to model stationary particle bed blankets of the TMR type, an experiment has been constructed where an annular packed bed of soda-lime glass microspheres contained by two concentric stainless steel tubes is cooled by air flowing down through the central tube. Heat is added to the bed at the outer wall of the annulus by electrical heating of the stainless steel tube. The helium purge through the blanket is modeled by a second, separate flow of air passing upward through the annular packing. The aim of this experiment has been to obtain heat transfer data for packed beds similar to the TMR blanket design as a function of the various design and operational parameters, namely coolant velocity, purge gas velocity, and particle size. The effect of heat flux has also been studied to separate out the radiant contribution. The outline of the research program is presented in Table 1.2-1 which lists the various combinations of experimental variables examined.

The literature presenting the heat transfer data for falling particle beds is scant. In designing such systems the effective thermal conductivity for a stationary packed bed with stagnant gas is generally used. The validity of this assumption was not previously known and has been assessed in this program.

Glass microspheres were allowed to flow by gravity through stainless steel tubes of various diameters. The tubes were heated electrically and the heat was transported away by the particles themselves. The aim of this experiment has been to obtain heat transfer data for flowing particle bed blankets of the SOLASE type

as a function of the various design and operational parameters, namely bulk particle velocity, particle size, and channel diameter. Variation with heat flux has also been studied to separate out the effect of radiation. The outline of the research program for this apparatus is presented in Table 1.2-2 where the various combinations of experimental variables examined are listed.

Table 1.2-1 Combinations of Experimental Variables Studied in the Stationary Packed Bed Experiments

Purge Air Superficial Velocity (cm/s)	Particle Size Range (μm)						Power Level (W)
	177-250		420-590		590-840		
	Coolant Air Velocity (cm/s)						
	200	500	200	500	200	500	
10	X	X	X	X	X	X	100
			X	X		X	150
20	X	X	X	X	X	X	100
				X	X	X	150
30	X	X	X	X	X	X	100
			X	X	X	X	150

Table 1.2-2 Range of Experimental Variables Studied in the Flowing Particle Bed Experiments

Tube Size (mm)	Particle Size Range (μm)			Heat Flux (W/cm^2)
	177-250	420-590	590-840	
	Bulk Particle Velocity Range (cm/s)			
7.75	(4) 4.4-11.6 (3) 7.7-13.3 (3) 7.6-11.8	(4) 3.0-10.9 (3) 6.2-12.3 (3) 5.8-10.9	(4) 2.1-10.7 (3) 4.7-10.4 (3) 5.5-11.5	2.55 3.35 4.20
13.8	(9) 3.5-11.8+ (8) 4.4-13.9+ (8) 4.9-15.3+	(9) 3.7-13.3+ (9) 2.4-14.3+ (9) 3.7-15.1+		2.55 3.35 4.20
24.8	(7) 1.3-7.2 (12) 1.8-6.6*	(6) 1.3-3.7 (6) 1.1-3.7 (5) 1.8-3.8	(5) 0.9-3.0 (4) 1.8-3.6 (3) 2.2-3.5	2.10 2.55 3.35

(#) Number of data points collected in the indicated range of velocity.

* Entire range of data repeated to demonstrate reproducibility.

+ Radial exit temperature profiles collected.

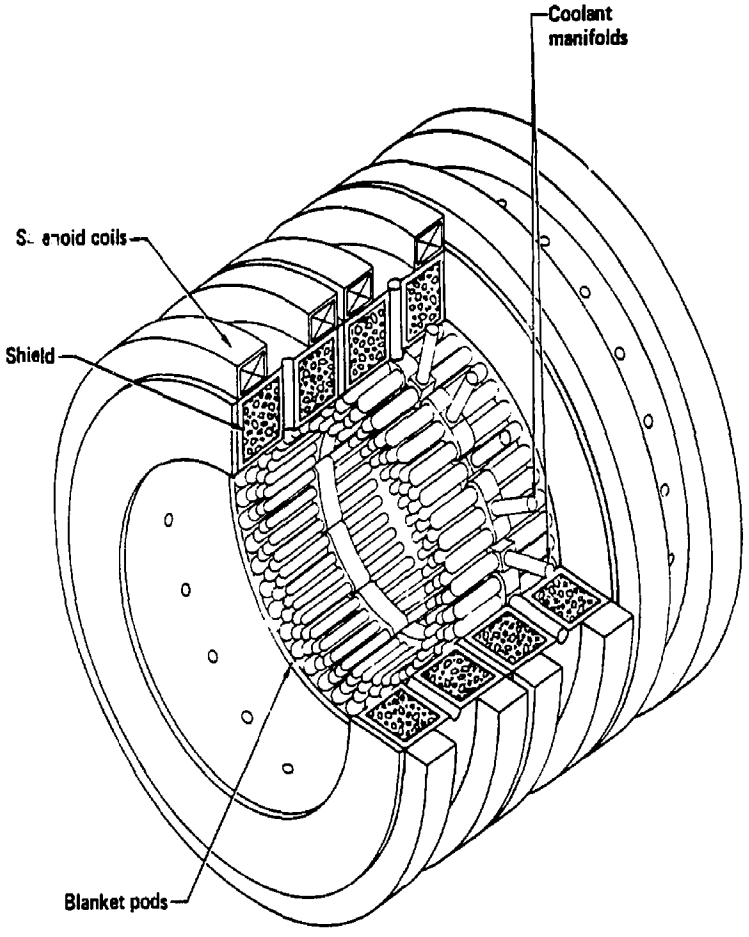

Figure 1.1-1. TMR central cell layout obtained from Carlson et al. (1979).

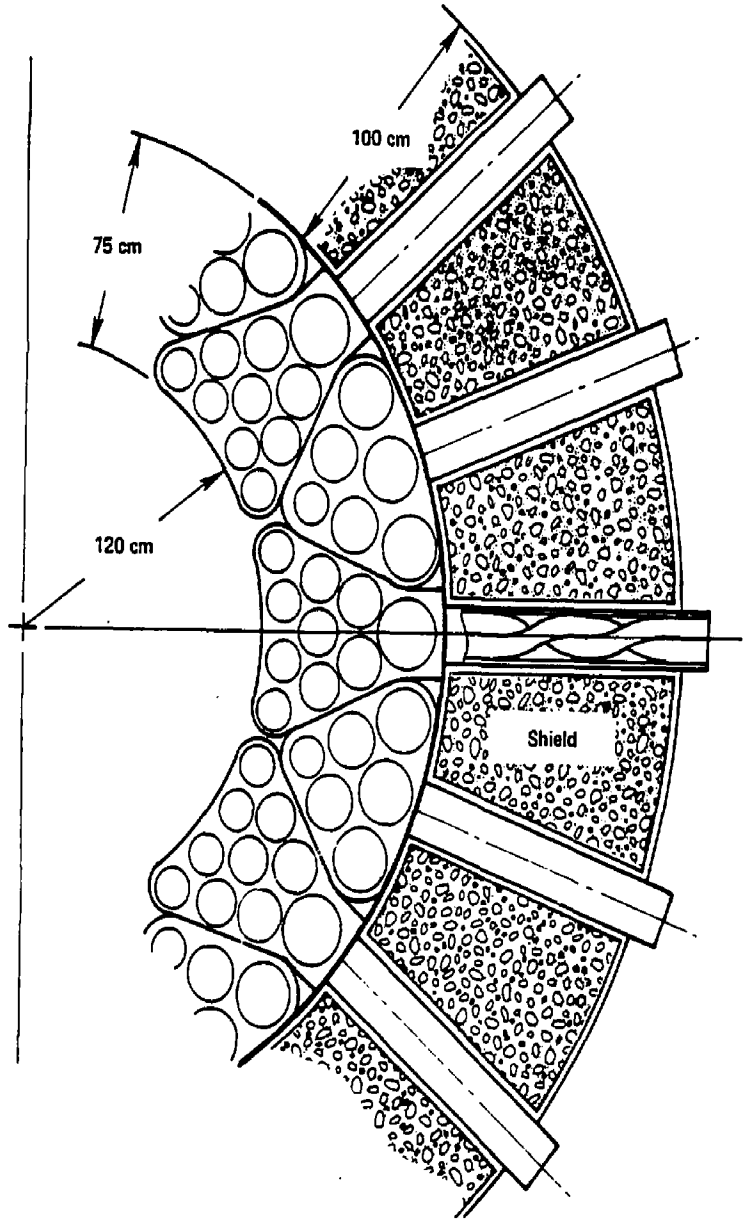

Figure 1.1-2. TMR blanket and shield obtained from Carlson et al. (1979).

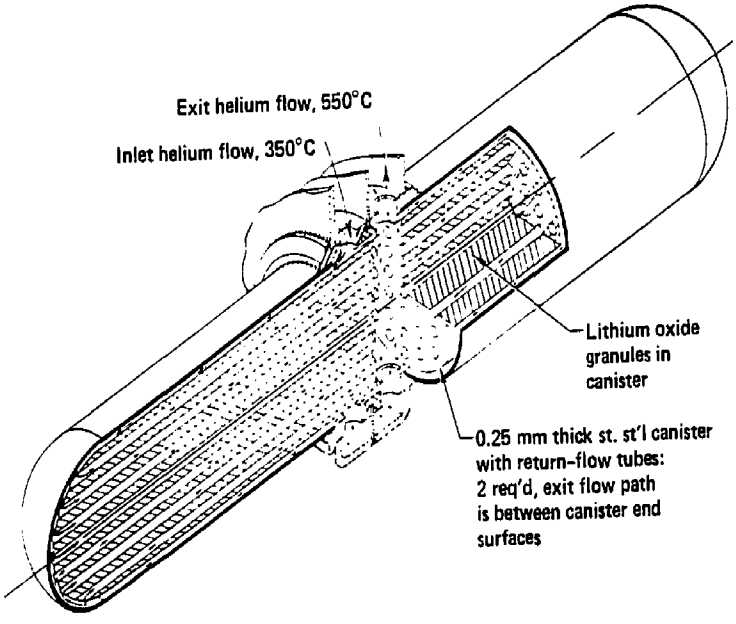

Figure 1.1-3. TMR blanket pod obtained from Carlson et al. (1979).

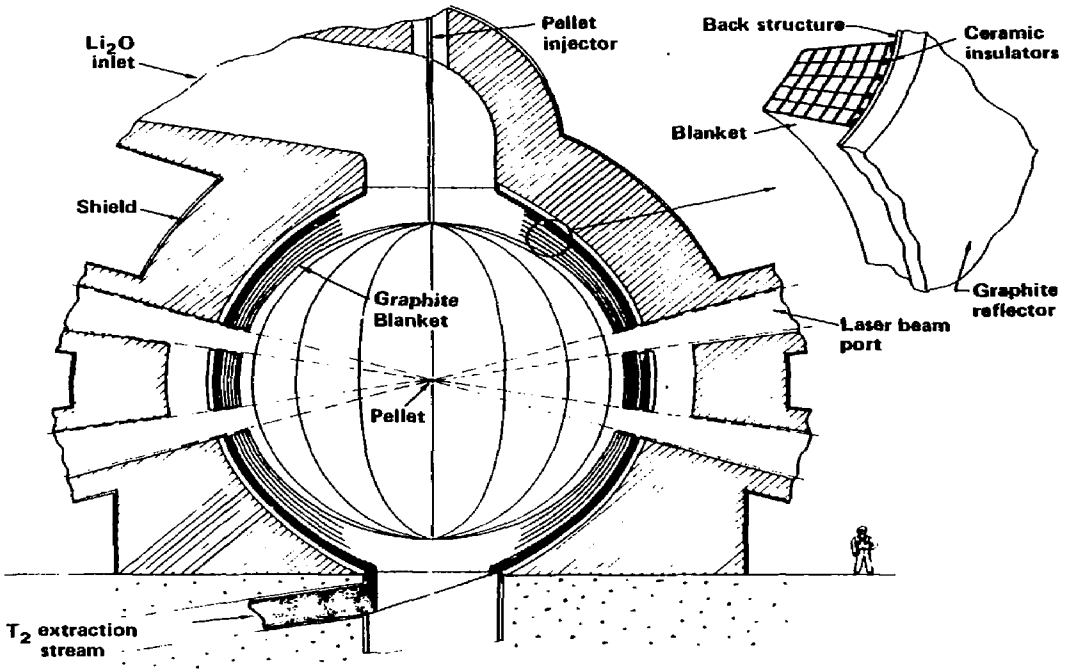

Figure 1.1-4. The SOLASE laser fusion reactor system presented by Conn et al. (1977).

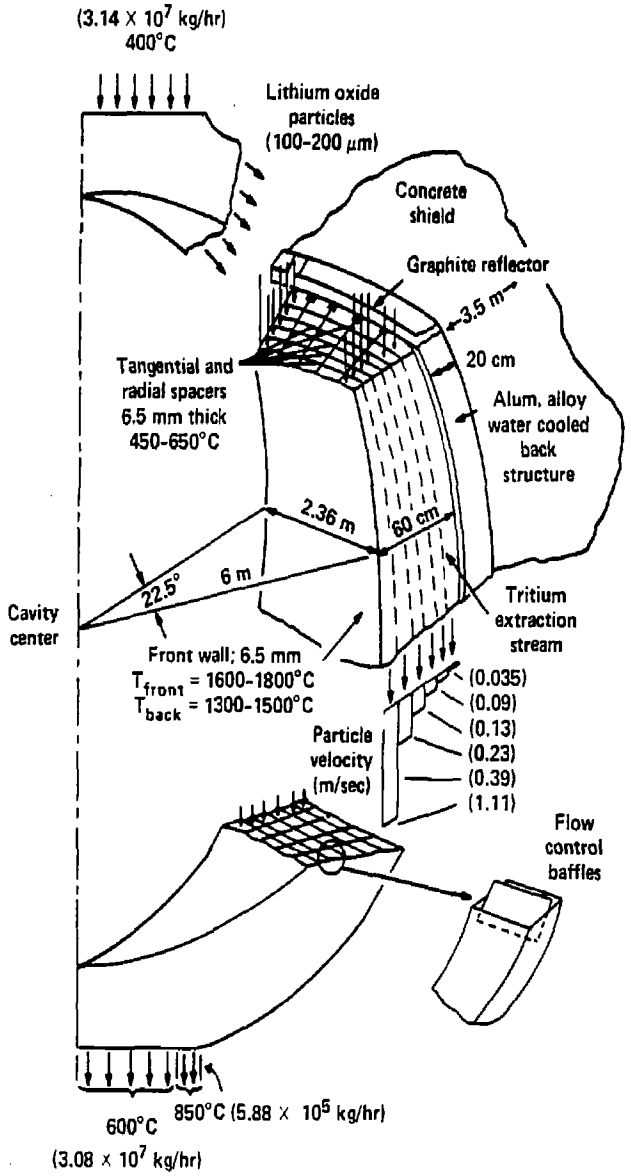

Figure 1.1-5. Schematic of SOLASE blanket segment obtained from Conn et al. (1977).

CHAPTER 2

EXPERIMENTAL METHODS IN PACKED BED HEAT TRANSFER

Research into the heat transfer aspects of packed bed systems has generally been attacked using the "pseudohomogeneous" approach. The solid-fluid system is treated as if it were a single phase through which all the heat transfer occurs. Although the physical properties expressed in the defining differential equations and boundary conditions are greatly simplified by this process, they are merely mathematical simplifications to the true system; thus, they are generally termed the effective properties of the packed bed. These ideas have been reviewed by Yagi and Wakao (1959), Baddour and Yoon (1961), Specchia, Baldi, and Sicardi (1980), and especially by Kulkarni and Doraiswamy (1980).

The earliest studies attacked the situation in a one-dimensional fashion analogous to that of flow through empty tubes. An overall heat transfer coefficient for the system, h_0, was defined based upon the log-mean temperature difference between the average gas temperatures in the inlet and exit planes and the wall temperatures at these planes. The heat transfer coefficient h_0 obtained in this fashion depended on the particle to tube diameter ratio and was generally proportional to a fractional power of the modified Reynolds number of the gas stream, which was based upon the particle diameter and the average superficial gas velocity.

The previous method defined the overall system behavior quite well, but did not provide the opportunity to predict the temperature distribution within the bed. Such predictions became necessary when the temperature in the packed bed was to be prescribed within narrow limits so as to obtain the most efficient conversion in a chemical reaction or to avoid sintering which would cause grave changes in the heat transfer characteristics of the system. To this aim, two-dimensional methods have been developed incorporating one, two, or three parameters to describe the temperature profile. These parameters were obtained by matching as closely as possible the experimental and pseudohomogeneous theoretical temperature profiles or differential equations.

The first of these two-dimensional models incorporated an overall effective thermal conductivity, k_0. The early investigators treated the superficial gas velocity, and therefore the overall effective thermal conductivity, as constant across the tube diameter. Later investigations demonstrated that the velocity profile in fact varied with radius exhibiting a peak near and decreasing at the tube wall. This peak was attributed to the increase in void fraction near the wall which was caused by forcing the particles to conform to a specific boundary. The decrease at the wall was attributed to skin friction. Thus, modifications of the two-dimensional one-parameter method have been conducted relaxing the assumption of constant velocity. In this aim, reported isothermal profiles or simultaneously measured nonadiabatic velocity profiles were utilized and pointwise values of the overall effective thermal conductivity were computed

based upon these data. The distribution of the overall effective thermal conductivity with tube radius obtained in this fashion was then similar to the velocity profile. The studies also showed that the assumption of constant velocity became increasingly valid for a given tube diameter as the particle diameter was decreased. The overall effective thermal conductivity k_0 was found to be dependent upon the modified Reynolds number and the particle to tube diameter ratio.

For packed beds with a practical particle to tube diameter ratio, the experimental results tended to show that the superficial gas velocity and the thermal resistance varied significantly, although only within a particle diameter of the wall. Thus, a two-parameter method was developed which incorporated an effective thermal conductivity, k_e, constant throughout the packed bed. In addition, the increase in thermal resistance near the wall was accounted for by an additional wall heat transfer coefficient, h_w, effective only in this narrow zone. Again, k_e was an integral part of the defining differential equation but h_w was introduced through a boundary condition at the wall. This method described the radial temperature profile much better than the one-parameter method. The effective conductivity was generally found to vary linearly with the modified Reynolds number. The exact dependence of h_w on the modified Reynolds number has been a source of considerable disagreement.

The effective thermal conductivity incorporated the effects of conduction, convection, and radiation between the different solid, stagnant film, and gas region combinations and did not relate specifically to the conductivity of the solid k_p or that of the gas k_g. The natural extension, therefore, was to segregate k_e into two parts, k_{er} and k_{ez}, acting in the radial and axial directions respectively. Axial conduction was usually negligible in comparison to bulk flow and such extension to three-parameter methods became useful only for shallow beds or for flow at low gas velocities.

The purpose of this chapter is to review these experimental methods and their results which served as a basis for theoretical treatment. Discussion of the specific models proposed will be deferred to the next chapter. Section 2.1 reviews the overall heat transfer coefficient. The overall effective thermal conductivity is reviewed in Section 2.2. Next, the two-parameter method is extensively reviewed in Section 2.3. Finally, Section 2.4 briefly discusses the three-parameter method.

2.1 Overall Heat Transfer Coefficient

The earliest experimental analyses of packed beds paralleled those of fluid flow in tubes. Heating as well as cooling experiments have been conducted. In all of the heating experiments, gas was introduced to the packed bed and was heated by means of a steam jacket which surrounded the tube and held the tube wall at constant temperature. In the cooling experiments, the packed bed system was surrounded by a constant temperature liquid jacket. The gas, which

was introduced at a higher temperature, was thus cooled by the bed. The correlations obtained from heating and cooling experiments conducted in the same packed bed were found to be identical.

The studies which will be discussed here are listed in Table 2.1-1 along with the various parameters of the system studied. All of the particles used in these studies were quite large, being on the order of a few millimeters. All of the tube diameters were likewise small, the largest being about 80 mm. The particle to tube diameter ratio was therefore large, a parameter of great importance as will be discussed. Metallic as well as lower conductivity ceramic particles of various shapes have been studied. When the actual particle dimensions were not obtainable an equivalent diameter, as defined by the respective authors, was tabulated. Various gases have been studied, air being the one most often encountered.

The overall heat transfer coefficients are calculated from:

$$Q = h_o A \Delta t_{ln} \qquad (2.1\text{-}1)$$

where Q is the heat input or output from the packed bed, A is the inside surface area of the packed tube, and Δt_{ln} is the logarithmic mean temperature difference between the air and the tube wall at the inlet and exit of the bed. The correlations for h_o that have been presented are listed along with their respective ranges of applicability in Table 2.1-2.

Colburn (1931) was perhaps the first to study heat transfer in packed beds. Colburn's correlation was presented in terms of a, a

function of d_p/D_t (Figure 2.1-1). Colburn argued that the effect of the particle to tube diameter ratio was based upon its effect on the void fraction. Forcing the particles against a specific boundary at the wall caused a localized increase in the void fraction compared to the center of the bed. As d_p/D_t was increased, a greater proportion of gas flowed next to the wall increasing h_o. As d_p/D_t exceeded 0.15, Colburn argued that the particles did not pack closely in the center of the tube and increased the void fraction there. The flow next to the wall, and therefore h_o, then decreased.

Leva (1947) conducted experiments similar to those of Colburn and correlated the overall heat transfer coefficient in terms of the modified Reynolds number. The correlation depicted a maximum in h_o for $d_p/D_t = 0.15$ which was found experimentally and also agreed with the results of Colburn. Leva claimed that no correlation existed between h_o and the void fraction in the range studied; however, the void fraction did correlate with pressure drop. For a constant pressure drop through the bed, the superficial gas velocity increased with increasing void fraction. For constant G_o, the pressure drop increased with decreasing void fraction.

The correlation predicted that h_o was proportional to $(k_g/\mu_g)^{0.90}$, a sole property of the gas. Leva tested the packed bed using both air and carbon dioxide; large variations in Prandtl number were not analyzed.

Leva and Grummer (1948) extended Leva's original work. They tested particles of various physical shapes and thermal conductivities.

Leva's original correlation was then slightly modified to take these changes into account.

The effects of surface characteristics were first studied using particles of approximately the same thermal conductivity as Leva's earlier work. Leva's 1947 correlation was assumed to apply to the data and was used to calculate an effective d_p. For beds with spherical particles of nonuniform sizes, the correlated value of d_p was found to agree closely with the arithmetic average diameter obtained on a volume basis. For Raschig rings it was found that the nominal diameter should be used, while for cylinders the best agreement was obtained when the average diameter of an equivalent volume sphere was used for d_p.

Data for particles with widely different thermal conductivities were then obtained. For aluminum, cast iron, copper, and zinc the observed values of h_0 were considerably higher than predicted using Leva's original correlation; therefore, the correlation was multiplied by a function of k_p. This function f_1 is reproduced in Figure 2.1-2. Leva and Grummer stressed that f_1 was approximately equal to unity for many materials of interest such as ceramics.

Leva, Weintraub, Grummer and Clark (1948) developed a correlation similar to that of Leva (1947) but for cooling of hot air injected into the bed. A slightly different dependence upon the modified Reynolds number was observed. The variation with particle to tube diameter ratio was also different in comparison to the heating case. The maximum in h_0 was observed for $d_p/D_t = 0.153$. An attempt

was made but no correlation between the overall heat transfer coefficient and the tube length to diameter ratio was found.

Leva (1950) was concerned with extending his original correlation of 1947 to systems where the particle to tube diameter ratio exceeded 0.35. The power of the modified Reynolds number variation was taken to be 0.75 and only the variation with d_p/D_t was correlated.

Campbell and Huntington (1952) studied the heating and cooling of natural gas. Results similar to those found above were observed. In place of the particle diameter, the reciprocal significant length was taken as the surface area per unit volume of particles, S. The effect of the Prandtl number was not studied.

Chu and Storrow (1952) analyzed the heating case and found results that were much more complicated than previously obtained. Two different correlations for the Nusselt number were presented for the regions above and below a critical Reynolds number, based on the tube diameter, of approximately 1600. These Nusselt numbers were again correlated as functions of the modified Reynolds number and d_p/D_t but correlation with the tube length to diameter ratio was also found. As all the runs were made with air, the effect of Prandtl number was not studied.

The authors indicated that for $N_{Re} < 1600$ there was no effect of k_p on h_o; however, for $N_{Re} > 1600$, k_p did begin to correlate with h_o. This would tend to agree with Leva and Grummer (1948) who ran most of their tests at high flow rates.

Gelperin and Kagan (1966) defined critical modified Reynolds numbers and divided the flow into three separate regimes. These were characterized as:

- $N'_{Re} < 40$ (laminar flow)
- $40 \leq N'_{Re} \leq 1200$ (unstable turbulent flow)
- $N'_{Re} > 1200$ (turbulent flow)

Both heating and cooling experiments were run and correlated together. The authors did not observe the maximum in h_o as reported by Colburn or Leva et al. They claimed that the error of previous authors resulted from the fact that a single correlation should not be used for both laminar and turbulent flow.

The authors then studied the effects of surface roughness on the overall heat transfer coefficient and presented additional correlations. To this aim, they defined an equivalent diameter which takes into account the surface characteristics of the particles and the tube:

$$d_e = \frac{4\epsilon}{S_p + 0.75\,A} \qquad (2.1\text{-}2)$$

The critical Reynolds numbers based upon this equivalent diameter then became $d_e G_o/\mu_g = 42$ and 1200, respectively.

2.2 Overall Effective Thermal Conductivity

To report heat transfer data in a form suitable for predicting the temperature profile within a packed bed, the concept of the overall effective thermal conductivity has been introduced. Several assumptions are made in order to derive the governing differential equation for such a system:

1. The actual heat transfer can be described by an equivalent mechanism consisting only of conduction and bulk gas flow;
2. at each point in the bed, the particle and gas temperatures are equal;
3. radial conduction can be described by Fourier's law and the overall effective thermal conductivity, k_0, which may or may not be treated as a constant;
4. axial conduction is negligible;
5. no heat is generated within the bed; and
6. the experiments are operated in the steady state.

Various schemes have been used in the literature to obtain k_0 from the defining differential equation or temperature profiles derived from the above assumptions. The first investigators assumed that the superficial gas velocity and the overall effective thermal conductivity were constant across the entire tube diameter (Section 2.2.1). The defining differential equation could then be integrated and comparison of the experimental and pseudohomogeneous theoretical temperature profiles yielded k_0. Other early authors also assumed

that the superficial gas velocity was constant but that k_o varied across the tube diameter (Section 2.2.2). Pointwise values of the overall effective conductivities were then computed by directly applying the defining differential equation to the experimental data. Later investigators demonstrated that the superficial gas velocity did indeed vary with radial position (Section 2.2.3). Previously reported isothermal velocity profiles or simultaneously obtained nonadiabatic velocity profiles were then utilized to modify the existing correlations (Section 2.2.4).

Experiments have been run for both heating and cooling of gas flowing in either the upflow or downflow directions. Each of the methods described above will be discussed in turn. Table 2.2-1 lists the different studies to be reviewed in this section along with the various parameters used.

2.2.1 Constant Superficial Gas Velocity, Constant k_o

Early investigators assumed that the superficial gas velocity and the overall effective thermal conductivity were constant across the bed diameter. In this case, the defining differential equation is:

$$k_o \left(\frac{1}{r}\frac{\partial t}{\partial r} + \frac{\partial^2 t}{\partial r^2}\right) = G_o c_p \frac{\partial t}{\partial z} \qquad (2.2\text{-}1)$$

Equation (2.2-1) is easily integrated with a constant wall temperature boundary condition; in addition, this solution is averaged over the bed cross section to give:

$$\frac{t_w - t_e}{t_w - t_i} = 4\sum_i \frac{1}{\alpha_i^2} \exp(-\alpha_i^2 \tau) \qquad (2.2\text{-}2)$$

where:

$$\tau = \frac{4\, Lk_0}{c_p G_0 D_t^2} \qquad (2.2\text{-}3)$$

and the α_i are the roots of $J_0(\alpha_i) = 0$. The overall effective thermal conductivity in this case is a truly average quantity for the packed bed. It is obtained by matching the experimental temperature profile to the pseudohomogeneous theoretical equation presented in Equation (2.2-2); the correlations obtained by this method are presented in Table 2.2-2.

Verschoor and Schuitt (1951) studied the heating of air flowing downward. The relevant parameter describing the reciprocal particle length was taken to be the surface area of the particles per unit volume of packed material, S. The size, surface characteristics, and shape were thus accounted for and correlation with respect to SD_t instead of d_p/D_t was presented. The effect of void fraction was not studied. The correlation presented incorporated a static overall conductivity effective even when there was no gas flow. The static term was found to be proportional to a fractional power of k_p/k_g.

Hougen and Piret (1951) studied hot air flowing downward through a packed bed cooled by a water jacket. Cylindrical as well as spherical shaped particles were studied; the relevant particle length was taken to be the square root of the surface area of the

particle, $\sqrt{S_p}$.

The void fraction was accounted for and the solution for the temperature profile was given by Equation (2.2-2) with τ replaced by $\epsilon\tau$. The overall effective conductivity was obtained by a method incorporating the modified Graetz number:

$$N'_{Gz} = \frac{c_p D_t^2 G_o}{4 \epsilon L k_o} \qquad (2.2\text{-}4)$$

The series on the right hand side of Equation (2.2-2) is denoted as E and can be plotted as a function of the modified Graetz number. Such a plot, called an E-chart, is reproduced in Figure 2.2-1. Since the temperature ratio in Equation (2.2-2) is determined experimentally, the E-chart can be used to determine k_o.

Note that the presented correlation does not predict a static conductivity that would exist even when G_o approaches zero. For this reason, equations of this type have received considerable criticism in the literature. The authors did not suggest using this correlation outside the region of modified Reynolds number studied.

Molino and Hougen (1952) repeated the work of Hougen and Piret, but for heating of air flowing downward. The authors stated that their correlation determined for the heating case fitted the data of Hougen and Piret (1951) for the cooling case quite well. Thus, they suggested their correlation applied to both heating and cooling. A stagnant thermal conductivity was not presented. A variation with particle to tube diameter ratio was not observed.

2.2.2 Radially Varying k_0

Other early investigators chose not to treat k_0 as an average quantity for the entire packed bed. Although Equation (2.2-1) is based upon a constant k_0, it is used as the defining differential equation for this case also. Graphical differentiation of the experimental temperature profiles gives the quantities necessary to evaluate pointwise values of k_0 directly from Equation (2.2-1). In this method, the superficial gas velocity is treated as a constant but the overall conductivity is found to vary with position throughout the system. Correlations published by this group are presented in Table 2.2-3.

Hall and Smith (1949) studied the upflow of air. The temperature of the gas stream was measured at seven positions along a given diameter at several bed depths. The particle temperature at these same points was measured by inserting a thermocouple in the center of a pellet. Smoothed radial temperature profiles were then obtained from a plot of the measured temperatures. The profiles were found to be nearly parabolic and the difference between the particle and gas temperature was small.

Originally, Hall and Smith tried to relax the assumption of equality of particle and gas temperature. To this end they postulated a solid to gas heat transfer coefficient and a separate overall effective thermal conductivity for the solid and gas, k_0^p and k_0^g, respectively. Analysis showed that wide variations in k_0^p and k_0^g were caused by large fluctuations in terms containing $(t_p - t_g)$. A

difference of only two degrees was found to cause more than 100% change in the overall thermal conductivities calculated. They and many other authors have discovered that the difficulty in accurately placing thermocouples in their proper radial positions easily cause errors of this magnitude.

Since the particle and gas temperatures were found to be nearly identical, final data analysis was presented in terms of the single conductivity, k_0. Table 2.2-4 lists the computed pointwise values of k_0 for the 3.2 mm alumina cylindrical pellets studied. These values were averaged over the bed depth at a given r/R and are also reported in Table 2.2-4. Although the data were not conclusive, the authors claimed that k_0 decreased as the wall was approached.

The work of the previous authors was continued by Bunnell, Irvin, Olson, and Smith (1949). This time, the superficial gas velocity was varied.

The temperature of the gas and pellets at all positions in the bed were found to be approximately identical. The radial temperature gradients were again quite steep resulting in nearly parabolic temperature profiles. The authors suggested this verified that heat was carried off in bundles and did not mix readily in the radial direction. Typical results of these two characteristics are presented in Figure 2.2-2 for a bed depth of 152 mm and various gas velocities.

The authors reported that the considerable variation with bed depth was not consistent and was presumed to be due to local nonuniformities in the packing. The overall effective thermal

conductivity was thus first averaged over bed depth and these values were then correlated; a linear dependence upon the modified Reynolds number resulted. No variation of k_o/k_g with radial position was reported for r/R less than about 0.8. However, as one approached the wall, the data tended to show a decrease. This decrease in k_o was suggested to be due to the channeling near the tube wall caused by the larger void space there. A correlation of k_o in the wall region was not presented.

The data of Bunnell, Irvin, Olson, and Smith (1949) was reanalyzed by Irvin, Olson, and Smith (1951). A slightly different way of correlating k_o was presented. Bunnell, Irvin, Olson, and Smith utilized the temperature gradients applied to Equation (2.2-1) to first obtain (k_o/Gc_p). To obtain k_o, this ratio was then multiplied by the specific heat and the mean value of the superficial gas velocity, which was assumed to be a constant. As was discussed above, straight lines were obtained from a plot of k_o versus G_o. Irvin, Olson, and Smith referred to studies of the velocity variation in packed beds and explained these results as follows: G was actually not constant across the bed cross section and thus what was actually being plotted was (k_o/c_pG) (c_pG_o) versus G_o. This was simply plotting a variable against itself, which of course gave a linear relationship.

This discrepancy was avoided by not applying the assumption of constant gas velocity and correlating k_o directly in a ratio of (k_o/c_pG). This correlation was presented in terms of a_1, a function of r/R that was not presented. This was the first time that the

superficial gas velocity was suggested to be other than a constant. This idea motivated additional investigations to verify the exact form of the radial velocity profile and its effect on the overall effective conductivity. These will be discussed next.

2.2.3 Velocity Distributions in Packed Beds

As has been discussed, the variation of k_o, especially near the wall, has often been explained by the existence of a different void fraction there than in the packing near the center of the tube. The assumption of a constant gas velocity across the bed cross section was therefore questioned also. For this reason, Smith and coworkers analyzed the radial variation of G in isothermal beds.

Circular hot wire anemometers concentric with the tube axis were used to measure the radial velocity profile. In this method, nonuniformities in the bed were suppressed since the average velocity at a given radial position was measured. Dependence upon the bed height and depth as well as particle size was studied.

Morales, Spinn, and Smith (1951) argued the fact that (k_o/c_pG) varied with radial position provided additional evidence that the mass velocity was not constant across the tube diameter. The average velocity was measured at radial positions chosen by the equation:

$$\frac{r}{R} = \left[\frac{(2n - 1)}{10}\right]^{0.5} \qquad (2.2\text{-}5)$$

for $n = 1$ through 5. Use of these positions allowed the average

velocity across the bed cross section to be computed from a single arithmetic average. The thickness of the wire was sufficiently smaller than the size of the pellets so that variations of the flow due to the presence of the anemometer were ignored. Reproducibility was excellent for identical runs made on a given bed without repacking; packing effects for these beds with large d_p/D_t ratios made reproducibility difficult to achieve when disassembly and repacking was involved.

Figure 2.2-3 shows typical results for the radial velocity profile with G_0 as a parameter. A decrease in the velocity at the center of the bed as well as at the wall was observed with a maximum located at approximately r/R = 0.7. The decrease near the tube wall was attributed to skin friction and the decrease near the center of the tube was attributed to a lower void fraction there than near the wall. The packing depth was found also to be of importance. The effect of skin friction near the tube wall was increasingly dampened so that the velocity there increased with packing depth over that found in the empty tube. Similarly, the effect of packing was found to depress the velocity near the center of the tube so that the velocity there decreased as the depth was increased.

The authors claimed a similarity between the radial velocity profiles and the radial variations of (k_o/c_pG) obtained by various authors. This variation was postulated to be due at least in part to the radial variation of G. Since the isothermal profiles could

not be guaranteed to be independent of temperature, no attempts were made to obtain k_0 from these data.

A more comprehensive investigation of this earlier study was reported by Schwartz and Smith (1953). Their objectives were to obtain a correlation for the velocity profile and to determine the effect of D_t/d_p, i.e. when the assumption of a flat velocity profile would be approximately valid.

The anemometers were calibrated by measuring the velocity profile in an empty tube via the usual laminar expression for the velocity profile:

$$\frac{u}{V} = 2\left[1 - \left(\frac{r}{R}\right)\right]^2 \qquad (2.2\text{-}6)$$

Reproducibility of results was shown generally to decrease with increasing d_p/D_t. The bed was disassembled and repacked three times; the average of these three tests was studied in each case. Divergence from a flat profile was observed to increase with increasing d_p and decreasing D_t. For large values of D_t/d_p, the velocity profile was quite flat in the core of the tube and exhibited a peak near the wall. This peak was only about 20% higher than at the center for $D_t/d_p = 32$. For low values of D_t/d_p, the velocity profile exhibited large gradients even near the center of the tube. For $D_t/d_p = 8$, the peak velocity was 100% above that at the center line. The peak near the wall was observed to occur at approximately one particle diameter from the tube wall independent of the particle or tube size. These

results are compared in Figure 2.2-4. Following these observations, it was concluded that deviation from the assumption of a uniform velocity is less than 20% for D_t/d_p greater than about 30.

The authors then derived a correlation for the velocity profile based upon the Prandtl mixing length theory and experimentally determined pressure drop data. This correlation is presented in Table 2.2-5 and was compared with the experimental data as the solid line in Figure 2.2-4. This correlation was shown to fit the observed data quite well.

2.2.4. Effect of Velocity Distribution on k_0

Because of the results presented in the previous section, various authors have relaxed the assumption of constant mass velocity in their computations of k_0. Actual pointwise values of k_0 can be computed without the assumption of constant velocity by applying the previously observed isothermal velocity profiles, or by simultaneously observing nonisothermal velocity profiles. Both methods have been attempted. Equation (2.2-1) assumes a constant overall effective thermal conductivity. Modification of this equation is thus required to account for the variation of k_0 with r that was described above. Allowing for variation of k_0 and G with r, Equation (2.2-1) becomes:

$$k_0\left(\frac{1}{r}\frac{\partial t}{\partial r} + \frac{\partial^2 t}{\partial r^2}\right) + \frac{dk_0}{dr}\frac{\partial t}{\partial r} = Gc_p\frac{\partial t}{\partial z} \qquad (2.2\text{-}7)$$

The mathematical equations used by the various authors to analyze the data and obtain k_0 are listed in Table 2.2-6.

Schuler, Stallings, and Smith (1952) studied a system which was identical to that used by Bunnell, Irvin, Olson, and Smith (1949) in their studies of the temperature profile. It was also identical to that used by Morales, Spinn, and Smith (1951) to study isothermal velocity profiles. Equation (2.2-7) is a first order differential equation in the unknown k_0 with all of the coefficients, $f_1(r)$ and $f_2(r)$ (Table 2.2-6), known at any radial position. Thus, a numerical solution resulted in the radial variation of k_0.

In carrying out the above procedure, the nonisothermal velocity profile of Morales, Spinn, and Smith (1951) was first converted to account for nonisothermal conditions. To do this, the pressure drop in a nonisothermal bed was assumed to be the same as that in an isothermal bed operating at the same bulk temperature and variation of the friction factor was taken to be proportional to the -0.25 power of the Reynolds number. Such a correction leads to a very moderate change of the results presented in Figure 2.2-3 or 2.2-4.

Results of k_0 obtained in this fashion are reproduced in Figure 2.2-5. The authors noted the similarity between this and the radial velocity profiles presented previously. The mass velocity of the gas remained an important parameter. Again, as d_p/D_t decreased, the radial variations in velocity became insignificant except near the wall.

Kwong and Smith (1957) developed a Sturm-Liouville solution to the problem so that numerical integration of Equation (2.2-7) resulted in k_0. In this method, the necessity of first graphically differentiating the temperature profile was eliminated. Only $T_0 = (t_0 - t_w)$ and $T_L = (t_L - t_w)$, the radial temperature difference profiles at the entrance and at some axial position L, were required. Here, L was not necessarily the bed exit.

Only radial variation of k_0 was assumed; a proper choice of the axial position z = L had to be made. If L was too small, errors in neglecting higher order terms were significant. If L was too large, the temperature profile was found to be so flat that sizeable numerical errors involved in computation were introduced. The isothermal velocity profile data of Schwartz and Smith (1953) were used in the computational process. It was assumed that the velocity profile was independent of temperature.

Results of the radial profile of k_0 were similar in form to those discussed earlier. k_0 was found to decrease near the wall and in the center of the bed with a peak being exhibited at about one pellet diameter from the wall. The radial profile for k_0 was found to be invariant with axial position above a bed height of approximately 0.05 m. The usual increase of k_0 with increasing G_0 was observed and no variation with temperature for the temperature levels studied was found. Since the particles themselves offered only a small part of the thermal resistance in the bed, the resulting effect of k_p on k_0 was observed to be small. The

higher c_p of ammonia was found to result in a sizable increase in k_0. A correlation for their results was not presented.

Schertz and Bischoff (1969) computed k_0 in the same fashion as Kwong and Smith. However, simultaneous nonisothermal velocity profile data and a correlation for k_0 were obtained. Typical results for the measured radial velocity profile are presented in Figure 2.2-6; the isothermal profile is also shown for comparison. Large differences between the isothermal and nonisothermal profiles were observed. The variations were found to be most pronounced when a temperature gradient existed throughout the bed and when the center of the bed was hotter than the edge.

A hydraulic radius was defined in order to correlate the velocity profile to the physical properties of the system:

$$r_H = \frac{\epsilon d_p}{6(1 - \epsilon)} \qquad (2.2\text{-}8)$$

Such a definition allowed the hydraulic radius to vary with r as is shown in Figure 2.2-7. To obtain Figure 2.2-7, Schertz and Bischoff used the data of Benenati and Brosilow (1962) and the data of Roblee, Baird, and Tierney (1958). The velocity correlation is presented in Figure 2.2-8. Here μ is the viscosity of the gas at the hydraulic radius in question and at the temperature measured there. μ_0 is the viscosity of gas at room temperature.

Smoothed temperature profiles and the equation listed in Table 2.2-6 were used to obtain k_0. Results for the correlation of k_0

are pictured in Figure 2.2-9. A linear relationship with the modified Peclet number was suggested and a static overall effective conductivity was observed. A correlation was also presented (Table 2.2-6) where it was approximately calculated that: $k_0^0/k_g=7$ and $c_2=0.055$.

2.3 Effective Thermal Conductivity and Wall Heat Transfer Coefficient

Failure of the assumption of constant overall effective thermal conductivity and the inherent complexities of utilizing a radially varying conductivity led other researchers to expand their analyses to two-dimensional methods which incorporated two parameters. For most packed beds of interest where D_t/d_p exceeds 30, the superficial gas velocity is nearly constant across the core of the bed. The first of these two parameters, called the effective thermal conductivity k_e, is therefore treated as a constant. This has the advantage of retaining mathematical simplicity in the defining differential equation. The decrease in the thermal resistance near the tube wall is then accounted for by the following method. The second parameter, called the wall heat transfer coefficient h_w, is postulated to occur simultneously with k_e in the narrow zone near the wall. Assumption of a constant effective thermal conductivity and a simultaneous wall heat transfer coefficient describes the temperature profile much more accurately than the one-parameter method. The differential equation used is:

$$k_e\left(\frac{1}{r}\frac{\partial t}{\partial r}+\frac{\partial^2 t}{\partial r^2}\right)=G_0 c_p\frac{\partial t}{\partial z} \qquad (2.3\text{-}1)$$

The boundary conditions are now modified to account for the wall heat transfer coefficient. Table 2.3-1 summarizes the parameters of the packed beds which will be discussed in this section. Again the same form of presentation is used as in Table 2.1-1.

Various methods have been utilized to obtain the two parameters from the experimental data. These include applying simple energy balances to the packed bed, graphically differentiating the data and applying the defining differential equation, and analytically or numerically integrating the differential equation and matching the solution to the observed temperature profile. Since these are all simply different methods of obtaining results for the same model, they will all be discussed here. The specific correlations are listed in Table 2.3-2.

Quinton and Storrow (1956) have presented perhaps the only experimental study utilizing a constant wall heat flux instead of a constant wall temperature. They found various advantages in such a method: i) The variation of surface temperature along the length of the tube was easy to measure. ii) The temperature profiles obtained were parabolic in nature and this fact could be exploited to conveniently find average temperatures. They argued that a parabolic profile was not actually obtained by the constant wall temperature heating method and that the magnitude of error varied with the fluid Graetz number. iii) The axial temperature gradient in Equation (2.3-1) became a constant independent of r for large z.

Values of k_e and h_w were determined as follows: Beyond a certain entrance length, $\partial t/\partial z$ became a constant independent of r/R. Solution of Equation (2.3-1) for constant $\partial t/\partial z$ is then straight forward. An energy balance over a section of the bed then relates the constant wall heat flux to the constant axial temperature gradient so that k_e could be written in terms of known quantities.

Hanratty (1954) reviewed the Ph.D. theses of Felix (University of Wisconsin, June 1951) and Plautz (University of Illinois, November 1953). The wall heat transfer coefficient for both of these authors in systems with heating of air flowing upwards through beds of spherical particles was found to be independent of d_p/D_t and proportional to a fractional power of the modified Reynolds number. This independence of the wall heat transfer coefficient on particle to tube diameter ratio was not observed with cylindrical particles. Also, a different dependence on the modified Reynolds number was observed. The results of Felix for cylindrical particles were written in terms of a constant, c_1, which depended on d_p/D_t as reproduced in Table 2.3-3. No trend with d_p/D_t was observed.

Plautz suggested that the difference in dependence on G_o results from the method of contact between the spherical or cylindrical particles and the wall. The spherical particles possess only point contacts whereas the cylinders may greatly obstruct the flow there. The possibility for such a "noncontinuous" liquid film to exist is therefore much greater. Using a mathematical treatment developed by Dankwerts for such a case and using certain order of magnitude

estimates, Hanratty developed a theoretical correlation identical to Felix's correlation. It is interesting to note that the value of c_1 derived was equal to 0.95, the same as in three of the five cases reported in Table 2.3-3.

Plautz and Johnstone (1955) reported similar results for Plautz's work. A copper-constantan high velocity probe was used to measure the radial variation of the bed temperature at various depths. Eight readings 45^{o} apart at a single radial position were averaged together to give the gas temperature at that position.

The wall heat transfer coefficient was calculated from an energy balance on the entire column. No variation of h_w with L was found. A trial and error method was used to obtain k_e incorporating these values of h_w. A value of k_e was assumed and a finite difference scheme was used to solve Equation (2.3-1). This process was continued until the predicted and observed temperature profiles matched closely. The effective thermal conductivity was found to vary by less than 10% up to a distance of one particle diameter from the wall.

Perhaps the earliest and most quoted work incorporating two parameters was that of Coberly and Marshall (1951). High velocity copper-constantan thermocouples were used to measure the temperature profiles at numerous radial locations for various bed depths. The observed temperature profiles were first plotted, then smoothed. Such smoothed plots were reported to fit the data more closely than the original curves. These smoothed curves were then graphically differentiated to obtain the effective conductivity. Since this

procedure was identical to that used to obtain the overall effective conductivity, variation of k_e with position was observed. The average of k_e obtained for each gas velocity and particle size was used as the constant k_e assumed in Equation (2.3-1). It was these values that were subsequently used and correlated. A graphical determination of the second derivative with respect to axial position verified that axial conduction was indeed negligible.

To obtain values of h_w, further mathematical treatment had to be presented. Since this mathematical treatment is perhaps the authors' greatest contribution, it will be briefly reviewed. Equation (2.3-1) is integrated to give a Sturm-Liouville solution that is used to compare with experimental data. The boundary conditions used and the series solution are presented in Table 2.3-4. Here t_0 is constant across the inlet plane and t_R is the temperature of the gas extrapolated to the inside surface of the wall. For $\beta_1 z$ greater than about 0.2, the authors stated that the series converges so rapidly that only the first term needs to be retained. A semilogarithmic plot of the temperature ratio versus axial position yields the slope $-\beta_1\lambda_1^2$. Since β_1 is defined in terms of k_e and other known parameters, λ_1, and therefore h_w, is obtained from the eigencondition.

The effective thermal conductivity was correlated with respect to the modified Reynolds number based upon the square root of the particle surface area. The authors claimed that isothermal velocity measurements verified the assumptions of constant G_0 throughout the bed.

The apparatus of Campbell and Huntington (1952) was mentioned previously when they analyzed their data to arrive at overall heat transfer coefficients. They also presented two-parameter data. Since the axial temperature profiles were obtained along the centerline of the bed, a specialized form of Equation (2.3-1) was used to graphically differentiate the observed temperature profiles. Outside of this discrepency, their method of data analysis was identical to that of Coberly and Marshall (1951). The authors quoted a minimum probable error in graphical differentiation of 20%. They claimed that their correlation for k_e applied not only to their data using natural gas, but also to the data of Coberly and Marshall (1951) using air.

Calderbank and Pogorski (1957) calculated k_e and h_w in the same manner as Coberly and Marshall (1951). In carrying out the analysis, radial velocity measurements confirmed that G was approximately constant across the tube diameter for D_t/d_p greater than 10. The peak was again observed at one pellet diameter from the tube wall. The results for k_e obtained confirmed those presented by Coberly and Marshall; the correlations were almost identical. The results obtained for the wall heat transfer coefficient were closer to those found by Coberly and Marshall than by Hanratty (1954). The mean deviation of both of the correlations was expected by the authors to be about 10%.

Yagi and Wakao (1959) studied packed beds with various packing materials, including higher conductivity metals. The mathematical

analysis used was identical to that of Coberly and Marshall. Only two points were considered necessary on the semilogarithmic plot of temperature ratio versus axial position, thus only two packing depths were used.

Except for some scattering at relatively low modified Reynolds numbers, the effective conductivity was correlated as:

$$\frac{k_e}{k_g} = \frac{k_e^o}{k_g} + (\alpha\beta)\, N_{Pr} N'_{Re} \qquad (2.3\text{-}2)$$

Again a linear relationship with the modified Reynolds number was obtained. The stagnant contribution was obtained by extrapolation of the best fit line to no flow conditions. Yagi and Wakao stated that $(\alpha\beta)$ is the parameter characterizing the radial fluid mixing and is defined as the inverse of the modified Peclet number due to turbulent diffusion of the fluid:

$$N'_{Pe} = \frac{d_p c_p G_o}{k_e^t} \qquad (2.3\text{-}3)$$

where:

$$k_e = k_e^o + k_e^t \qquad (2.3\text{-}4)$$

In the theoretical developments of Chapter 3, equations similar to Equation (2.3-2) will be encountered repeatedly. It is for this reason

that the correlation is listed here. The values of k_e^o/k_g and $(\alpha\beta)$ obtained are listed in Table 2.3-5. The value of k_e^o/k_g for metal spheres is twice that for glass spheres and cement clinker particles. Yagi and Wakao thus concluded that k_e^o is dependent upon k_p itself.

The correlation presented for h_w was found to be equally valid for the data of Plautz and Johnstone (1955) and of Felix (1951). No variation of h_w with k_p was observed. The effect of the gas Prandtl number was not studied.

Phillips, Leavitt, and Yoon (1960) used the same defining equation for the temperature profile as Coberly and Marshall but also used a different method in which graphical differentiation became unnecessary. They studied systems using various different gases and studied the effect when these gases were actually adsorbed by the packing material.

$\beta_1\lambda_1^2$ was graphically obtained in a similar fashion as Coberly and Marshall. $\ln (t_w - t_o)/(t_w - t)$ was plotted as a function of z for various ξ. The slope of these lines gave $\beta_1\lambda_1^2$. The value obtained for each line gave a check on the consistency of the data. The magnitude of the vertical distance between any line and the line for $\xi = 0$ was equal to $\ln J_o(\lambda_1\xi)$. Thus λ_1 could be used to determine k_e. Previously, graphical differentiation to evaluate k_e was necessary so that λ_1 could be calculated. Again λ_1 and k_e were used to obtain h_w.

The static contribution to k_e was obtained in transient experiments with stagnant gas contained in the packed bed. The differential equation describing the process is similar to Equation

(2.3-1). This differential equation, the initial conditions, and the solution are presented in Table 2.3-6. The same method is used to obtain k_e^o as was described above for the steady state flow case. The only difference is that plotting was done versus θ and the slope is equal to $\beta'\lambda_1^2$. Of course since these experiments were run with static gas, $k_e = k_e^o$.

The static conductivity was correlated with two contributions one of which depended on the gas conductivity. The propane and methane gases were adsorbed to a significant extent by the molecular sieve pellets but the correlation was found to apply equally well to the case of nonadsorbed gases. No presentation of h_w was made.

Yagi, Kunii, and Wakao (1961) utilized the analytical temperature profile derived by Coberly and Marshall in a similar fashion as previous methods to obtain k_e and h_w. The data were again correlated by Equation (2.3-3). Results for k_e^o/k_g and $(\alpha\beta)$ are presented in Table 2.3-7.

Agnew and Potter (1970) mounted bed thermocouples only along the tube axis. Coberly and Marshall's analytical temperature profile equation evaluated at r = 0 was used to analyze the data. The data were correlated by Equation (2.3-3). Values of k_e^o/k_g and $(\alpha\beta)$ are reported in Table 2.3-8. The values of k_e^o/k_g obtained agreed closely with the predictions of theory to be presented in Chapter 3. $(\alpha\beta)$ was in the range of that reported by Yagi and Kunii (1957).

DeWasch and Froment (1972) utilized a system similar to Coberly and Marshall, and Calderbank and Pogorski. D_t/d_p varied between

10.4 and 27.6. A "bump" in the temperature profile was obtained at approximately one particle diameter from the tube wall due to the range of D_t/d_p used.

The authors claimed that the graphical differentiations involved in the method of Coberly and Marshall could introduce scattering as high as 40%. For this reason, a scheme was utilized to minimize the sum of the squares of the difference between the predicted and observed temperatures along the exit cross section.

The procedure was as follows: k_e and h_w were estimated so that m (Table 2.3-4) could be obtained. The λ_n were then obtained from the transcendental eigenconditions and the predicted temperature ratio was computed. The first three terms in the series were used and convergence was rapid. The parameters k_e and h_w were then iterated to minimize the above error.

The correlations for k_e and h_w were both presented in a form which incorporated static contributions. The static contributions are presented for the different particles in Table 2.3-9. Figure 2.3-1 reproduces the radial exit profile for the 9.5 mm V_2O_5 pellets in the 157.5 mm diameter 1.345 m long tube. Good agreement between the predicted and measured values was obtained except for adjacent to the tube wall.

Specchia, Baldi, and Sicardi (1980) averaged the temperature profile presented by Coberly and Marshall over any given bed cross section and it was this equation that was matched to the experimental data. A minimization scheme similar to that used by DeWasch and

Froment (1972) was used to obtain the values of k_e and h_w. The first seven terms were necessary to obtain good convergence. The best fit of the radial temperature profile for a bed of 6 mm glass spheres is presented in Figure 2.3-2. The solid line predicted by the two-parameter method is seen to fit the data quite well. The broken line represents the best fit predicted for the one-parameter method. This line was predicted by DeWasch and Froment (1972) but was not discussed previously. As can be seen, the one-parameter method is less accurate.

An extensive analysis of the literature was used by the authors largely to modify theoretical treatment of k_e and develop theoretical treatment for h_w. Discussion of these will be delayed until the next chapter. Correlations for h_w^t were, however, given (Table 2.3-2). The flow regime was divided into two separate regions and correlations were presented for each. The modified Reynolds number was based upon d_o, the diameter of a sphere with the same external surface area as the actual particle.

Although many investigators have used the method of Coberly and Marshall, data reduction was very complicated. For this reason, three experiments were conducted where the temperature profile could be expressed in a much simpler fashion.

Yagi and Kunii (1960) criticized the correlations presented by Hanratty, and Yagi and Wakao for h_w as they predicted that $h_w = 0$ for no flow. Yagi and Kunii sought to correlate h_w in a form incorporating a stagnant contribution.

Yagi and Kunii claimed that these earlier studies revealed radial temperature distributions which approached that of the constant wall temperature. They thus designed an annular packed bed where the heat flowed purely radially. Since there was no variation in the temperature with axial position, the temperature profile was described by the simple composite wall conduction expressions.

The temperature difference at the outer wall was found to be too small to correlate h_w there. Only h_w at the inner wall was reported. The effective thermal conductivity was correlated according to Equation (2.3-2). Again, k_e^o/k_g was found to vary with k_p. The experimental values agreed closely with the theoretical predictions of Yagi and Kunii (1957) which will be discussed in Chapter 3. Table 2.3-10 lists the results of k_e^o/k_g and $(\alpha\beta)$ obtained for the different packing materials. The quantity $(\alpha\beta)$ was found to vary with $D_e = 2b$ as shown in Figure 2.3-3.

A static contribution to the wall heat transfer coefficient was found and a linear variation with the modified Reynolds number was obtained. $h_w^o d_p/k_g$ and α_w are reproduced in Table 2.3-11. Assuming there were no differences between annular and cylindrical packed beds, Yagi and Kunii (1960) successfully applied their correlation to the data of Felix, Plautz and Johnstone, and Yagi and Wakao. The values of $h_w d_p/k_g$ and α_w are also reported in Table 2.3-11. Yagi and Kuni attributed the different values of α_w to differences in the packing states of the two systems. The data of Coberly and

Marshall for cylindrical celite particles were found to have too much of a spread to be correlated easily by Yagi and Kunii's correlation.

Kunii and Suzuki (1966) studied a system similar to that used by Yagi and Kunii (1960). The effective thermal conductivity was correlated by Equation (2.3-2). $(\alpha\beta)$ was again a function of d_p/D_e but the values obtained were somewhat higher than was reported in Figure 2.3-3. Instead of presenting h_w, heat transfer near the wall was presented in terms of the effective thermal conductivity in the near wall region. This was defined in terms of the temperatures evaluated at $d_p/2$ from the wall, t', and extrapolated to the tube wall, t_R, which were used in forming the gradient. k_{ew} was correlated in an analogous fashion to k_e:

$$\frac{k_{ew}}{k_g} = \frac{k^0_{ew}}{k_g} + \alpha_v N_{Pr} N'_{Re} \qquad (2.3\text{-}5)$$

The values of k^0_e/k_g, $(\alpha\beta)$, k^0_{ew}/k_g, and α_v obtained from the experimental data are summarized in Table 2.3-12. Since the average wall heat flux could be written in terms of k_{ew} and $(t_w - t')$ or k_e and $(t_R - t')$, a relationship between h_w, k_e, and k_{ew} was obtained:

$$\frac{h_w d_p}{k_g} = 2\left[\frac{1}{(k_{ew}/k_g)} - \frac{1}{(k_e/k_g)}\right]^{-1} \qquad (2.3\text{-}6)$$

Kunii, Suzuki, and Ono (1968) continued with the above treatment in systems with high modified Reynolds numbers. This time a cylindrical packed bed was used.

Equation (2.3-5) for the effective conductivity in the wall region was found to be only approximate. It applied only to systems in which the modified Reynolds number was considerably less than 1000. Equation (2.3-6) was still found to be valid with the following change in the definition of k_{ew}:

$$\frac{k_{ew}}{k_g} = \frac{k^0_{ew}}{k_g} + \left[\frac{1}{\alpha_v N_{Pr} N'_{Re}} + \frac{1}{h^*_w d_p/2k_g}\right]^{-1} \qquad (2.3\text{-}7)$$

where:

$$\frac{h^*_w d_p}{k_g} = \frac{1}{2}(N_{Pr})^{1/3}(N'_{Re})^{3/4} \qquad (2.3\text{-}8)$$

Here, h^*_w was called "the heat transfer coefficient of the boundary layer on the wall." In calculating k_e and h_w, an analysis similar to that of Phillips, Leavitt, and Yoon was used. Again k_e correlated as Equation (2.3-2) where $k^0_e/k_g = 14.0$ and $(\alpha\beta) = 0.12$. The extrapolated value of k^0_{ew}/k_g was 8.0 as compared to a theoretical value of 9.0 calculated by the Yagi-Kunii model to be presented in Chapter 3. Since Equations (2.3-5) through (2.3-8) will be encountered again in the theoretical development of Chapter 3, they have been listed here.

2.4 Axial Effective Conductivity

The assumption that the effective thermal conductivity is identical in the axial and radial directions is seldom found to be in serious error. In certain cases, however, some authors have found it necessary to divide k_e into two components. The first is the usual radial effective thermal conductivity, k_{er}. The second is the axial effective thermal conductivity, k_{ez}. Since axial conduction is often neglected, few authors have expressed any interest in k_{ez}. Those few papers dealing with k_{ez} which can be found wi'l briefly be discussed here.

In the case of the three-parameter model, axial conduction is not neglected. The defining differential equation is thus:

$$k_{er}\left(\frac{1}{r}\frac{\partial t}{\partial r} + \frac{\partial^2 t}{\partial r^2}\right) + k_{ez}\frac{\partial^2 t}{\partial z^2} = G_o c_p \frac{\partial t}{\partial z} \qquad (2.4\text{-}1)$$

The variables studied and correlations presented are listed in Tables 2.4-1 and 2.4-2, respectively.

Yagi, Kunii, and Wakao (1960) studied a packed bed which had no radial temperature gradients. Since the axial temperature gradients became quite steep for high air flow rates, the experiments were restricted to lower flow. With the above simplifications, Equation (2.4-1) was easily integrated. Straight lines were then obtained from semilogarithmic plots of the temperature difference, $(t - t_o)$, versus bed depth. Comparison of these profiles and the data yielded k_{ez}.

The axial effective conductivity was correlated in a form analogous to that for the radial effective thermal conductivity which was presented in Equation (2.3-2):

$$\frac{k_{ez}}{k_g} = \frac{k^o_{ez}}{k_g} + \delta' N_{Pr} N_{Re} \qquad (2.4\text{-}2)$$

The stagnant axial conductivity k^o_{ez} was obtained by extrapolation to zero flow rate. The values obtained for k^o_{ez}/k_g and δ' are reported in Table 2.4-3.

The stagnant contribution, k^o_{ez}/k_g, was compared to the theoretical prediction of the stagnant radial effective conductivity presented by Yagi and Kunii. These values are also given in Table 2.4-3. Agreement was found to be quite good; the authors found this to be quite natural "because the random bed of solids is homogeneous in all directions for heat transfer when no fluid is flowing."

The value of $(\alpha\beta)$ for the radial effective conductivity was previously found to be on the order of 0.1 to 0.3. δ' was found to be 0.7 to 0.8. Thus at zero flow, $k_{er} = k_{ez}$, and k_{ez} increased somewhat more than k_{er} with increasing flow.

Some authors have assumed that $k_{ez} = k_{er}$ in calculations to verify that axial conduction was negligible in comparison to bulk flow. These results tended to show that this assumption was valid. Furthermore, at low gas flow rates when axial conduction cannot be neglected, systems can be analyzed by a method where $k_{ez} = k_{er} = k_e$.

Kunii and Smith (1961) eliminated radial conduction in their packed bed in a much more elaborate method. The temperature was found to be constant across the exit cross section. A slightly different temperature profile was presented and k_{ez} was obtained by comparison to the experimental data. Typical results for the air runs are reproduced in Figure 2.4-1. Similar results were obtained for the CO_2 and He gases studied.

Bischoff (1962) estimated the values of k_{ez} at higher flow rates than had been previously presented based upon existing data for k_{er} and theoretical grounds. He compared the second moments of the pseudohomogeneous temperature profile based upon a flat and generalized velocity profile, respectively, to obtain a theoretical form of k_{ez}/k_g as related to k_{er}/k_g. Bischoff's correlation incorporated a term that accounted for radial variations of the velocity profile in k_{er}. Bischoff claimed his correlation showed that no simple linear dependence on N'_{Re} could occur for k_{ez} except at high flow rates. He also compared the data of Yagi, Kunii, and Wakao (1960) and obtained fair agreement.

Votruba, Hlavacek, and Marek (1972) studied a packed bed incorporating the experimental method of Yagi, Kunii, and Wakao (1960). Their aim was to extend values of k_{ez} obtained to a much higher range of the modified Reynolds number. A nonlinear regression scheme was used to match the obtained temperature profiles to a theoretical temperature profile and thus to obtain k_{ez}.

In obtaining correlations, an equivalent diameter was defined as:

$$D_o = \frac{(4/6)D_t\epsilon}{(1-\epsilon)(D_t/d_p) + 1} \qquad (2.4\text{-}3)$$

The values of k^o_{ez}/k_g and c_3 obtained are presented in Table 2.4-4.

Gunn and Khalid (1975) presented an elaborate mathematical treatment of the pseudohomogeneous problem incorporating three parameters. A solution similar to that presented by Coberly and Marshall for the two-parameter method was presented. A minimization technique similar to that used by DeWasch and Froment was used in obtaining the values of k_{er}, k_{ez}, and h_w. Results for the modified Reynolds number in excess of 40 were then compared to the literature. k_{er} obtained in this fashion were in good agreement with previous authors. The wall coefficient was also found to be in agreement with some of the literature. Disagreement with the balance was probably not due to the different method used (i.e. three parameters instead of two), but due to disagreement in the literature to date among those utilizing the two-parameter method.

Specchia, Baldi, and Sicardi (1980) quoted the work of Dixon, Cresswell, and Paterson (1978) on axial effective conductivity. These authors found that accounting for a separate k_{ez} independent of k_{er} was only important for shallow beds and at low fluid velocity. When studying beds of ceramic beads and steel spheres with D_t/d_p between 5.6 and 11.2, L/d_p greater than 10 or 15, and N'_{Re} between 70 and 380, the temperature profiles calculated with the two- and three-parameter methods were found to be nearly identical.

Table 2.1-1 Parameters Involved in Experiments to Determine the Overall Heat Transfer Coefficient, h_o

Investigator	L(m)	D_t (mm)	Particle Characteristics			Gases Used
			Size (mm)	Material	Shape	
Colburn (1931)	0.457	34.9	4.76	(2 types)	pellets	air
			9.53		pellets	
	1.16	78.7	3.18		granules	
			6.35		granules	
			14.3		pebbles	
			22.9	porcelain	balls	
			25.4	zinc	balls	
Leva (1947)	0.914	12.7	3.20	glass beads	sphere	air
			3.31	glass beads	sphere	
		50.8	3.61	glass beads	sphere	CO_2
			4.37	glass beads	sphere	
			5.79	glass beads	sphere	N_2
			9.86	glass beads	sphere	
			8.84	clay	sphere	
			12.9	porcelain	sphere	
Leva and Grummer (1948)	0.356	20.9	4.29	glass	smooth sphere	air
			7.54	glass	smooth sphere	
	0.914	52.5	7.98	glass	smooth sphere	
			9.98	glass	smooth sphere	
			10.2x	tungsten	smooth	
			8.1	sulfate	cylinder	
			3.2x	cobalt oxide	smooth	
			6.4		cylinder	
			4.8x	cobalt oxide	smooth	
			5.6		cylinder	
			6.4	clay	smooth Raschig ring	
			9.5	clay	smooth Raschig ring	
			2.3	lead shot	smooth sphere	
			15.1	cast iron	smooth sphere	
			25.4	zinc		
			6.4x	aluminum	smooth	
			6.4		cylinder	

Table 2.1-1 (Continued)

Investigator	L(m)	D_t (mm)	Particle Characteristics			Gases Used
			Size (mm)	Material	Shape	
			6.4x 6.4	copper	smooth cylinder	
			3.8x5	alundum	rough cylinder	
			4.0	aloxite	irregular sharp	
			4.3	aloxite	irregular sharp	
Leva, Weintraub, Grummer, and Clark (1948)	0.232	20.9	3.3	glass beads	sphere	air
			4.3	glass beads	sphere	
	0.308	52.5	5.2	glass beads	sphere	CO_2
			5.7	glass beads	sphere	
	0.356		5.8	glass beads	sphere	
			9.9	glass beads	sphere	
	0.914		12.9	porcelain	sphere	
Leva (1950)		15.8	4.4	glass beads		air
			5.2	glass beads		
		20.9	5.8	glass beads		
			7.6	glass beads		
		52.5	9.4	glass beads		
			10.0	glass beads		
			10.4	glass beads		
			12.7	porcelain	sphere	
			18.6	porcelain	sphere	
			9.5	porcelain	Raschig ring	
			7.7	clay	sphere	
			8.3	clay	sphere	
			8.9	clay	sphere	
			7.0	copper	cylinder	
			9.5	brass	ring	
Campbell and Huntington (1952)		51	4.9	silica-alumina	cylinder	natural gas
		102	8.0	hydrated alumina	cylinder	
		152	7.2	tabular alumina	sphere	

Table 2.1-1 (Continued)

Investigator	L(m)	D_t (mm)	Particle Characteristics			Gases Used
			Size (mm)	Material	Shape	
			8.3	aluminum	cylinder	
			11.2	tabular alumina	sphere	
			16.3	aluminum	cylinder	
			19.0	glass	sphere	
			25.4	glass	sphere	
Chu and Storrow (1952)	0.305	25.4	3.7	"SOVA" catalyst	sphere	air
	0.610		0.99	glass beads	sphere	
			4.9	glass beads	sphere	
	0.762		1.1	lead shot	sphere	
			2.4	lead shot	sphere	
	0.914		3.2	lead shot	sphere	
			4.6	lead shot	sphere	
	1.07		6.5	lead shot	sphere	
			6.4	steel balls	sphere	
	1.22					
Gelperin and Kagan (1966)		12	1.8	lead balls		air
			2.5	lead balls		
			4.2	lead balls		H_2
			5.2	lead balls		
			2.6	steel balls		CO_2
			5.1	steel balls		
			5.4	iron balls	rough surface	75% H_2
			1.5	silica gel balls		25% N_2
			2.5	silica gel balls		90% H_2 10% N_2
			1.5	silica gel balls	irregular shape	
			2.5	silica gel balls	irregular shape	
			5.9	silica gel balls	irregular shape	
			5x5x1	copper	Raschig ring	
			5x5x1	glass	Raschig ring	

Table 2.1-1 (Continued)

Investigator	L(m)	D_t (mm)	Particle Characteristics			Gases Used
			Size (mm)	Material	Shape	
			2.5	ammonia synthesis	irregular shape	
			---	alumina gel	cylinder	
			50% 1.8 50% 2.5	lead balls	mixture	
			50% 1.8 50% 4.2	lead balls	mixture	
			50% 1.8 50% 5.2	lead balls	mixture	

Table 2.1-2 Range of Validity and Specific Correlations Proposed for the Overall Heat Transfer Coefficient, h_o

---

Colburn (1931) $\qquad 200 \leq \frac{d_p G_o}{\mu_g} \leq 15{,}000$

$$h_o = 240\, a \left(G_o[m^2 s/kg] \right)^{0.83}$$

Leva (1947) $\qquad 100 \leq \frac{d_p G_o}{\mu_g} \leq 4000$

$$\frac{h_o D_t}{k_g} = 0.813 \exp(-6 d_p/D_t) \left(\frac{d_p G_o}{\mu_g} \right)^{0.90} \quad ; \quad d_p/D_t < 0.35$$

Leva and Grummer (1948) $\qquad 100 \leq \frac{d_p G_o}{\mu_g} \leq 10{,}000$

$$\frac{h_o D_t}{k_g} = 0.813\, f_1 \exp(-6 d_p/D_t) \left(\frac{d_p G_o}{\mu_g} \right)^{0.9}$$

Leva, Weintraub, Grummer, and Clark (1948) $\qquad 250 \leq \frac{d_p G_o}{\mu_g} \leq 3000$

$$\frac{h_o D_t}{k_g} = 3.50 \exp(-4.6 d_p/D_t) \left(\frac{d_p G_o}{\mu_g} \right)^{0.7}$$

Table 2.1-2 (Continued)

Leva (1950) $\qquad 800 \leq \frac{d_p G_o}{\mu_g} \leq 13{,}000$

$$\frac{h_o d_p}{k_g} = 0.125\left(\frac{d_p G_o}{\mu_g}\right)^{0.75}\left(\frac{D_t}{d_p}\right)^{1.0} \quad ; \quad 0.35 \leq d_p/D_t \leq 0.60$$

$$\frac{h_o D_t}{k_g} = 0.120\left(\frac{d_p G_o}{\mu_g}\right)^{0.75}\left(\frac{D_t}{d_p}\right)^{1.05} \quad ; \quad d_p/D_t > 0.60$$

Campbell and Huntington (1952) $\qquad 15 \leq \frac{G_o}{\mu_g S} \leq 1000$

$$\frac{h_o}{c_p G_o} = 0.76\exp(-0.0225 S D_t)\left(\frac{G_o}{\mu_g S}\right)^{-0.42}$$

Chu and Storrow (1952)

$$\frac{h_o D_t}{k_g} = 0.134\left(\frac{d_p}{D_t}\right)^{-1.13}\left(\frac{L}{D_t}\right)^{-0.9}\left(\frac{d_p G_o}{\mu_g}\right)^{1.17} \quad ; \quad \frac{D_t G_o}{\mu_g} \leq 1600$$

$$\frac{h_o D_t}{k_g} = 15\left(\frac{L}{D_t}\right)^{-1.82}\left(\frac{d_p}{D_t}\right)^{-0.90}\left(\frac{d_p G_o}{\mu_g}\right)^{m'}$$

where: $m' = 0.55\left(\frac{L}{D_t}\right)^{0.165} \quad ; \quad 1600 \leq \frac{d_t G_o}{\mu_g} \leq 3500$

Table 2.1-2 (Continued)

Gelperin and Kagan (1966)

$$\frac{h_o D_t}{k_g} = 0.001 \left(\frac{d_p G_o}{\mu_g}\right)^{1.5} \left(\frac{D_t}{d_p}\right)^{1.4} ; \quad \frac{d_p G_o}{\mu_g} < 40$$

$$\frac{h_o D_t}{k_g} = 0.004 \left(\frac{d_p G_o}{\mu_g}\right)^{1.21} \left(\frac{D_t}{d_p}\right)^{1.24} ; \quad 40 \leq \frac{d_p G_o}{\mu_g} \leq 1200$$

$$\frac{h_o D_t}{k_g} = 0.048 \left(\frac{d_p G_o}{\mu_g}\right)^{0.9} \left(\frac{D_t}{d_p}\right)^{1.0} ; \quad \frac{d_p G_o}{\mu_g} > 1200$$

$$\frac{h_o d_e}{k_g} = 0.00118 \left(\frac{d_e G_o}{\mu_g}\right)^{1.5} \left(\frac{c_p \mu_g}{k_g}\right)^{0.68} \left(\frac{\mu_g}{\mu_w}\right)^{0.7} \left(\frac{k_g}{k_w}\right)^{0.65} ;$$

$$\frac{d_e G_o}{\mu_g} < 42$$

$$\frac{h_o d_e}{k_g} = 0.00355 \left(\frac{d_e G_o}{\mu_g}\right)^{1.21} \left(\frac{c_p \mu_g}{k_g}\right)^{0.68} \left(\frac{\mu_g}{\mu_w}\right)^{0.7} \left(\frac{k_g}{k_w}\right)^{0.65} ;$$

$$42 \leq \frac{d_e G_o}{\mu_g} \leq 1200$$

$$\frac{h_o d_e}{k_g} = 0.0295 \left(\frac{d_e G_o}{\mu_g}\right)^{0.9} \left(\frac{c_p \mu_g}{k_g}\right)^{0.68} \left(\frac{\mu_g}{\mu_w}\right)^{0.7} \left(\frac{k_g}{k_w}\right)^{0.65} ; \quad \frac{d_e G_o}{\mu_g} > 1200$$

Table 2.2-1 Parameters Involved in Experiments to Determine the Overall Effective Thermal Conductivity, k_o

Investigator	L(m)	D_t (mm)	Particle Characteristics			Gases Used
			Size (mm)	Material	Shape	
Hall and Smith (1949)		51	3.2	alumina	clyinder	air
Bunnell, Irvin, Olson, and Smith (1949)		51	3.2	alumina	cylinde·	air
Irvin, Olson, and Smith (1951)		51	3.2	alumina	cylinder	air
Verschoor and Schuit (1951)	0.21-0.30	29-50	3-10	pumice terrana glass steel lead		air H_2
Hougen and Piret (1951)	0.16-0.32	35-95	9.8x 12.3	celite	cylinder	air
			9.7x 8.6	celite	cylinder	
			6.5x 7.1	celite	cylinder	
			15.8x 4.3	celite	cylinder	
			3.1x 3.1	celite	cylinder	
			2.3	celite	sphere	
			3.1	celite	sphere	
Molino and Hougen (1952)	0.160	34.8	3.7x 3.3	celite	pellet	air
	0.164	95.3	4.5x 4.5	celite	pellet	

Table 2.2-1 (Continued)

Investigator	L(m)	D_t (mm)	Particle Characteristics			Gases Used
			Size (mm)	Material	Shape	
	0.30		6.8x 6.4	celite	pellet	
			9.8x 12.3	celite	pellet	
Schuler, Stallings, and Smith (1952)	0-0.152	51	3.2		cylinder	air
			4.8		cylinder	
			6.4		cylinder	
Kwong and Smith (1957)		51	4.0	steel	sphere	air
		102	6.4	steel	sphere	
			6.4	alumina	sphere	ammonia
			9.5	alumina	sphere	
Schertz and Bischoff (1969)		102	7.6	stoneware	sphere	air

Table 2.2-2 Range of Validity and Specific Correlations Proposed for Constant Overall Effective Thermal Conductivity, k_o, Assuming Constant Superficial Gas Velocity

---

Verschoor and Schuit (1951) $\quad 7 \leq \frac{G_o}{\mu_g S} \leq 1000$

$$\frac{k_o}{k_g} = 1.72 \left(\frac{k_p}{k_g}\right)^{0.26} + 0.10 \left(SO_t\right)^{0.50} \left(\frac{G_o}{\mu_g S}\right)^{0.69}$$

Hougen and Piret (1951) $\quad 100 \leq \frac{\sqrt{S_p} G_o}{\mu_g} \leq 400$

$$\frac{k_o}{k_g} = \frac{2.74}{\epsilon} \left(\frac{\sqrt{S_p} G_o}{\mu_g}\right)^{1/3}$$

Molino and Hougen (1952) $\quad 50 \leq \frac{\sqrt{S_p} G_o}{\mu_g} \leq 4000$

$$\frac{k_o}{k_g} = \frac{1.23}{\epsilon} \left(\frac{\sqrt{S_p} G_o}{\mu_g}\right)^{0.43}$$

Table 2.2-3 Range of Validity and Specific Correlations Proposed for Radially Varying Overall Effective Thermal Conductivity, k_o

Bunnell, Irvin, Olson and Sm'	(1949)	$30 \leq \frac{d_p G_o}{\mu_g} \leq 100$

$$\frac{k_o}{k_g} = 5.0 + 0.061 \frac{d_p G_o}{\mu_g}$$

Irvin, Olson and Smith	(1951)	$30 \leq \frac{d_p G_o}{\mu_g} \leq 100$

$$\frac{k_o}{c_p G} = a_1 \left(\frac{d_p G_o}{\mu_g} \right)^{-0.51}$$

Table 2.2-4 Pointwise Values of k_0 and k_0 Averaged Over Bed Depth Obtained by Hall and Smith (1949)

Radial Position (r/R)	Bed Depth (mm)	k_0 (W/mK)	k_0, ave (W/mK)
0.2	1.27	16.7	0.20
	43.4	126	
	85.3	126	
	133.8	109	
	195.6	54.5	
0.4	1.27	37.7	0.29
	43.4	163	
	85.3	167	
	133.8	142	
	195.6	105	
0.6	1.27	29.3	0.24
	43.4	---	
	85.3	192	
	133.8	109	
	195.6	66.9	
0.8	1.27	12.6	0.17
	43.4	29.3	
	85.3	105	
	133.8	163	
	195.6	46.0	

Table 2.2-5 Correlation of the Velocity Profile in a Packed Bed as Presented by Schwartz and Smith (1953)

$$\frac{\ln\left(\frac{u}{V}\right) + \left[\left(\frac{u}{V}\right)^2 - \left(\frac{u_0}{V}\right)^2\right]^{.2}}{\frac{u_0}{V}} = k' \left(\frac{r}{R}\right)^{1.5}$$

where:

$$k' = \frac{2}{3}\left(\frac{D_t}{d_p}\right)^{1.5}\left(\frac{0.0012\, d_p \Delta p \gamma}{\rho_g V^2}\right)^{0.5}$$

and:

$$\gamma = \left(\frac{\epsilon}{\epsilon_0}\right)^3 \frac{(1-\epsilon_0)}{(1-\epsilon)}$$

Table 2.2-6 Equations Used by Various Authors to Obtain k_o Accounting for Radial Variation of G

Schuler, Stallings, and Smith (1952)

$$\frac{dk_o}{dr} = f_1(r)k_o + f_2(r)$$

where:

$$f_1(r) = -\left(\frac{\partial^2 t}{\partial r^2} + \frac{1}{r}\frac{\partial t}{\partial r}\right)\Big/\frac{\partial t}{\partial r}$$

and:

$$f_2(r) = c_p G \left(\frac{\partial t}{\partial z}\right)\Big/\frac{\partial t}{\partial r}$$

Kwong and Smith (1957)

$$\lambda_1 = -\frac{1}{L}\ln\left(\frac{\int_o^R T_o T_L c_p G r\, dr}{\int_o^R T_L T_L c_p G r\, dr}\right)$$

$$k_o = -\lambda_1 \left(\int_o^r c_p G r T_L\, dr\right)/\left(r\frac{\partial T}{\partial r}\right)_L$$

Table 2.2-6 (Continued)

Schertz and Bischoff (1969)

$$k_o = \left(\int_0^r c_p G r \frac{\partial T}{\partial z} \, dr \right) / \left(r \frac{\partial T}{\partial r} \right)$$

$$\frac{k_o}{k_g} = \frac{k_o^0}{k_g} + c_2 \frac{d_p G}{\mu_g} \frac{c_p \mu_g}{k_g}$$

Table 2.3-1 Parameters Involved in Experiments to Determine the Effective Conductivity, k_e, and the Wall Coefficient, h_w

Investigator	L(m)	D_t (mm)	Particle Characteristics			Gases Used
			Size (mm)	Material	Shape	
Coberly and Marshall (1951)		127	3.2x 3.2	celite	cylinder	air
			6.4x 6.4	celite	cylinder	
			9.5x 12.7	celite	cylinder	
Hanratty (1954)		76	3.2x 3.2	celite	cylinder	air
		127	6.4x 6.4	celite	cylinder	
		203	9.5x 12.7	celite	clyinder	
			3.2	celite	sphere	
			6.4	celite	sphere	
			12.7	glass	sphere	
			19.1	glass	sphere	
Plautz and Johnstone (1955)		203	12.7	glass	sphere	air
			19.1	glass	sphere	
Quinton and Storrow (1956)	0.75	41	4.4	glass	sphere	air
Calderbank and Pogorski (1957)	0-1.8 (various)	51-127 (various)	3.2	celite	cylinder	air
			6.4	celite	cylinder	
			6.4	alundum	sphere	
			12.7	alundum	sphere	
Yagi and Wakao (1959)	0.2	36	0.764	glass	sphere	air
	0.36		0.909	glass	sphere	
			2.60	glass	sphere	
			6.00	glass	sphere	

Table 2.3-1 (Continued)

Investigator	L(m)	D_t (mm)	Particle Characteristics			Gases Used
			Size (mm)	Material	Shape	
			1.28	cement clinker	granular	
			1.81	cement clinker	granular	
			1.97	cement clinker	granular	
			2.57	cement clinker	granular	
			4.31	cement clinker	granular	
			0.764	lead shot	sphere	
			1.08	lead shot	sphere	
			1.50	lead shot	sphere	
			3.10	steel balls	sphere	
Yagi and Kunii (1960)		22x7 (annular)	0.57	glass	sphere	air
			0.94	glass	sphere	
			2.75	glass	sphere	
			5.1	glass	sphere	
			12.3	glass	sphere	
			3.0	lead shot	sphere	
			11.2	steel balls	sphere	
Phillips, Leavitt, and Yoon (1960)		102 203	3.0x 4.4	Linde molecular sieve	pellets	air H_2 propane methane Ar He
Yagi, Kunii, and Wakao (1961)		60	1.09	glass beads		air
			2.6	glass beads		
			6.3	glass beads		

Table 2.3-I (Continued)

Investigator	L(m)	D_t (mm)	Particle Characteristics			Gases Used
			Size (mm)	Material	Shape	
			12.4	glass beads		
Kunii and Suzuki (1966)		76x140 (annular)	1.20	glass	sphere	air
			3.72	glass	sphere	
			6.43	glass	sphere	
			8.70	glass	sphere	
			12.2	glass	sphere	
			6.40	glass	sphere	
Kunii, Suzuki, and Ono (1968)		140	28	celite	sphere	air
			42	celite	sphere	
Agnew and Potter (1970)		18.5	1.6x 3.2	carbon	cylinder	N_2
			1.6x 3.2	stainless steel	cylinder	C_2H_2
			1.6x 1.6	steel	cylinder	Ar
			20ga. x20ga.	steel	cylinder	
			23ga. x23ga.	steel	cylinder	
			3.0	glass	sphere	
			4.2	glass	sphere	
			0.7	glass	sphere	
			1.9	thermofor catalyst	sphere	
DeWasch and Froment (1972)	0.2-1.4 (various)	99	5.6	Fe_3O_4	pellets	air
			5.9	V_2O_5	pellets	
		157.5	5.7	V_2O_5	pellets	
Specchia, Baldi, and Sicardi (1980)	0.35	141	6	glass	sphere	air
			12.9	porcelain	sphere	
			6	porcelain	Raschig ring	

Table 2.3-2 Range of Validity and Specific Correlations Proposed for the Effective Thermal Conductivity, k_e, and the Wall Heat Transfer Coefficient, h_w

---

Quinton and Storrow (1956) $\quad 30 \leq \frac{d_p G_o}{\mu_g} \leq 1100$

$$k_e = \left(0.0415 + 0.00019 \frac{d_p G_o}{\mu_g}\right) \text{ W/mK}$$

$$h_w = 167.5 G_o \text{ Ws/kgK}$$

Hanratty (1954) $\quad 80 \leq \frac{d_p G_o}{\epsilon \mu_g} \leq 500$

$$\frac{h_w d_p}{k_g} = 0.12 \left(\frac{d_p G_o}{\epsilon \mu_g}\right)^{0.77} \quad \text{(spheres)}$$

$$\frac{h_w d_p}{k_g} = c_1 \left(\frac{d_p G_o}{\epsilon \mu_g}\right)^{0.5} \quad \text{(cylinders)}$$

Plautz and Johnstone (1955) $\quad 90 \leq \frac{d_p G_o}{\mu_g} \leq 2000$

$$k_e = \left(0.76 + 0.00223 \frac{d_p G_o}{\mu_g}\right) \text{ W/mK}$$

$$h_w = (72.2 \text{ W/m}^2\text{K}) \left(G_o \left[\text{m}^2\text{s/kg}\right]\right)^{0.75}$$

Table 2.3-2 (Continued)

Coberly and Marshall (1951) $\quad 50 \leq \dfrac{G_o\sqrt{S_p}}{\mu_g} \leq 2000$

$$k_e = \left(0.31 + 0.017\ \frac{G_o\sqrt{S_p}}{\mu_g}\right)\ \text{W/mK}$$

$$h_w = (148\ \text{W/m}^2\text{K})\left(G_o\left[\text{m}^2\text{s/kg}\right]\right)^{0.33}$$

Campbell and Huntington (1952) $\quad 40 \leq \dfrac{G_o}{\mu_g S} \leq 500$

$$k_e/k_g = 10.0 + 0.267\ (G_o/\mu_g S)$$

$$h_w = 2.38\ (G_o/\mu_g S)^{0.47}\ \text{W/m}^2\text{K}$$

Calderbank and Pogorski (1957)

$$k_e = \left(0.35 + 0.0016\ \frac{\sqrt{S_p}G_o}{\mu_g}\right)\ \text{W/mK};\quad 100 \leq \frac{\sqrt{S_p}G_o}{\mu_g} \leq 2000$$

$$\frac{h_w d_p}{k_g} = 3.6\left(\frac{d_p G_o}{\epsilon\mu_g}\right)^{0.365};\quad 100 \leq \frac{d_p G_o}{\epsilon\mu_g} \leq 10{,}000$$

Table 2.3-2 (Continued)

Yagi and Wakao (1959) $20 \leq \frac{d_p G_o}{\mu_g} \leq 800$

$$\frac{k_e}{k_g} = \frac{k_e^o}{k_g} + (\alpha\beta) \frac{c_p \mu_g}{k_g} \frac{d_p G_o}{\mu_g}$$

$$\frac{h_w d_p}{k_g} = 0.18 \left(\frac{d_p G_o}{\mu_g}\right)^{0.80}$$

Phillips, Leavitt, and Yoon (1960) $15 \leq \frac{d_p G_o}{\mu_g} \leq 200$

$$k_e = 0.14 \text{ W/mK} + 0.65\, k_g + \frac{d_p G_o c_p}{9.1}$$

DeWasch and Froment (1972) $100 \leq \frac{D_t G_o}{\mu_g} \leq 400$

$$k_e = k_e^o + \left(\frac{0.0029 \text{ W/mK}}{1 + 46(d_p/D_t)^2}\right) N_{Re}$$

$$h_w = h_w^o + (0.0177 \text{ W/m}^2\text{K}) \frac{D_t}{d_p} N_{Re}$$

Table 2.3-2 (Continued)

Specchia, Baldi, and Sicardi (1980)

$$\frac{h_w^t d_o}{k_g} = 0.0835 \left(\frac{d_o G_o}{\mu_g}\right)^{0.91} ; \qquad 10 \leq \frac{d_o G_o}{\mu_g} \leq 1200$$

$$\frac{h_w^t d_o}{k_g} = 1.23 \left(\frac{d_o G_o}{\mu_g}\right)^{0.53} ; \qquad 1200 \leq \frac{d_o G_o}{\mu_g} \leq 10{,}000$$

Yagi and Kunii (1960) $\qquad \frac{d_p G_o}{\mu_g} \leq 2000$

$$\frac{h_w d_p}{k_g} = \frac{h_w^o d_p}{k_g} + \alpha_w N_{Pr} N_{Re}'$$

Kunii and Suzuki (1966) $\qquad \frac{d_p G_o}{\mu_g} \leq 1000$

$$\frac{k_{ew}}{k_g} = \frac{k_{ew}^o}{k_g} + \alpha_v N_{Pr} N_{Re}'$$

Table 2.3-2 (Continued)

Kunii, Suzuki, and Ono (1968) $\quad 300 \leq \frac{d_p G_o}{\mu_g} \leq 8000$

$$\frac{k_{ew}}{k_g} = \frac{k^o_{ew}}{k_g} = \left(\frac{1}{\alpha_v N_{Pr} N'_{Re}} + \frac{1}{h^*_w d_p / 2k_g} \right)^{-1}$$

$$\frac{h^*_w d_p}{k_g} = c(N_{Pr})^{1/3} (N'_{Re})^{3/4}$$

Table 2.3-3 The Constant c_1 as Applied to the Data of Felix (1951)

Particle Size (mm)	D_t (mm)	c_1
3.2 x 3.2	127	0.95
6.4 x 6.4	127	1.33
9.5 x 12.7	127	1.44
6.4 x 6.4	76	0.95
9.5 x 12.7	76	0.95

Table 2.3-4 The Analytical Solution of Coberly and Marshall (1951)

Boundary Conditions:

$$@\ z = 0,\ t = t_o$$

$$@\ r = 0,\ \partial t/\partial r = 0$$

$$@\ r = R,\ -k_e(\partial t/\partial r) = h_w(t_w - t_R)$$

Solution:

$$\frac{t_w - t}{t_w - t_o} = 2\sum_n \frac{J_o(\lambda_n \xi)\ \exp(-\beta_1 \lambda_n^2 z)}{\lambda_n \left[(\lambda_n m)^2 + 1\right] J_1(\lambda_n)}$$

Eigencondition:

$$\frac{J_o(\lambda_n)}{J_1(\lambda_n)} = \lambda_n m$$

where:

$$\xi = r/R$$

$$\beta_1 = k_e/G_o c_p R^2$$

$$m = k_e/h_w R$$

Table 2.3-5 k_e^o/k_g and $(\alpha\beta)$ Obtained by Yagi and Wakao (1959)

Material	d_p/D_t	k_e^o/k_g	$(\alpha\beta)$
Cement clinker	0.021-0.072	6.0	0.11
Cement clinker	0.12-0.17	6.0	0.09
Metal spheres	0.021-0.086	13	0.11

Table 2.3-6 The Transient Analytical Solution of Phillips, Leavitt, and Yoon (1960)

Differential Equation:

$$k_e^0 \left(\frac{1}{r} \frac{\partial t}{\partial r} + \frac{\partial^2 t}{\partial r^2} \right) = \rho_g c_p \frac{\partial t}{\partial \theta}$$

Initial Condition:

@ $\theta = 0$, $t = t_0$ for all points in the bed

Solution:

$$\frac{t_w - t}{t_w - t_c} = 2 \sum_n \frac{J_0(\lambda_n \xi) \exp(-\beta' \lambda_n^2 \theta)}{\lambda_n \left[(\lambda_n m)^2 + 1 \right] J_1(\lambda_n)}$$

where:

$$\beta' = \frac{k_e^0}{\rho_g c_p R^2}$$

Table 2.3-7 k_e^o/k_g and $(\alpha\beta)$ Obtained by Yagi, Kunii and Wakao (1961)

d_p/D_t	k_e^o/k_g	$(\alpha\beta)$
0.043	8.0	0.11
0.10	8.0	0.084
0.207	8.0	0.061

Table 2.3-8 k_e^0/k_g and $(\alpha\beta)$ Obtained by Agnew and Potter (1970)

Material	d_p (mm)	k_e^0/k_g	$(\alpha\beta)$
Carbon cylinders	1.6 x 3.2	5	0.16
Stainless steel cylinders	1.6 x 3.2	16	0.23
Steel cylinders	1.6 x 1.6	15	0.19
Steel cylinders	20 ga. x 20 ga.	14	0.15
Steel cylinders	23 ga. x 23 ga.	13	0.14
Glass spheres	3.0	5	0.17
Glass spheres	4.2	5.5	0.15
Glass spheres	0.7	6	0.10
Thermofor catalyst spheres	1.9	5	0.14

Table 2.3-9 k_e^o and h_w^o Obtained by DeWasch and Froment (1972)

Material	d_p/D_t	k_e^o(W/mK)	h_w^o(W/m^{2}K)
V_2O_5	0.037	0.205	19.8
V_2O_5	0.060	0.279	59.4
V_2O_5	0.036	0.280	18.9
V_2O_5	0.058	0.261	81.5
Fe_3O_4	0.060	0.419	36.1
Fe_3O_4	0.096	0.407	98.9

Table 2.3-10 k_e^0/k_g and $(\alpha\beta)$ Obtained by Yagi and Kunii (1960)

Material	d_p (mm)	$d_p G_0/\mu_g$	k_e^0/k_g	$(\alpha\beta)$
Glass beads	0.57	0-80	8.5	0.061
Glass beads	0.94	0-80	8.5	0.061
Glass beads	2.75	0-400	9	0.054
Glass beads	5.1	0-400	9	0.054
Lead shot	3.0	0-400	20	0.054
Glass balls	12.3	0-800	9	0.038
Steel balls	11.2	0-800	18	0.038

Table 2.3-11(a) $h_w^o d_p/k_g$ and α_w Obtained by Yagi and Kunii (1960)

Material	d_p/D_e	$d_p G_o/\mu_g$	$h_w^o d_p/k_g$	α_w
Glass beads	0.0119	0-80	3.2	0.041
Glass beads	0.0196	0-80	3.2	0.041
Glass beads	0.0572	0-400	7	0.041
Glass beads	0.106	0-400	12	0.041
Lead shot	0.0625	0-400	12	0.041
Glass balls	0.256	0-800	19	0.041
Steel balls	0.233	0-800	25	0.041

Table 2.3-11(b) $h_w^o d_p/k_g$ and α_w for the Data of Felix, Plautz and Johnstone, Yagi and Wakao

Glass beads, cement clinker	0.021-0.036	0-100	1.2	0.054
Celite balls, glass beads, cement clinker	0.0417-0.0722	0-1000	3 6.5	0.054
Celite balls, glass beads, cement clinker	0.0833-0.167	0-2000	5 8	0.054
Lead shot, steel balls	0.021-0.042	0-800	3	0.054

Table 2.3-12 k_e^o/k_g, $(\alpha\beta)$, k_{ew}^o/k_g, and α_v Obtained by Kunii and Suzuki (1966)

Material	d_p/D_e	k_e^o/k_g	$(\alpha\beta)$	k_{ew}^o/k_g	α_v
Glass spheres	0.019	8.0	0.13	3.5	0.025
Glass spheres	0.057	7.0	0.10	3.0	0.025
Glass spheres	0.10	8.5	0.090	5.5	0.023
Glass spheres	0.14	12.0	0.092	5.5	0.023
Glass spheres	0.19	9.5	0.090	6.0	0.019
Steel spheres	0.10	21	0.095	10	0.020
Glass spheres	0.097	7.0	0.010	3.0	0.025

Table 2.4-1 Parameters Involved in Experiments to Determine the Axial Effective Thermal Conductivity, k_{ez}

Investigator	L(m)	D_t (mm)	Particle Characteristics			Gases Used
			Size (mm)	Material	Shape	
Yagi, Kunii, and Wakao (1960)		50	0.91	glass beads		air
			2.6	glass beads		
		68	6.0	glass beads		
			1.5	lead shot		
			3.0	steel balls		
			4.8	steel balls		
			1.3	limestone pieces	broken	
			2.0	linestone pieces	broken	
			3.4	limestone pieces	broken	
			4x4x1	porcelain	Raschig ring	
			9x9x 1.3	porcelain	Raschig ring	
Kunii and Smith (1961)		25.4	0.11	glass beads		air
			0.37	glass beads		
			0.57	glass beads		He
			1.02	glass beads		
			0.11	sand		CO_2
			0.24	sand		
Votruba, Hlavacek, and Marek (1972)		26	0.45	glass	sphere	O_2
			2.25	glass	sphere	
			3.9	glass	sphere	N_2
			6.5	glass	sphere	
			2.25	lead	sphere	N_2-air
			5.0	iron	sphere	
			5.15	iron	sphere	air
			3.4	alumina	sphere	
			5.6x4	alumina	cylinder	
			6.5x 6.5x3	ceramic	Raschig ring	
			1.32	duracryl	particles	
			0.25	sand		

Table 2.4-2 Range of Validity and Specific Correlations Proposed for the Axial Effective Thermal Conductivity, k_{ez}

Yagi, Kunii, and Wakao (1960) $\quad 2 \leq \frac{d_p G_o}{\mu_g} \leq 12$

$$\frac{k_{ez}}{k_g} = \frac{k^o_{ez}}{k_g} + \delta N_{Pr} N'_{Re}$$

Bischoff (1962) $\quad 1 \leq \frac{d_p G_o}{\mu_g} \leq 100$

$$\frac{k_{ez}}{k_g} = \frac{k^o_e}{k_g} + \left[(\alpha\beta)\, N'_{Re} N_{Pr} + \frac{h}{4} \left(\frac{D_t}{d_p}\right)^2 (N'_{Re} N_{Pr})^2 \left(\frac{1}{k^o_e/k_g - (\alpha\beta)\, N'_{Re} N_{Pr}} \right) \right]$$

Votruba, Hlavacek, and Marek (1972) $\quad 0.1 \leq \frac{D_o G_o}{\mu_g} \leq 1000$

$$\frac{k_{ez}}{G_o c_p d_p} = \frac{k^o_{ez}/k_g}{N'_{Re} N_{Pr}} + \frac{14.5 \text{ mm}}{d_p [1 + (c_3/N'_{Re} N_{Pr})]}$$

Table 2.4-3 k^o_{ez}/k_g and δ' Obtained by Yagi, Kunii, and Wakao (1960)

Material	d_p (mm)	k^o_{ez}/k_g	δ'	k^o_e/k_g, calc
Glass beads	2.6, 6.0	7.5	0.65	7.9, 8.4
Steel balls	4.8	13	0.70	19
Broken limestone	2.0, 3.4	10	0.80	10, 10
Porcelain Raschig rings	4.0, 9.0	7	0.70	9.0, 6.7

Table 2.4-4 k^o_{ez}/k_g and c_3 Obtained by Votruba, Hlavacek, and Marek (1972)

Material	d_p (mm)	Gas	k^o_{ez}/k_g	c_3
Glass spheres	3.9	O_2	38.8	4.9
Glass spheres	2.25	O_2	8.3	2.9
Lead spheres	2.25	N_2	29.8	0.0
Iron spheres	5.15	N_2	23.3	0.0
Ceramic Raschig rings	6.5x6.5x3	N_2-air	19.6	11.4
Glass spheres	0.45	N_2-air	27.5	0.0
Iron spheres	5.0	air	25.0	5.1
Alumina spheres	3.4	air	4.5	0.5
Alumina cylinders	5.6x4	air	7.27	3.2
Duracryl particles	1.32	air	34.2	2.9
Sand	0.25	air	11.2	0.03
Glass spheres	6.5	air	228.0	70.8

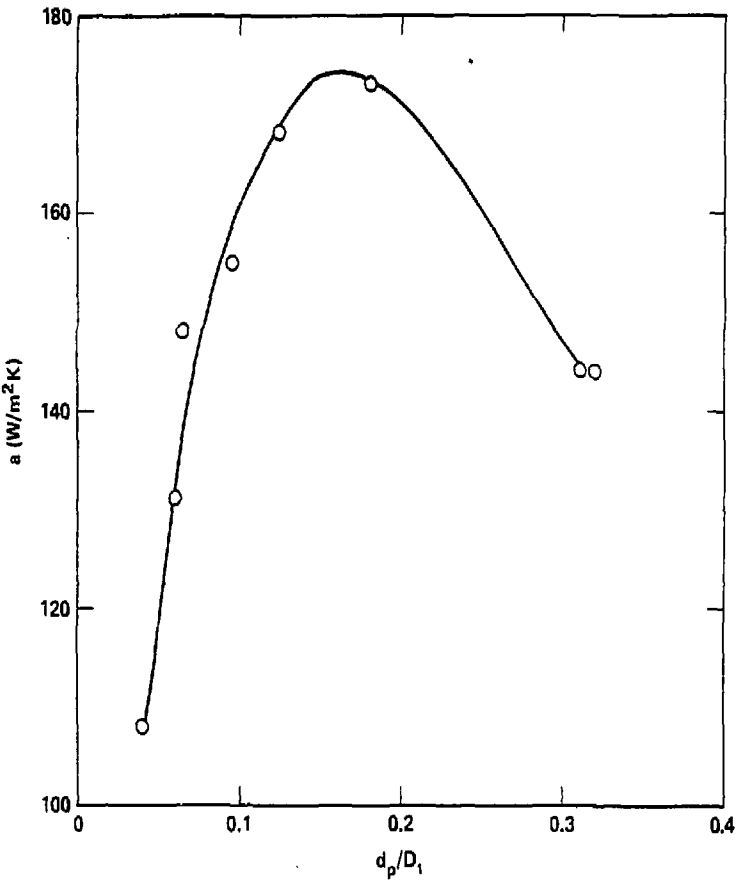

Figure 2.1-1. The parameter a as presented by Colburn (1931).

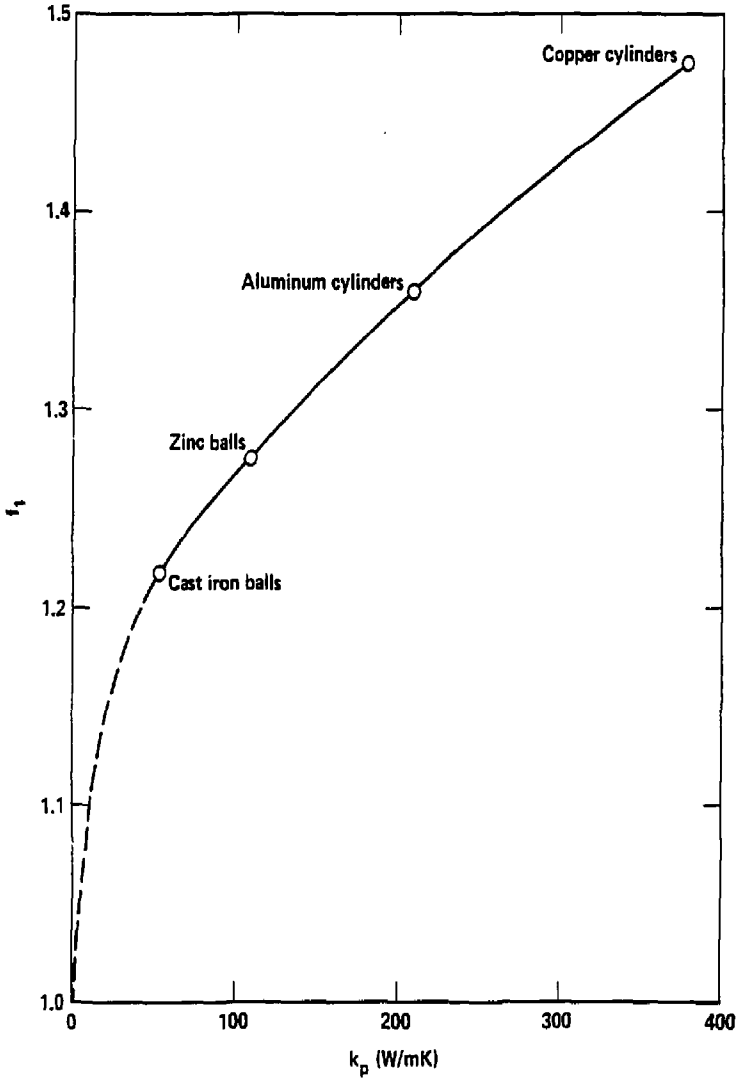

Figure 2.1-2. Correction factor f_1 presented by Leva and Grummer (1948).

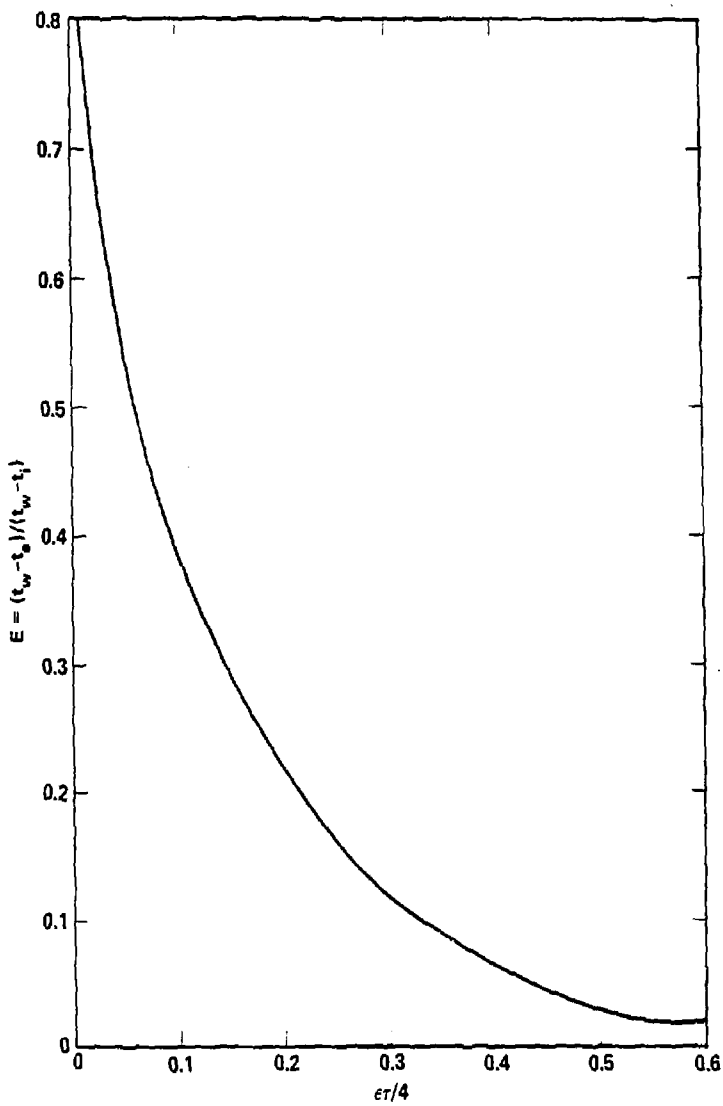

Figure 2.2-1. E chart presented by Hougen and Pirat (1951).

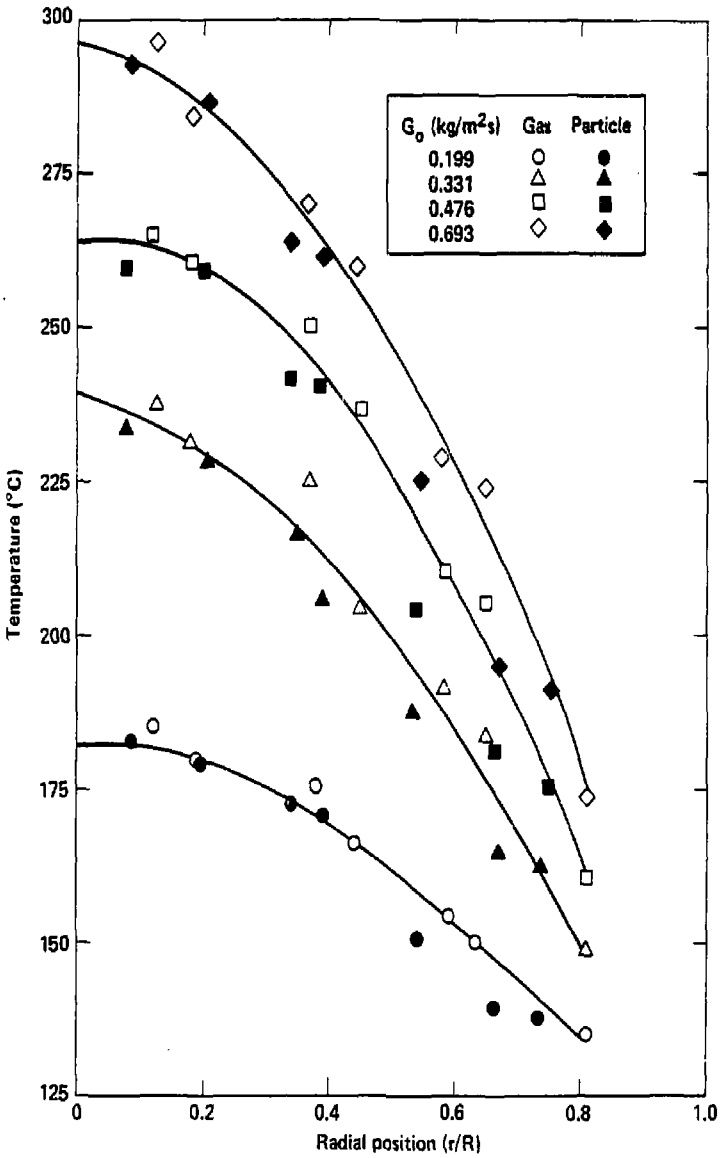

Figure 2.2-2. Radial temperature profiles reported by Bunnell, Irvin, Olson, and Smith (1949).

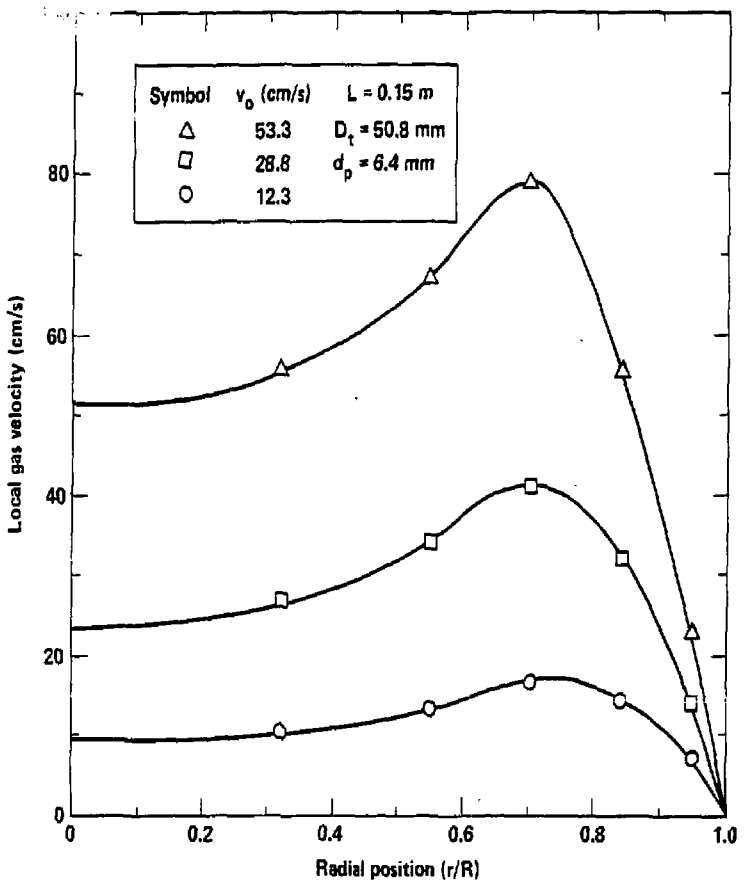

Figure 2.2-3. Variation of velocity profile with gas flow rate as reported by Morales, Spinn, and Smith (1951).

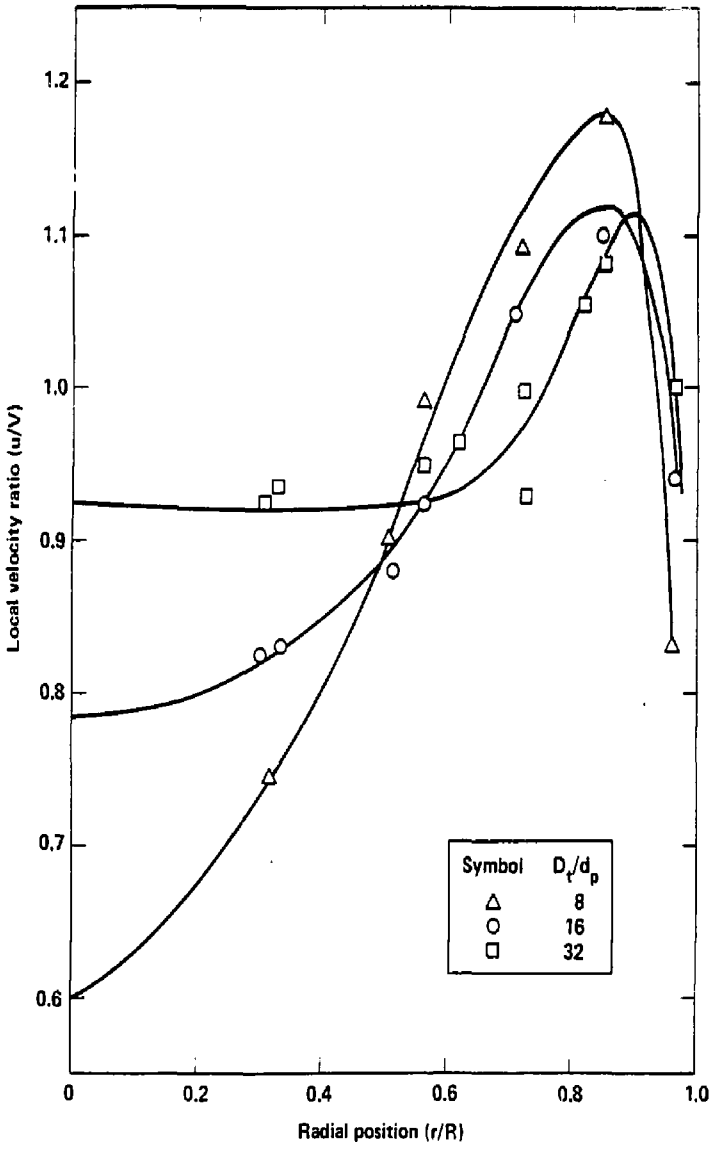

Figure 2.2-4. Radial velocity profiles as presented by Schwartz and Smith (1953).

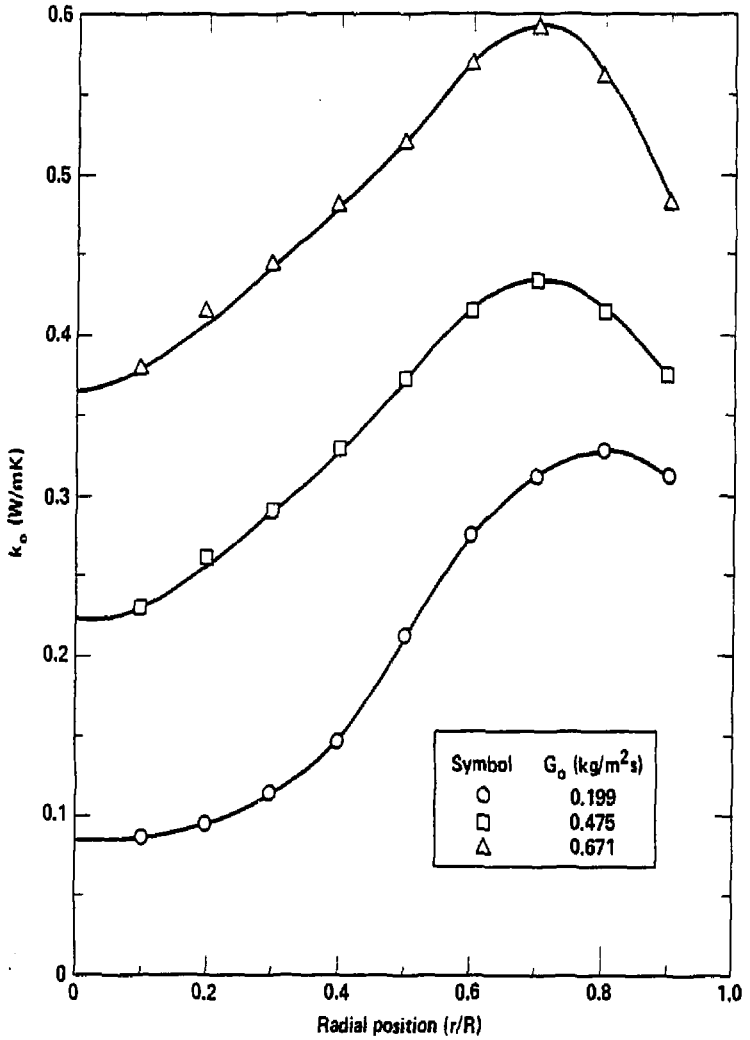

Figure 2.2-5. Variation of overall effective thermal conductivity with radial position reported by Schuler, Stallings, and Smith (1952).

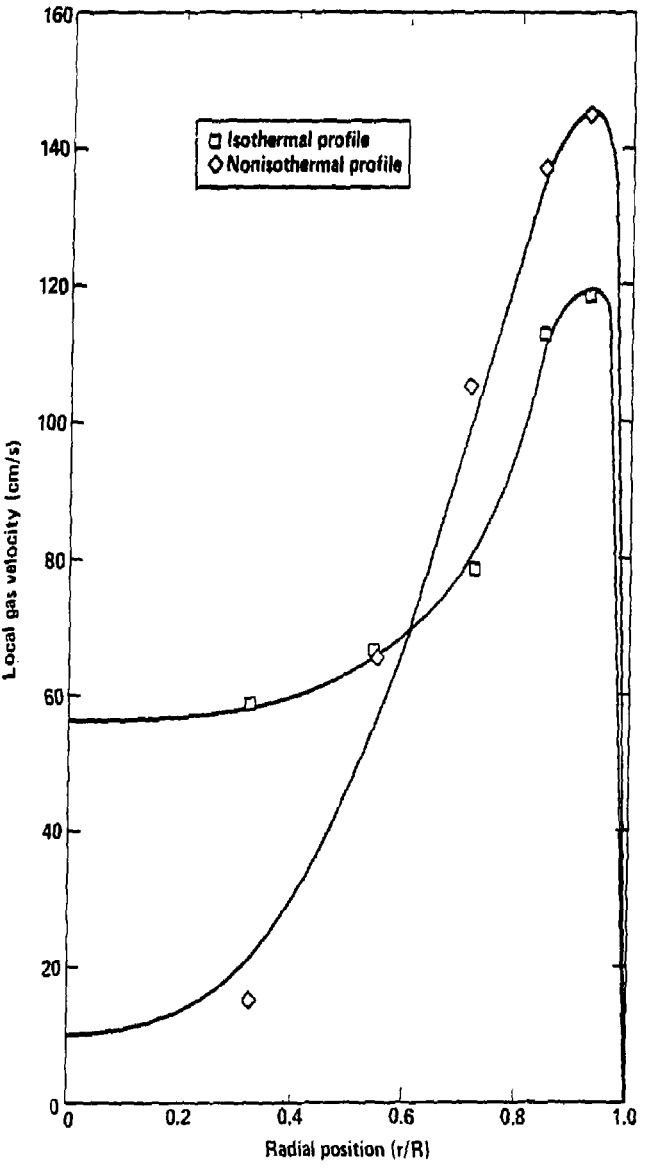

Figure 2.2-6. Radial velocity profiles reported by Schertz and Bischoff (1969).

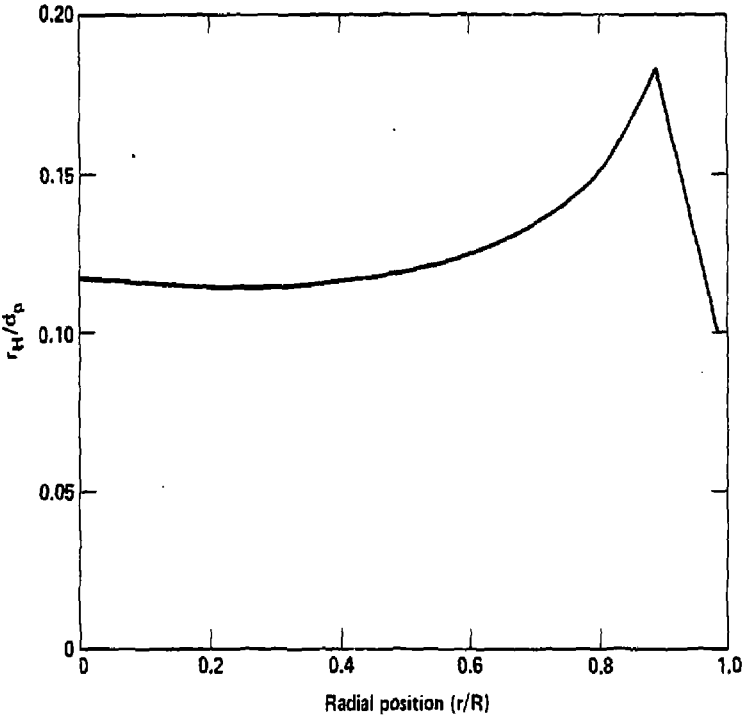

Figure 2.2-7. The radially varying hydraulic radius used by Schertz and Bischoff (1969).

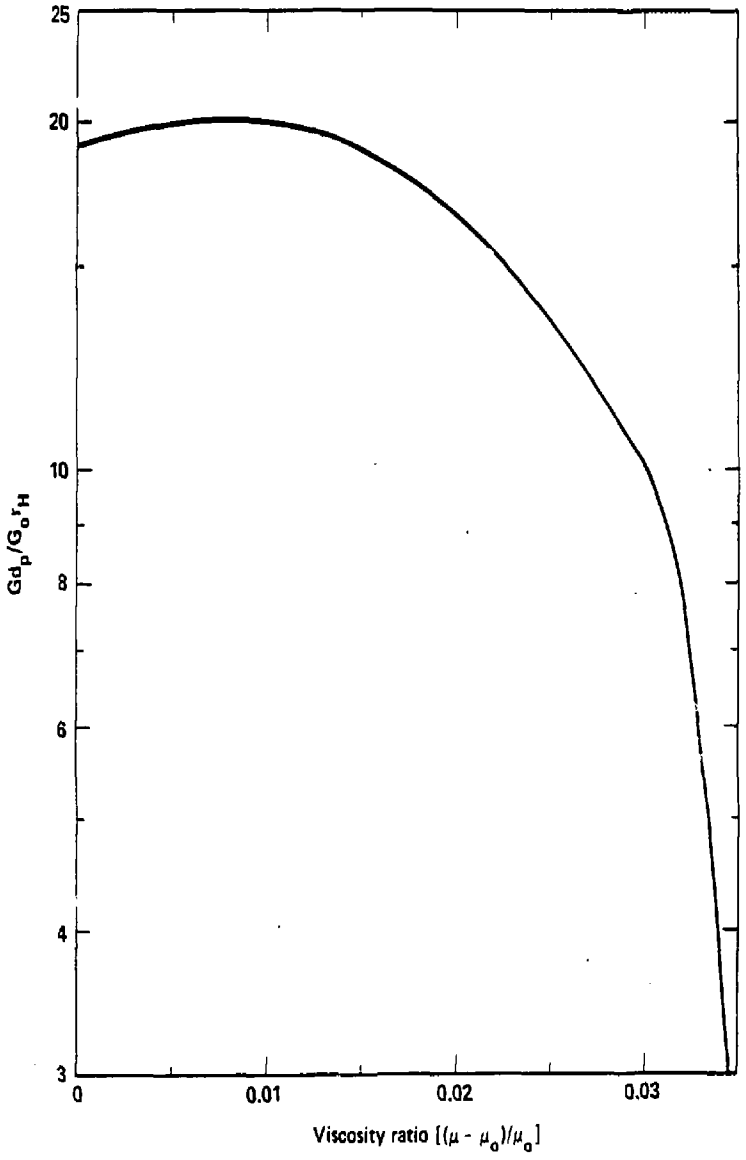

Figure 2.2-8. Velocity correlation of Schertz and Bischoff (1969).

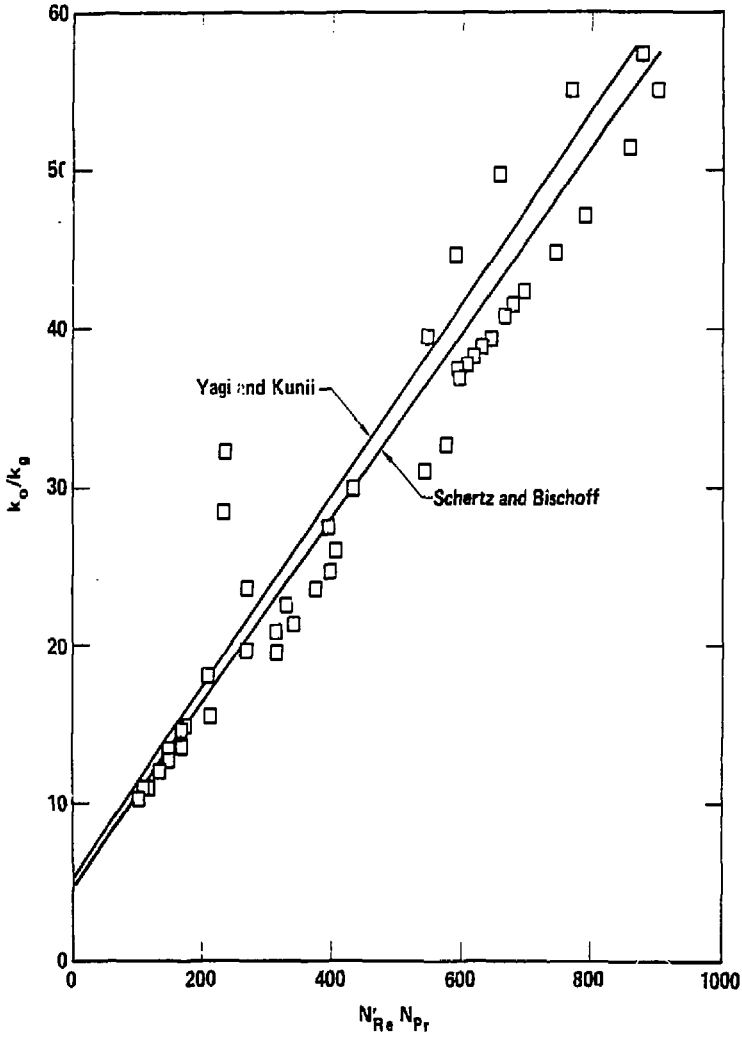

Figure 2.2-9. Overall effective thermal conductivity correlation presented by Schertz and Bischoff (1969).

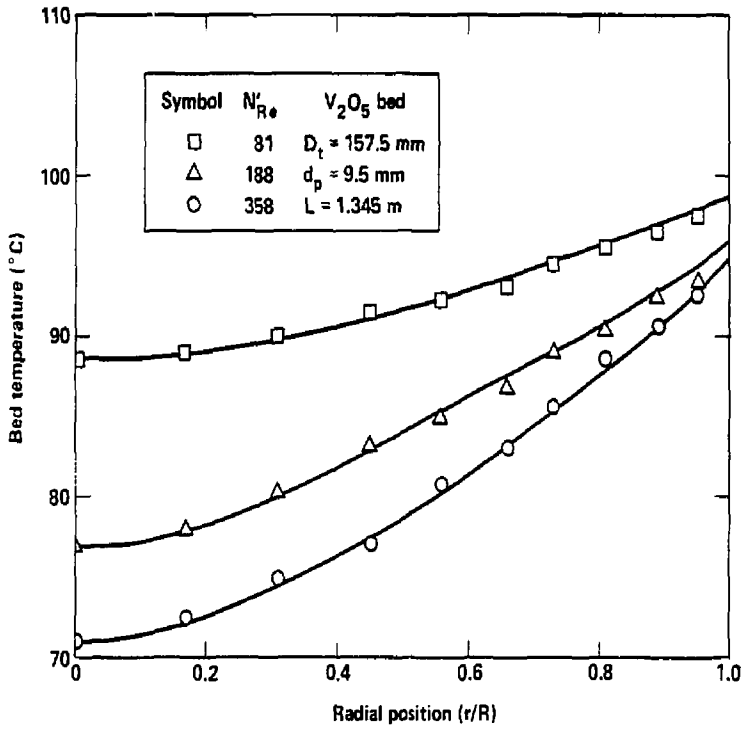

Figure 2.3-1. Experimental and two-parameter theoretical radial temperature profiles reported by Dellesch and Froment (1972).

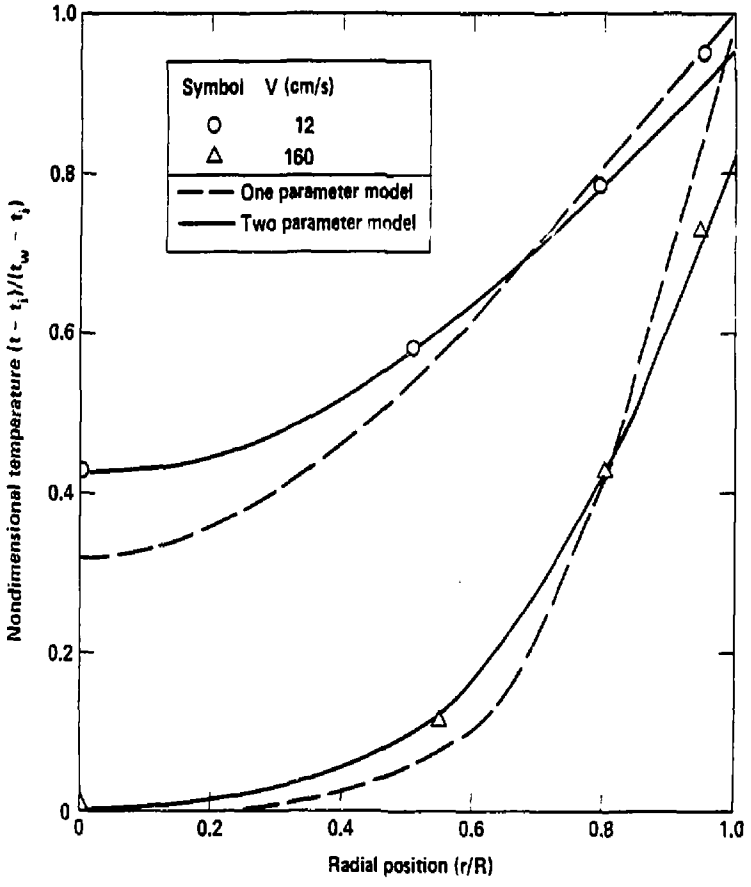

Figure 2.3-2. Experimental and theoretical radial temperature profiles reported by Specchia, Baldi, and Sicardi (1980).

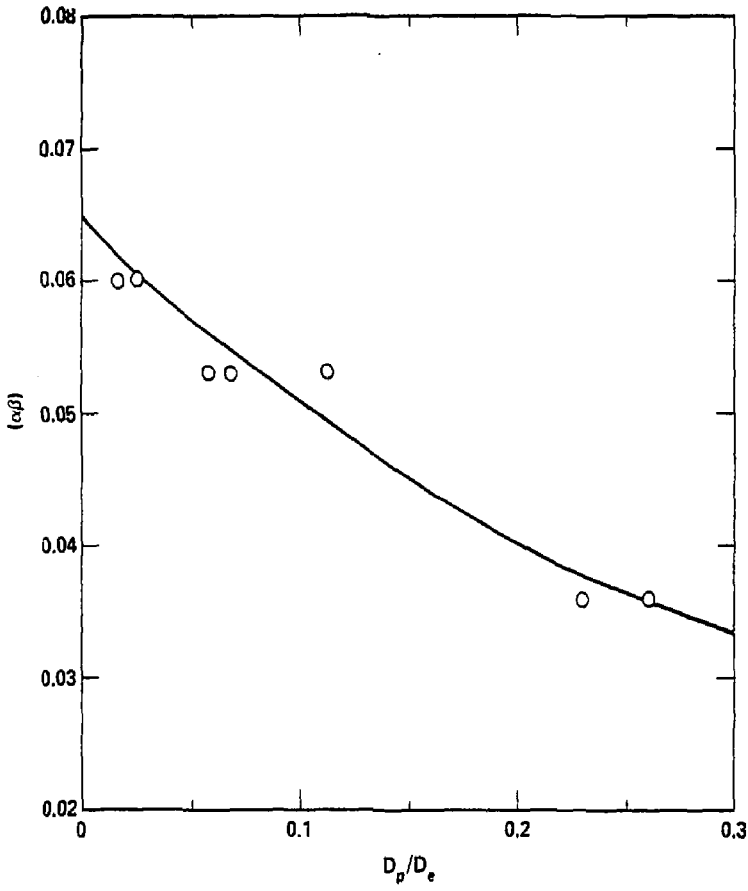

Figure 2.3-3. The parameter ($\alpha\beta$) in the annular bed of Yagi and Kunii (1960).

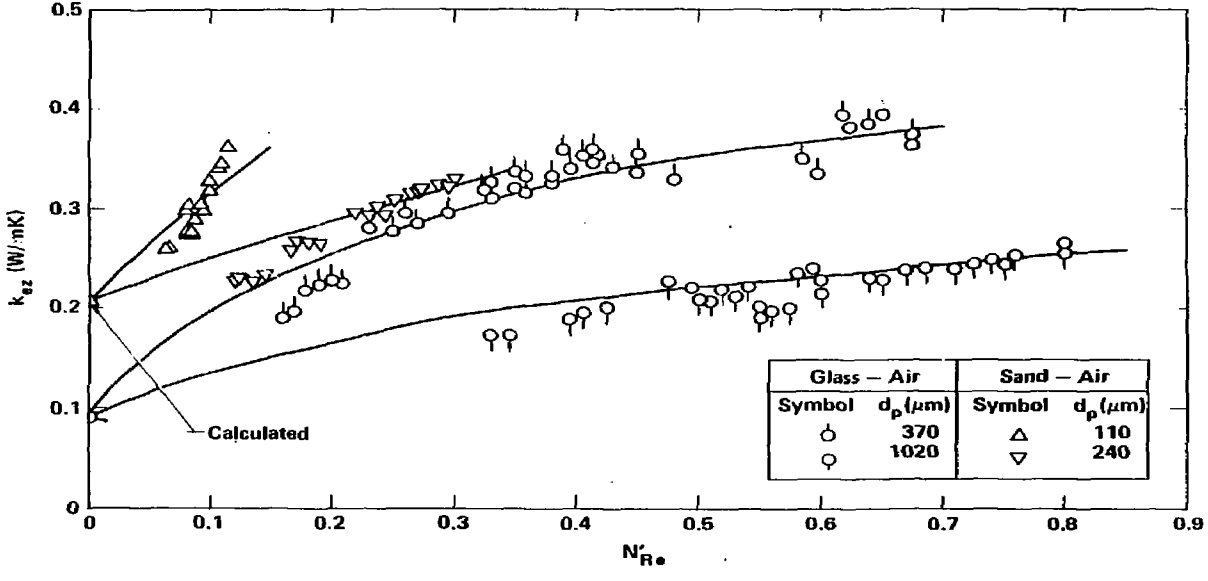

Figure 2.4-1. Axial effective thermal conductivity correlation reported by Kunii and Smith (1961).

CHAPTER 3

TWO PARAMETER PACKED BED MODELS

The various methods for treating heat transfer in packed beds were discussed in the last chapter. In order to realistically explain the temperature profiles, one of the two-dimensional methods described must be used. In addition, the existence of an additional thermal resistance near the wall requires that models incorporating more than one parameter be utilized. As has been discussed, extention to a three-parameter model has usually proven unnecessary; great success has resulted by describing the temperature profile in terms of the two-dimensional, two-parameter methods. Therefore, most of the theoretical treatments of packed bed heat transfer have been aimed at expressing the two heat transfer parameters, k_e and h_w, in terms of k_p, k_g, the void fraction, N_{Pr}, N'_{Re}, and other known system variables.

The greatest number of theoretical models presented in the literature have been concerned with expressing the form of the static effective thermal conductivity. Although this assumes the existance of an eddy contribution k_e^t relatively few studies have been presented to explain its form. It is generally accepted that the stagnant conductivity is due to heat transfer via conduction through the particle, the points of particle contact, the voids, the stagnant film near the points of contact, and by radiation. Various arrangements of these thermal resistances have been proposed in the different models. It is generally accepted that k_e^t is proportional to the modified

Reynolds number, but has been presented only in terms of correlated experimental data; purely theoretical predictions have not been made. Other models have been proposed for k_e based upon the particle-to-gas heat transfer coefficient. As these are generally more complicated, explanation in terms of h_{pg} relies heavily upon experimental correlation.

Very few studies have presented models for the wall heat transfer coefficient. The bulk of these have discussed the various contributions to h_w in terms of the effective conductivity near the wall. One, however, was based upon a combination of thermal resistances similar to that proposed for k_e^o.

The purpose of this chapter is to present the theoretical models for k_e and h_w that have been proposed in the literature. Section 3.1 discusses the effective conductivity with much of the work aimed at estimating the static conductivity. The few models explaining the wall heat transfer coefficient are presented in Section 3.2.

3.1 Models of the Effective Thermal Conductivity

Many models have been proposed for k_e. These models can be segregated into two classes. The first type postulates a local temperature difference between the particles and the gas stream. Here the rate of conduction through the solid is affected by the particle-to-gas heat transfer coefficient, h_{pg}, which depends upon the fluid velocity. Many authors have expressed the opinion that such a model describes the actual phenomena more precisely, but is clearly much more complicated. These difficulties make it impossible to obtain an a

priori model; dependence upon experimental correlations of the particle-to-gas heat transfer coefficient becomes necessary.

The second type is based upon the usual pseudohomogeneous model which postulates the equivalence of the solid and fluid temperatures. The effective conductivity is generally segregated into two independent parts: the stagnant effective thermal conductivity that exists even when there is no gas flow and the eddy contribution due to flow and turbulent mixing. Experimental observations have tended to agree with the assumptions of this type of model; a temperature difference between the solid and fluid has been found in general to be nonexistent and the segregation of the effective conductivity into two parts has been experimentally observed.

Only two models have been proposed for k_e^0 based upon the particle-to-gas heat transfer coefficient (Section 3.1.1); the correlations that have been presented for h_{pg} will also be discussed (Section 3.1.2). Most work, and therefore the bulk of this section, has concentrated on models of the pseudohomogeneous type. Various methods have been utilized in developing a form for k_e^0. The simplest models were based upon various parallel-series combinations of the postulated heat transfer mechanisms (Section 3.1.3). Other models reported the variation of the static effective conductivity at low pressure due to the variation of k_g in that regime (Section 3.1.4). The final method was presented in graphical form (Section 3.1.5); in this regard, solutions of the problem at hand were obtained numerically.

3.1.1 Models Based Upon the Particle-to-Gas Heat Transfer Coefficient

The first type of models to be discussed is based upon the particle-to-gas heat transfer coefficient. These are expected to describe the heat transfer processes more accurately than those based upon the pseudohomogeneous model. They are inherently more complex; dependence upon experimental correlation becomes necessary. For these reasons, only two models of this type have been reported. Table 3.1-1 lists the final forms of the models presented.

Argo and Smith (1953) considered the radial heat transfer in a packed bed to be a parallel combination of the part passing through the void space and the part passing through the solid particles (Table 3.1-1). The heat passing through the void was postulated to be a combination of molecular conduction, turbulent diffusion, and radiation all in parallel with one another. The heat passing through the particle was taken to be a series combination of radiation, convection from the gas stream, conduction through the points of particle contact, and conduction through the stagnant gas adjacent to the particle.

In the void, the gas conduction contribution, k_c', was assumed to be equal to k_g. The turbulent diffusion contribution, k_{td}', was obtained in analogy to mass transfer from the Peclet number for mass transfer. The work of Bernard and Wilhelm (1950) was quoted to be one source of obtaining the Peclet number for mass transfer in terms of the modified Reynolds number. The work of Schuler, Stallings, and Smith (1952) was quoted as a basis for estimating the form of k_r' which depended upon the temperature level and gradient, and therefore,

position. These authors found that the temperature level was more important than the gradient. Argo and Smith thus stated that the expression of Damköhler (1937) applied even though only the bulk temperature of the bed was used. This was stated to be acceptable for most practicle packed beds, i.e. for beds with T_a less than about 400°C.

The estimation of k'_{series} was much more complicated. Several assumptions were made by the authors in order to obtain a useful solution; an expression was derived for k'_{series} in terms of h', the total heat transfer coefficient between the surface of the particle and the fluid or other particles. For nonspherical particles, the authors suggested that d_p be replaced by d_o.

For the convection coefficient, h_{pg}, the correlations of Gamson, Thodos, and Hougen (1943) were suggested. A derivation based upon the same assumptions that were used to derive k'_{series} gave the radiation coefficient h_r in terms of k'_r which was mentioned above. The conduction coefficient h_p was similarly expressed. Heat transfer by conduction through the points of particle contact and through the stagnant gas near these points was accounted for by the correlation of Wilhelm, Johnson, Wynkoop, and Collier (1948).

For temperatures in the bed less than 300°C, the authors stated that the radiation contributions could be neglected. This final form was compared to experimental data for k_e which did not include a wall resistance. The predicted values agreed well with the data of Schuler, Stallings, and Smith (1952) and disagreed with the values of Coberly

and Marshall (1951). Argo and Smith suggested the correlation of Bernard and Wilhelm used to evaluate k'_{td} did not apply to the apparatus of Coberly and Marshall.

Kunii and Smith (1961) presented a method in which the effective thermal conductivity could be expressed in terms of the particle-to-gas heat transfer coefficient and the "apparent" conductivity. Such an expression was felt to be necessary because accurate values of k_e were difficult to measure at low flow rates. The apparent conductivity was taken to represent the solid-phase contribution to k_e and was given the symbol k_e^*.

Differential equations describing the heat flows in both the solid and gas phases, respectively, were described in terms of k_e^* and h_{pg}. The temperature profile for t_g was taken to be the same as that used to compute k_e by the method of Kunii and Smith (1961) which was discussed in Chapter 2. With these assumptions, the particle-to-gas heat transfer coefficient was expressible in terms of k_e and k_e^*. It was emphasized that this method would only be applicable for heat transfer parallel to fluid motion as was implied by the assumed temperature profile.

3.1.2 Particle-to-Gas Heat Transfer Coefficients

In the above section, the models proposed were based upon a particle-to-gas heat transfer coefficient. None of the experimental methods discussed in Chapter 2 observed a temperature difference between the two phases; the additional studies incorporating methods

different from those previously discussed in order to provide data for h_{pg} will be presented in this section. The correlations presented are listed in Table 3.1-2.

Gamson, Thodos, and Hougen (1943) presented h_{pg} in terms of the j-factors for heat transfer:

$$j_H = \frac{h_{pg}}{c_p G_o}\left(\frac{c_p \mu_g}{k_g}\right)^{2/3} \qquad (3.1\text{-}1)$$

Most of the results for h_{pg} have been subsequently correlated in this fashion.

Glaser and Thodos (1958) studied a packed bed with heat generated in the bed by passing an electric current through metallic particles. The modified Reynolds number was based upon the surface area of the particle, the void fraction, and a shape factor ϕ':

$$N'_{Re} = \frac{\sqrt{S_p}\, G_o}{\mu_g (1 - \epsilon)\, \phi'} \qquad (3.1\text{-}2)$$

For spheres, the shape factor was taken to be 1.0. The j-factor was correlated in terms of j_{Ho}, which was taken to be independent of particle shape. The shape factor for cubes or cylinders was varied until the curve of j_{Ho} versus N'_{Re} coincided with that for spheres; values of 0.81 and 0.88, respectively, were obtained for ϕ'.

Baumeister and Bennett (1958) utilized induction heating of steel balls to obtain a temperature difference between the particles and gas. The parameters were functions of D_t/d_p. N'_{Re} was the usual modified Reynolds number.

McConnachie and Thodos (1963) studied simultaneous heat and mass transfer in the drying of spheres saturated with water by dry air flowing through a packed bed. The modified Reynolds number was once again given by Equation (3.1-2) with $\phi' = 1$ and $S_p = d_p$ for spheres.

Gupta, Chaube, and Upadhyay (1974) reanalyzed existing data on h_{pg}. They claimed the scattering in the curves of j_H versus N'_{Re} was reduced by accounting for the void fraction in their correlation.

Cybulski, Van Dalen, Verkerk, and Van Den Berg (1975) studied heat transfer from silicon-copper particle packed beds at low modified Reynolds numbers.

Bhattacharyya and Pei (1975) used microwave power to heat their packed bed. The particle-to-gas heat transfer coefficient was correlated in terms of the Archimedes number.

3.1.3 Simple Models of the Effective Thermal Conductivity

The first group of theoretical predictions for k_e based upon the pseudohomogeneous model are very straightforward to derive. These have been referred to most often and have compared well with the extensive experimental data.

The effective thermal conductivity is assumed to consist of separate static and flow terms as described by Equation (2.3-4). Although it is generally accepted that k_e^t is proportional to the modified Reynolds number, the proportionality constant has to date been determined from experiment. The majority of the models proposed have been concerned only with k_e^o. Here, various heat transfer mechanisms through the

solid, stagnant gas, and void are postulated to occur in different parallel-series combinations. The different models that have been proposed are listed in Table 3.1-3.

Ranz (1952) concentrated on explaining the form of k_e^t. While an average mass velocity G_0 of fluid flowed axially through a packed bed, a radial mass velocity αG_0 was postulated to occur to the right and to the left simultaneously through randomly oriented channels. This lateral motion of fluid flowed through each of N planes with openings that allowed for N distinct changes. Based upon this model k_e^t was derived to be proportional to αG_0 and inversely proportional to N.

Ranz's equation thus gave physical meaning to the results presented in Equation (2.3-2); α was that fraction of the average axial flow of gas that moved back and forth laterally in a given cross section. As was shown in Chapter 2, the form of this equation described well the form of the eddy contribution to k_e.

One of the most quoted and thoroughly tested models is the one first presented by Yagi and Kunii (1957). They proposed seven heat transfer mechanisms which occurred in a packed bed: i) thermal conduction through the solid; ii) thermal conduction through the points of particle contact; iii) radiant heat transfer between particle surfaces; iv) radiant heat transfer between neighboring voids; v) thermal conduction through the fluid film near the point of contact of two adjacent packings; vi) heat transfer by convection, solid-fluid-solid; and vii) heat transfer by lateral mixing of fluid.

They postulated that the first five processes occurred independent of fluid flow and could be accounted for in predicting a static effective thermal conductivity. Actually, mechanism v) could be affected by fluid flow, but Yagi and Kunii claimed that the film of fluid near the point of contact was embedded well into the boundary layer and that the above postulation applied. The final two mechanisms were dependent upon fluid flow. At high Reynolds numbers, process vii) controlled the heat transfer. The authors further assumed that mechanism vi) was unimportant at all Reynolds numbers.

The effective thermal conductivity due to lateral mixing was taken to be that proposed by Ranz. The factor β was defined as the ratio of the average length ℓ_p between the centers of two neighboring solids in the direction of heat flow and the diameter of the particle d_p:

$$\beta = \frac{\ell_p}{d_p} \qquad (3.1\text{-}3)$$

The authors stated that β took a value between 0.82 and 1.0 depending upon the packing characteristics of the bed. From the definition of $N = 1/\beta d_p$, Ranz's form for k_e^t could be written as was presented in Equation (2.3-2). The parameter β then also had physical meaning; α also depended on the packing state of the system.

The bulk of the Yagi-Kunii model concerned itself with a presentation of the static effective thermal conductivity. The effective area for heat transfer was divided into three portions. The

fraction of this area that accounted for radiation between neighboring voids (mechanism iv) was ϵ. The fraction of area for conduction through the points of contact (mechanism ii) was designated by δ_1. The remaining three processes occurred through the balance of this area. These three groups were postulated to occur in parallel with one another. This parallel-series combination is depicted schematically in Figure 3.1-1(a). An energy balance for this combination of thermal resistances yielded the general form of Yagi and Kunii's model (Table 3.1-3). The heat transfer coefficient for radiation between solid surfaces was taken to be analogous to Damköhler's radiant conductivity with $k_r' = d_p h_{rs}$. Radiation between the voids was similarly expressed.

Two further definitions were made; γ was the ratio of the length of solid affected by thermal conductivity, ℓ_s, and the particle diameter; ϕ was the ratio of the effective thickness of fluid film in void for conduction, ℓ_v, and the particle diameter. That is:

$$\gamma = \frac{\ell_s}{d_p} \qquad (3.1\text{-}4)$$

$$\phi = \frac{\ell_v}{d_p} \qquad (3.1\text{-}5)$$

For gas filled voids, $\delta_1 = 0$. For fine particles, the radiation contributions can be neglected. The parameter γ was then taken for practical purposes to be unity resulting in the form of the Yagi-Kunii (1957) model most often quoted (Table 3.1-3).

The experimental data of Bunnell, Irvin, Olson, and Smith (1949); Campbell and Huntington (1952); Coberly and Marshall (1951); Schuler, Stallings, and Smith (1952); and Plautz and Johnstone (1955) were reanalyzed and put into the form of Equation (2.3-2) which is identical to the model of Yagi and Kunii presented here. k_e^0 was obtained by extrapolation to zero flow rate. Comparison with theory showed that the term containing δ_1 was negligible; the points of particle contact contributed little to the static conductivity at atmospheric pressure. The two forms of the Yagi-Kunii (1957) model were applied to the experimental results to obtain ϕ for the various gases studied in terms of the void fraction. k_e^0/k_g was found to increase with increasing T_a. Radiant heat transfer from solid to solid was found to be important only for materials with high k_p. On the other hand, radiation from void to void was found to be important even for low conductivity solids when T_a was higher than about 400°C. Above a certain minimum, k_e^0/k_g increased significantly with increasing d_p.

The Yagi-Kunii model agreed well with the experimental data inasmuch as it relied heavily upon experimental correlation for the most important parameters, $(\alpha\beta)$ and ϕ. Kunii and Smith (1960) sought to relax this restriction, so far as the static conductivity was concerned. The same five nonradiant mechanisms were postulated; in addition, a sixth mechanism was included in the derivation of k_e^0 to account for conduction between adjacent voids. A slightly different parallel-series combination of these six mechanisms was utilized. The combination used is depicted schematically in Figure 3.1-1(b).

An energy balance for this combination of thermal resistances yielded the general form of the Kunii and Smith (1960) model (Table 3.1-3). Conduction through the points of contact was expressed in terms of the heat transfer coefficient h_p. Again, ℓ_s was the thickness of a slab of solid material which would offer the same resistance as a spherically shaped particle; ℓ_v was the thickness of a slab of stationary gas which would offer the same resistance as the stagnant fluid near the points of contact.

Except at low pressure, the term accounting for conduction through the points of contact was negligible. A final simplification could be made when radiation was neglected; radiation was quoted as being negligible below about 500°C. This yielded the form of the Kunii-Smith (1960) model most often referred to (Table 3.1-3).

Kunii and Smith were concerned with developing theoretical derivations for β, γ, and ϕ. For close packing of spheres, β was presented as the average of the distance to next neighbors along each of the three axes. This resulted in $\beta = 0.895$. For the most open packing, β took on the maximum value of unity. ℓ_s was assumed to be the length of a cylinder having the same diameter and volume as a spherical particle; this resulted in $\gamma = 2/3$.

The parameter ℓ_v was a measure of the film thickness adjacent to the points of contact, and therefore depended upon the packing characteristics. Kunii and Smith made two assumptions in order to derive an expression for ϕ, which depended upon the packing state in addition to k_p/k_g. A theoretical relation between ϕ and k_p/k_g was

developed for both the close and loose packed states and is reproduced in Figure 3.1-2. Here the subscripts 1 and 2 are for the loose packed and close packed states respectively. Clearly the general case lies somewhere between these two limits. Kunii and Smith suggested that the general form of ϕ could be expressed by a linear combination of ϕ_1 and ϕ_2 as listed in Table 3.1-3.

With β, γ, and ϕ theoretically determined, the Kunii-Smith model had no dependence upon experimental correlation. The model was tested against the data from both stagnant systems and flowing systems extrapolated to zero flow rate. The agreement was reported to be good over the wide range of systems and materials studied.

Yagi, Kunii, and Wakao (1961) compared their experimental data to the Kunii-Smith model with $\beta = 1$ and $\gamma = 2/3$. The model agreed well with their observed results and the results of several other investigators. The values of k_e^0 obtained by extrapolation of data to zero flow rate seemed somewhat larger than values obtained directly in apparatus containing stagnant gas. The models of Kunii and Smith (1960) and Schotte (1960) were shown to be nearly identical when applied to the experimental results of Yagi and Kunii (1957) and of Hill and Wilhelm (1959) in high temperature packed beds where the radiation mechanism was significant.

Willhite, Kunii, and Smith (1962) suggested improvements in the Kunii-Smith model. At relatively low temperatures the final form applied. As can be seen by the relative weighting of the terms with respect to ϵ and $(1 - \epsilon)$ (Table 3.1-3), the second term was due to

processes in the effective nonvoid section. However, this included the contribution due to conduction through the stagnant film which was part of the void. A fraction of the effective nonvoided section, $\ell_v/(\ell_s + \ell_v)$, was thus actually voided. The weighting factors in the two terms of the equation for the effective voided and nonvoided sections should not have been be expressed in terms of the actual void fraction but a void fraction ϵ^* which was close to the actual ϵ. This type of model is pictured in Figure 3.1-3.

The void fraction ϵ^* was expressed in terms of ϵ and was inserted into the Kunii-Smith model in place of ϵ. β was replaced by $\gamma + \phi$. The Willhite-Kunii-Smith model was written in terms of $\alpha = \phi + \gamma k_g/k_p$ which depended on the number of contact points (Table 3.1-3). The parameter α was derived by Kunii and Smith (1960) for spherical particles in the packed bed. Since α was written in terms of the number of contact points, n, the authors quoted the theoretical expression of Foote, Smith, and Busang (1929) for n in terms of the actual voidage. The static conductivity was thus expressed in terms of the usual parameters ϵ, k_g, k_p, and γ.

The value of γ may range between 0 and 1; data collected in a packed bed in which the heat flowed purely radially correlated well with these predictions and a value for γ equal to 2/3. Experimental data available for k_e^o were also compared to the Willhite-Kunii-Smith model. Good agreement was obtained over the wide range of particle materials and gases used. A value for γ of 1/2 was used for nonspherical particles and for spherical particles of high conductivity

in order to improve agreement with the data. Since the corrected void fraction ϵ^* must be positive, the model will apply for most systems in which k_p/k_g is greater than about 1.

Specchia, Baldi, and Sicardi (1980) stated that assuming $\beta = 1$ in the Kunii-Smith model was acceptable, but choosing $\gamma = 2/3$ and the complicated equation for ϕ (as it was derived in order to obtain Figure 3.1-2) was open to criticism. The disagreement of the model with extrapolated data in nonstatic experiments was sited as a basis for these claims; Kunii and Smith checked their model primarily against data obtained from experiments incorporating motionless fluid.

An empirical approach to data collected in their own and others' packed beds was attempted to evaluate γ and ϕ in terms of ϵ. γ was found to be independent of ϵ and equal to the value of 2/3 assumed by Kunii and Smith. With $\gamma = 2/3$, the values obtained for ϕ were plotted against ϵ and subsequently correlated.

Specchia and Sicardi (1980) stated that comparison between mass and heat transfer at very low flow rates indicated that the Kunii-Smith model was in error. The nondimensionalized static conductivity predicted by the Kunii-Smith model when radiation was neglected for the case of no heat transfer through the particle, $k_p = 0$, was equal to the void fraction. Specchia and Sicardi stated that this should be equal to the nondimensionalized dispersion coefficient which has been reported to be $\epsilon/1.5$. The Kunii-Smith model was thus modified to take advantage of this heat-mass transfer analogy. Assuming that $\beta = 1$, the same procedure that was used by Specchia, Baldi, and Sicardi (1980)

again yielded $\gamma = 2/3$ but ϕ was correlated in a slightly different form.

In all of the pseudohomogeneous models discussed above, k_e^o was assumed to be independent of flow. Even though the model of Kunii and Smith (1960) has demonstrated remarkable success in predicting k_e^o for systems containing static gas, discrepancies have been observed for those values of k_e^o obtained in flow systems by extrapolation to zero flow. Kulkarni and Doraiswamy (1980) have discussed the work of Bhattacharyya and Pei (1975) who explained this discrepancy.

Bhattacharyya and Pei postulated that in addition to the normal static and eddy contributions the total heat transfer consisted also of a convective contribution to conduction. This was reflected in the particle-to-gas heat transfer coefficient that existed when there was gas flow. With this model, Equation (2.3-4) for the effective conductivity was modified:

$$k_e = k_e^o + k_e^d + k_e^t \qquad (3.1\text{-}6)$$

Here k_e^d was the dynamic contribution to the normal conductive contribution k_e^o. They argued that for a system with static gas, $k_e^d = 0$ in addition to k_e^t. This was why the Kunii-Smith model predicted k_e quite well for such a system. However, as soon as the gas began to flow, k_e^d took on a nonzero value; thus, extrapolation of data collected in flow experiments yielded $k_e^o + k_e^d$, not k_e^o.

To test this theory, microwave power was used for heating a packed bed. The particle-to-gas heat transfer coefficient was correlated in

terms of the Archimedes number as was discussed in Section 3.1.2. From this they were able to correlate the dynamic contribution to conduction in terms of the dynamic heat transfer coefficient h_d. By subtracting this contribution from the values for $k_e^o + k_e^d + k_e^t$ found in the literature, the true values of $k_e^o + k_e^t$ were obtained. These were plotted versus N_{Re}' and extrapolated to no-flow conditions to obtain the true values of k_e^o. The values for the static conductivity obtained in this fashion demonstrated excellent agreement with the Kunii-Smith model. The discrepancies reported in the literature were thus not due to failure of the Kunii-Smith model, but due to the method of obtaining k_e^o from flow data.

3.1.4 Static Effective Thermal Conductivity at Low Pressure

Several authors have studied the variation of k_e^o at low pressure. This characteristic is due to the variation of the gas thermal conductivity at low pressure as is described by kinetic theory. Such studies are important since under certain circumstances this effect may be observed even at atmospheric pressure. These models are presented in Table 3.1-4 and in the figures.

Deissler and Boegli (1958) examined the maximum and minimum limits of the static effective thermal conductivity of any two phase system containing a stagnant gas. The minimum k_e^o was taken to occur when solid slabs of material were alternately arranged with regions of pure gas, the normal to the planes aligning with the direction of heat flux. The maximum occurred when this normal was perpendicular to the

direction of heat flow. These maximum and minimum configurations were then a function of k_p, k_g and ϵ as reproduced in Figure 3.1.4. From this figure, Deissler and Boegli reported that for $\epsilon = 0.4$ and $k_p/k_g = 2$, the variation in k_e^o/k_g from the average was only about 7%, but for $k_p/k_g = 1000$, the variation was 99%. Since k_p/k_g was high for most solid-gas systems, it then followed that the arrangement of the material was an important effect on k_e^o.

Deissler and Boegli were interested in the variation of k_e^o with temperature and gas pressure. A linear variation of the static effective conductivity with temperature was assumed in order to compute k_e^o from the data. This variation was iterated until the assumed and computed values for k_e^o were identical. The results for the variation of k_e^o with temperature for MgO powder in various gases is reported in Figure 3.1-5. The results again showed a strong dependence on the gas thermal conductivity. Similar results were obtained for stainless steel and UO_2 powders except the UO_2 systems showed a flatter temperature variation.

The variation of k_e^o with gas pressure for MgO systems are reproduced in Figure 3.1-6. Similar results were obtained for the other systems. For each curve k_e^o became independent of pressure above a certain point called the breakaway pressure. The breakaway pressure varied with temperature and was different for different gases.

Schotte (1960) criticized the method of Yagi and Kunii (1957) finding the model did not yield satisfactory results for the case of small particles. The change in k_e^o below the breakaway pressure

was studied and a new correlation for the radiation contribution was presented.

When the distance over which conduction in a gas takes place is of the same order as the mean free path of the gas molecules, k_e^0 has been observed to decrease with decreasing pressure. The onset of this phenomena occurs at the breakaway pressure as was discussed above. The correlation of Deissler and Eian (1952) for the breakaway pressure is:

$$p_b = \frac{(4.26 \times 10^{-26} \text{ atm m}^3/\text{K})\, T_a}{d_p d_g^2} \qquad (3.1\text{-}7)$$

For small particles, the breakaway pressure may be comparable to atmospheric pressure. For air, $d_g = 0.0003\,\mu m$, atmospheric pressure is lower than the breakaway pressure for a packed bed with $d_p = 200\mu m$ at average bed temperatures above 150^oC.

A form for the apparent thermal conductivity of the gas at pressures below the breakaway pressure obtained from Kennard (1938) was modified by existing experimental data to become:

$$k_g' = \frac{k_g}{1 + 35.94\left(\frac{\gamma'}{1-\gamma'}\right)\left(\frac{1-\epsilon}{\epsilon}\right)\left(\frac{T_a k_B}{p d_p d_g^2 N_{Pr}}\right)} \qquad (3.1\text{-}8)$$

If p was less than p_b, Schotte suggested that k_g' should be used in place of k_g in order to obtain k_e^0 from the correlation of Deissler and Eian as is reproduced in Figure 3.1-7. When radiation

became important, Schotte suggested some sort of radiant thermal conductivity should be added to the value of k_e^o obtained from Figure 3.1-7. An expression was derived in terms of h_r which was equivalent to $(2 - \epsilon)h_{rs}$ (Table 3.1-4). Good agreement was obtained between the predicted value of k_e^o using Schotte's model and the high temperature experimental results of Yagi and Kunii (1957).

Masamune and Smith (1963) developed a model for k_e^o at low pressure using the method of Kunii and Smith (1960). The same six mechanisms as the Kunii-Smith model were proposed. Their thermal resistances were postulated to occur in a slightly different parallel-series combination. This model, with radiation neglected, is schematically represented in Figure 3.1-8(a) and pictured in Figure 3.1-9.

A heat balance applied in the usual fashion yielded an expression for the static conductivity (Table 3.1-4). Again k_g' was the gas thermal conductivity in the film near the points of contact which may be a function of pressure when the pressure was low enough. As was utilized by Willhite, Kunii, and Smith, the area fraction $\alpha^*\epsilon$ for the first term in the model was not equal to ϵ since some of the voided area was accounted for in the second term. Similarly, the nonvoided area was split between the last two terms. This area fraction α^* was related to ϵ and ϕ. The relationship between ϕ and the void fraction was derived in terms of the number of contact points n. The suggested relation between n and the void fraction was obtained from the work of Kunii and Smith (1960). All experimental data suggested to them that

the area fraction δ must be regarded as a specific parameter for each type of particle and therefore cannot be related simply to ϵ alone. Application of the model as the pressure approaches zero related δ to ϵ and the effective conductivity under vacuum conditions, k_e^v.

The authors ran experiments incorporating beds of fine particles in air over a large range of pressure. Results similar to those of Deissler and Eian (1952), and Schotte (1960) were obtained. Beds of glass beads between 29 and 470 microns in diameter showed that the effective conductivity did not change with pressure above atmospheric pressure. The experimental results for the vacuum conductivity k_e^v as well as other results obtained from the literature were tabulated. Thus, for packed beds of known k_e^v, k_e^o can be predicted by their model with the usual bed parameters ϵ, k_g, k_p, and d_p.

Imura and Takegoshi (1974) proposed a model accounting for the change in k_e^o with pressure incorporating the vacuum conductivity. The authors claimed that this new model agreed with the experimental data over a wider range of pressure than the Kunii-Smith model. Also, they claimed that the Kunii-Smith model did not agree with many experimental values at atmospheric pressure if k_p/k_g was greater than 1000. Five of the six processes that Kunii and Smith proposed were accounted for; only radiation in the void was neglected. The postulated parallel-series arrangement of the thermal resistances is presented schematically in Figure 3.1-8(b). As can be seen, radiation between particle surfaces across the film has been included. Comparison of Figures 3.1-8(a) and 3.1-8(b) shows that this is the same as the

Masamune-Smith model updated to account for radiation. Likewise, the area fractions for the respective processes are the same. The area fractions $\alpha^*\epsilon$ and $(1-\alpha^*\epsilon)\delta$ are written as ϵ' and δ^*, respectively.

An energy balance leads in the usual fashion to k_e^o (Table 3.1-4). The radiant heat transfer coefficient h_r was taken to be of a slightly different form than before. The area fraction ϵ' was expressed in terms of ϵ and ϕ. Both δ^* and ϕ were determined from experimental data obtained in packed beds of glass, bronze, and copper spheres. Various gases were studied over a wide range of pressure below atmospheric. The vacuum conductivity was expressed in terms of the above parameters. δ^* was found to be quite small and the observed values for h_r agreed well with the form proposed. A correlation for ϕ based upon the experimental data was also proposed. Although ϕ was found to vary with pressure, this was found not to effect the values predicted for k_e^o.

3.1.5 Models of k_e^o Based Upon Numerical Solutions

The last group of models were based upon numerical integration of the defining differential equation in simplified arrays of particles. In these models, the actual bending of the heatflow lines was accounted for. They are presented in Table 3.1-5 and Figures 3.1-10 through 3.1-12.

Dietz (1979) developed a simple formula for k_e^o in a hexagonal array of touching spheres with only point contacts. Radiation was neglected. Dietz claimed favorable agreement with published data over

the range of k_p/k_g from 1 to 3000.

Krupiczka (1967) attempted to obtain a rigorous mathematical solution which dispensed with the simplifying assumption of unidirectional flow of heat. Even when ignoring the contributions due to radiation, his solutions were extremely complicated. The complexity of these solutions greatly limit their usefulness. Comparison of these solutions with the experimental data in the literature suggested that both the theory and the experimental results could be correlated by a simpler function. The usual three parameters k_p, k_g, and ϵ were all that was needed to predict k_e^o with this function.

Deissler and Eian obtained the temperature profile in square and triangular arrays of cylinders, with void fractions of 0.214 and 0.093 respectively, using the relaxation method. From these profiles they were able to calculate theoretical values of k_e^o. Deissler and Boegli (1958) applied this method to a cubical array of spheres with a void fraction of 0.475. Both of these studies were for packed beds at relatively low temperatures so that radiation could be ignored. Wakao and Kato (1969) applied the relaxation method to an orthorhombic array of spheres with a void fraction of 0.395. In addition, heat transfer by radiation was added by including the radiation heat transfer coefficient in the nodal energy balances. A slightly different form for h_r was used (Table 3.1-5). The results obtained are reproduced in Figure 3.1-10. Here, k_e^o/k_g was a function of the radiation Nusselt number $h_r d_p/k_p$ in addition to k_p/k_g. The contribution to k_e^o above that for $N_{Nu}^r = 0$ was also correlated as a radiative

conductivity that could be added to predictions of k_e^0 neglecting radiation. Agreement with experimental data was reported to be fairly good.

Wakao and Vortmeyer (1971) applied the relaxation method to a unit cell consisting of a cylinder of gas $d_p/2$ in height containing a hemisphere of particle material. The void fraction was assumed to be 0.395. Variation of k_e^0 with p at low pressures was accounted for by utilizing a gas conductivity similar to Equation (3.1-8). The contribution due to contact between the particles was also studied by using areas of particle contact instead of points. k_e^0 was separated into three additive contributions which were expressed graphically: i) gas-solid conduction conductivity; ii) radiation conductivity; and iii) contact conductivity.

The conduction component of conductivity was evaluated alone at conditions where radiation was negligible and where the areas of contact were points so that the third mechanism was negligible also. k_e^0/k_g was plotted versus k_p/k_g and τ' as is reproduced in Figure 3.1-11. τ' was a parameter relating the pressure dependence. As can be seen from the figure, k_{cond} was very dependent upon pressure. To account for radiation, the radiant heat transfer coefficient of Wakao and Kato was once again incorporated into the nodal energy balances. Figure 3.1-10, which was from the work of Wakao and Kato (1969), illustrates the results of the first two contributions at $\tau' \rightarrow \infty$. The radiation conductivity was correlated in terms of k_{rad}^{∞} and f'. k_{rad}^{∞} can be obtained from Figure 3.1-10 as the difference between the

values for a given N_{Nu}^{r} and for N_{Nu}^{c} = 0 and f' is presented in Figure 3.1-12. k_{rad} was thus also found to be dependent upon pressure. The conductivity at the point of contact for finite areas of contact was modified by Λ, the contact area divided by the projected area of a particle. $k_{contact}$ was found to be related to Λ and k_p only. The usual S-shaped curves of k_e^o versus pressure were obtained when the three mechanisms were accounted for in the above fashion. For particles bigger than 500 μm in diameter, k_e was found not to change with pressure above atmospheric pressure.

The equations developed by Wakao and Kato and by Wakao and Vortmeyer were based on a stagnant gas with zero emissivity in the voids. Wakao (1973) investigated the effect of gas emissivity on the effective thermal conductivity. This change only modified the radiation Nusselt number N_{Nu}^{r}. The difference obtained was so small that in most cases gas radiation was found not to have an appreciable effect on the effective conductivity.

3.2 Models of the Wall Heat Transfer Coefficient

Theoretical models predicting the wall heat transfer coefficient have been developed to a much lesser extent than the treatment of the static conductivity. All of the models that will be discussed here are based upon the assumption of a static wall coefficient that has been observed experimentally. The wall coefficient h_w is postulated to be similar in form to the effective conductivity predicted by Equation (2.3-4):

$$h_w = h_w^o + h_w^t \qquad (3.2\text{-}1)$$

where h_w^t exists only when there is fluid flow and h_w^o is independent of flow. In many of the models, h_w^o was predicted in terms of the effective conductivity in the wall region as was presented experimentally in Section 2.3. In addition, the dependence upon point contact was expressed in terms of a new function, ϕ_w, that was similar to ϕ for the effective conductivity case. These models are listed in Table 3.2-1.

The earliest correlations for h_w of Yagi and Kunii (1960) were discussed in Section 2.3. They predicted h_w to be linearly related to the modified Reynolds number (Table 2.3-2). This correlation was valid only for N'_{Re} less than 2000. Yagi and Kunii (1961) extended their work to all ranges of modified Reynolds number. This was done by taking the turbulent contribution to h_w to be in series with the true film coefficient of heat transfer for the boundary layer on the wall surface, h_w^* (Table 3.2-1). For low N'_{Re}, the second term in the denominator of their model predominated and the correlation of Yagi and Kunii (1960) was again obtained. The Yagi-Kunii (1961) model then determined both h_w^o and h_w^*.

The determination of the stagnant wall heat transfer coefficient was concerned with the region within one half of one particle diameter from the wall. In this region a particle will have one point of contact with the wall but several with other particles. The model for heat transfer in this region was taken to be that proposed by Kunii and

Smith (1960); their determination of k_e^o was presented in Figure 3.1-1(b). Accounting for the points of contact, h_w^o was written in terms of k_w^o and k_e^o. k_w^o was defined in terms of ℓ_v^*, ℓ_s^*, and ϵ_w which are ℓ_v, ℓ_s, and ϵ in this near wall region. γ_w was taken to be one half of the value outside this near wall region, i.e. $\gamma_w = 1/3$. A derivation for the heat flow through the solid phase gave an expression for ϕ_w in terms of k_p/k_g. This expression was plotted for comparison with ϕ_1 and ϕ_2 in Figure 3.1-2. It will be noted that ϕ_w was independent of ϵ as opposed to the dependence of ϕ. Fairly good agreement with the experimental results of Yagi and Kunii (1960) were obtained when a value for ϵ_w of 0.7 was assumed. The true film coefficient for the boundary layer was correlated to be slightly different than that reported in Equation (2.3-8).

Ofuchi and Kunii (1965) obtained additional data for h_w^o in beds with stagnant fluid to test the validity of Yagi and Kunii's (1961) model. They mentioned that insertion of Equation (2.3-6), which applied to static beds, into the model of Yagi and Kunii (1961) showed that k_w^o was twice the static effective conductivity in the near-wall region, k_{ew}^o. It was concluded that when the Kunii-Smith theory was incorporated to determine k_e^o, the values of the static effective conductivity in the wall region and the static wall heat transfer coefficient could satisfactorily be predicted by the Yagi-Kunii model.

Specchia, Baldi, and Sicardi (1980) used the same simplified approach as was proposed by Kunii and Smith for k_e^o. In the near wall region, the heat flux was written in terms of the contributions

through the fluid in parallel with those through the solid. For nonspherical particles the author suggested d_p should be replaced by the diameter of a sphere with the same volume as the particle.

The static wall heat transfer coefficient was then obtained in terms of γ_w and ϕ_w by an energy balance (Table 3.2-1). It will be noted that $h_w^o d_p/k_g$ predicted by their model was the same as k_w^o/k_g predicted by the Yagi-Kunii model with negligible radiation. Correlation showed that γ_w was independent of other factors and equal to the value assumed by Yagi and Kunii (1961). With $\gamma_w = 1/3$, the values of ϕ_w were determined. ϕ_w was found to depend only upon D_t/d_p.

Table 3.1-1 Models of k_e which incorporate h_{pg}

Argo and Smith (1953):

General:

$$k_e = \epsilon(k_c' + k_{td}' + k_r') + (1 - \epsilon)\, k_{series}'$$

$$k_c' = k_g$$

$$k_{td}' = \frac{d_p c_p G_o}{\epsilon\, N_{Pem}}$$

$$k_r' = 4\left(\frac{e}{2 - e}\right) d_p\, \sigma T_a^3$$

$$k_{series}' = \frac{k_p h' d_p}{(2k_p + h' d_p)}$$

$$h' = h_{pg} + h_r + h_p$$

$$h_r = k_r' \frac{(2k_p + h' d_p)}{d_p k_p}$$

$$h_p = k_p' \frac{(2k_p + h' d_p)}{d_p k_p}$$

$$\log(k_p'[W/mK]^{-1}) = -1.52 + 0.00746\,[W/mK]^{-1}\,\frac{k_p}{\epsilon}$$

Table 3.1-1 (Continued)

Argo and Smith (1953): (continued)
For $t < 300^{\circ}C$:

$$k_e = \varepsilon(k' + k'_{td}) + \frac{(1 - \varepsilon)\, k_p(d_p h' + 2k'_p)}{d_p h' + 2k_p}$$

Kunii and Smith (1961)

General:

$$\frac{h_{pg} d_p}{k_g} = \frac{(N_{Pr} N'_{Re})^2}{6(1 - \varepsilon)} \frac{\left(1 - \varepsilon \frac{k_g}{k_e}\right)}{\frac{k_e}{k_g}\left[\frac{k_e}{k_e^*}\left(1 - \varepsilon \frac{k_g}{k_e}\right)^{-1}\right]}$$

For gases of low k_g:

$$\frac{k_e}{k_e^*} = \frac{1}{2}\left\{1 + \left[1 + \frac{2}{3(1 - \varepsilon)} \frac{(N_{Pr} N'_{Re})^2}{\frac{k_e^*}{k_g} N_{Nu}}\right]^{1/2}\right\}$$

Table 3.1-2 Range of Validity and Specific Correlations Proposed for the Particle-to-Gas Heat Transfer Coefficient, h_{pg}

Gamson, Thodos, and Hougen (1943)

$$\frac{h_{pg}}{c_p G_o}\left(\frac{c_p \mu_g}{k_g}\right)^{2/3} = 1.95\left(\frac{d_p G_o}{\mu_g}\right)^{-0.51} ; \qquad \frac{d_p G_o}{\mu_g} < 350$$

$$\frac{h_{pg}}{c_p G_o}\left(\frac{c_p \mu_g}{k_g}\right)^{2/3} = 1.06\left(\frac{d_p G_o}{\mu_g}\right)^{-0.41} ; \qquad \frac{d_p G_o}{\mu_g} > 350$$

Glaser and Thodos (1958) $\qquad 100 \leq N'_{Re} \leq 9200$

$$j_{Ho} = \frac{0.535}{(N'_{Re})^{0.30} - 1.6}$$

$$\frac{j_H}{j_{Ho}} = 1 + \frac{\sqrt{S_p}}{D_t} \log \frac{4984}{(N'_{Re})^{0.933}} ; \qquad \text{spheres}$$

$$\frac{j_H}{j_{Ho}} = 1 + \frac{\sqrt{S_p}}{D_t} \frac{23.1}{(N'_{Re})^{0.626}} ; \qquad \text{cubes}$$

$$\frac{j_H}{j_{Ho}} = 1 + \frac{\sqrt{S_p}}{D_t} \frac{10.78}{(N'_{Re})^{0.384}} ; \qquad \text{cylinders}$$

Table 3.1-2 (Continued)

Baumeister and Bennett (1958) $\quad 200 \leq N'_{Re} \leq 10{,}000$

$$j_H = a'(N'_{Re})^{b'}$$

$$a' = 0.918\{1 + 0.0148[\exp 0.565(18 - D_t/d_p)]\}$$

$$b' = -0.267 - \frac{0.257}{D_t/d_p - 8.70}$$

McConnachie and Thodos (1963) $\quad 70 \leq \frac{d_p G_o}{\mu_g(1 - \varepsilon)} \leq 7000$

$$j_H = \frac{1.192}{(N'_{Re})^{0.41} - 1.52}$$

Gupta, Chaube, and Upadhyay (1974) $\quad 10 \leq N'_{Re} \leq 10{,}000$

$$\varepsilon j_H = \frac{2.786}{(N'_{Re})} + \frac{0.3023}{(N'_{Re})^{0.35}}$$

Table 3.1-2 (Continued)

Cybulski, Van Dalen, Verkerk, and Van Den Berg (1975) $0.24 \leq N'_{Re} \leq 0.63$

$$\frac{h_{pg} d_p}{k_g} = 0.07\ N'_{Re}$$

Bhattacharyya and Pei (1975) $100 \leq N'_{Re} \leq 800$

$$\frac{h_{pg}}{c_p G_0}\left(\frac{c_p \mu_g}{k_g}\right)^{2/3} = 0.018\left[\frac{N_{Ar}(1-\varepsilon)^2}{(N'_{Re})^2}\right]^{0.25}$$

$$N_{Ar} = \frac{d_p^3 g \rho_g (\rho_p - \rho_g)}{\mu_g^2}$$

Table 3.1-3 Theoretical Predictions of the Effective Thermal Conductivity Based Upon Simple Heat Transfer Mechanisms

---

Ranz (1952)

$$k_e^t = \frac{\alpha G_o c_p}{N}$$

Yagi and Kunii (1957)

General:

$$\frac{k_e^t}{k_g} = (\alpha\beta)\, N'_{Re} N_{Pr}$$

$$\frac{k_e^o}{k_g} = \delta_1 \frac{k_p}{k_g} + \frac{(1 - \varepsilon - \delta_1)\,\beta}{\gamma \frac{k_g}{k_p} + \frac{1}{\frac{1}{\phi} + \frac{d_p h_{rs}}{k_g}}} + \varepsilon\beta \frac{d_p h_{rv}}{k_g}$$

$$h_{rs} = 4 \left(\frac{e}{2 - e}\right) \sigma T_a^3$$

$$h_{rv} = 4\left(\frac{1 - e}{e}\right)\left[1 + \frac{\varepsilon}{2(1 - \varepsilon)}\right] \sigma T_a^3$$

Fine Particles with Gas Filled Voids:

$$\frac{k_e^o}{k_g} = \frac{(1 - \varepsilon)\,\beta}{(k_g/k_p) + \phi}$$

Table 3.1-3 (Continued)

Kunii and Smith (1960)

General:

$$\frac{k_e^o}{k_g} = \varepsilon\left(1 + \frac{\beta h_{rv} d_p}{k_g}\right) + \frac{\beta(1-\varepsilon)}{\frac{1}{\frac{1}{\phi}\frac{d_p(h_p + h_{rs})}{k_g}} + \gamma\frac{k_g}{k_p}}$$

Neglectable Radiation and Point of Contact Conduction:

$$\frac{k_e^o}{k_g} = \varepsilon + \frac{\beta(1-\varepsilon)}{\phi + \gamma\frac{k_g}{k_p}}$$

$$\phi = \phi_2 + (\phi_1 - \phi_2)\frac{(\varepsilon - \varepsilon_2)}{(\varepsilon_1 - \varepsilon_2)} \quad ; \quad \varepsilon_1 \geq \varepsilon \geq \varepsilon_2$$

$$\phi = \phi_1 \quad ; \quad \varepsilon > \varepsilon_1 \quad ; \quad \varepsilon_1 = 0.476$$

$$\phi = \phi_2 \quad ; \quad \varepsilon < \varepsilon_2 \quad ; \quad \varepsilon_2 = 0.260$$

Table 3.1-3 (Continued)

Willhite, Kunii, and Smith (1962)

$$\frac{k_e^o}{k_g} = 1 + (1 - \varepsilon)\left(1 - \frac{k_g}{k_p}\right) + \frac{\gamma}{\alpha}\left(1 - \frac{k_g}{k_p}\right)^2 (1 - \varepsilon)$$

$$\frac{1}{2n}\left(1 - \frac{k_g}{k_p}\right)^2$$

$$\alpha = \frac{}{\ln\left[\frac{k_p}{k_g} - \left(\frac{k_p}{k_g} - 1\right)\left(1 - \frac{1}{n}\right)^{1/2} - \left(1 - \frac{k_g}{k_p}\right)\left[1 - \left(1 - \frac{1}{n}\right)^{1/2}\right]\right]}$$

$$n = \frac{15.03 - 25.26\ \varepsilon}{1.91 - 1.91\ \varepsilon}$$

Specchia, Baldi, and Sicardi (1980)

$$\frac{k_e^o}{k_g} = \varepsilon + \frac{\beta(1 - \varepsilon)}{\phi + \gamma\frac{k_g}{k_p}}$$

$$\phi = 0.220\ \varepsilon^2$$

Specchia and Sicardi (1980)

$$\frac{k_e^o}{k_g} = \frac{\varepsilon}{1.5} + \frac{\beta(1 - \varepsilon)}{\phi + \gamma\frac{k_g}{k_p}}$$

$$\phi = 0.130\ \varepsilon^{1.44}$$

Table 3.1-3 (Continued)

Bhattacharyya and Pei (1975)

$$\frac{h_d}{c_p G_o}\left(\frac{c_p \mu_g}{k_g}\right)^{2/3} = (2.05 \times 10^{-5})\ \frac{\rho_p c_p}{\rho_g c_{pp}}$$

Table 3.1-4 Models Proposed for the Static Effective Thermal Conductivity at Low Pressure

---

Schotte (1960)

$$\frac{k_r}{k_g} = \frac{\epsilon h_r d_p}{k_g} + \frac{1 - \epsilon}{\frac{k_g}{h_r d_p} + \frac{k_g}{k_p}}$$

Masamune and Smith (1963)

$$k_e^o = \alpha^* \epsilon\, k_g + \frac{(1 - \alpha^* \epsilon)(1 - \delta)}{\frac{\phi}{k_g} + \frac{1-\phi}{k_p}} + (1 - \alpha^* \epsilon)\delta\, k_p$$

$$\alpha^* = 1 - \frac{3}{2}\left(\frac{1 - \epsilon}{\epsilon}\right)\phi$$

$$\phi = n\left[1 - \left(\frac{\pi}{2} - \theta_2\right)\tan\theta_2\right](\sec\theta_2 - 1)^2$$

$$\cos\theta_2 = \left(1 - \frac{1}{n}\right)$$

$$n = 13.56 - 12.51\epsilon$$

$$\delta = \left(\frac{1}{1 - \alpha^* \epsilon}\right)\frac{k_e^v}{k_p}$$

Table 3.1-4 (Continued)

Imura and Takegoshi (1974)

$$k_e^o = \varepsilon'(k_g' + k_p h_r) + \frac{(1 - \varepsilon' - \delta^*)}{\frac{1}{k_g'/\phi + d_p h_r} + \frac{1 - \phi}{k_p}} + \delta^* k_p$$

$$h_r = 4e\sigma T_a^3$$

$$\varepsilon' = \frac{\varepsilon - \phi}{1 - \phi}$$

$$k_e^v = (1 - \delta^*)\, d_p h_r + \delta^* k_p$$

$$\phi = 0.3\, \varepsilon^{1.6} \left(\frac{k_p}{k_g}\right)^{-0.044}$$

Table 3.1-5 Models of k_e^o Based Upon Numerical Solutions

Dietz (1979)

$$\frac{k_e^o}{k_p} = 1.14 \left(\frac{k_p}{k_g}\right)^{1/2} \frac{K_0\left(\left[40\ \frac{k_n}{k_p}\right]^{1/2}\right)}{K_1\left(\left[40\ \frac{k_g}{k_p}\right]^{1/2}\right)}$$

Krupiczka (1967)

$$k_e^o = \left(\frac{k_p}{k_g}\right)^{A' + B' \log (k_p/k_g)}$$

$$A' = 0.280 - 0.757 \log \epsilon$$

$$B' = -0.057$$

Wakao and Katao (1969)

$$h_r = \frac{2}{2/e - 0.264}\ 4\sigma T_a^3$$

$$\frac{k_r}{k_g} = 0.707\ (N_{Nu}^r)^{0.96} \left(\frac{k_p}{k_g}\right)^{1.11}; \qquad 20 \leq \frac{k_p}{k_g} \leq 1000,\ 0 \leq N_{Nu}^r \leq 0.3$$

$$\frac{k_r}{k_g} = 1.3\ N_{Nu}^r \frac{k_p}{k_g}; \qquad 10 \leq \frac{k_p}{k_g} \leq 500,\ 0 \leq N_{Nu}^r \leq 0.1$$

Table 3.1-5 (Continued)

Wakao and Vortmeyer (1971)

$$\tau' = \frac{(d_p/\lambda_0)\ (p/p_0)}{2(2 - \alpha')/\alpha'}$$

$$k_{rad} = k_{rad}^{\infty} \cdot f'$$

$$k_{contact} = 0.18\ \Lambda \quad ; \quad \Lambda < 0.03$$

Table 3.2-1 Models of the Wall Heat Transfer Coefficient

Yagi and Kunii (1961)

$$\frac{h_w d_p}{k_g} = \frac{h_w^o d_p}{k_g} + \frac{1}{\frac{1}{h_w^* d_p / k_g} + \frac{1}{\alpha_w N_{Pr} N_{Re}}}$$

$$\frac{1}{h_w^o d_p / k_g} = \frac{1}{k_w^o / k_g} - \frac{0.5}{k_e^o / k_g}$$

$$\frac{k_w^o}{k_g} = \varepsilon_w \left(2 + \frac{h_{rv} d_p}{k_g}\right) + \frac{1 - \varepsilon_w}{\frac{1}{\frac{1}{\phi_w} + \frac{h_{rs} d_p}{k_g}} + \gamma_w \frac{k_g}{k_p}}$$

$$\frac{h_w^* d_p}{k_g} = 4.0 (N_{Pr})^{1/3} (N'_{Re})^{0.5}$$

Specchia, Baldi, and Sicardi (1980)

$$\frac{h_w^o d_p}{k_g} = 2\varepsilon + \frac{1 - \varepsilon}{\phi_w + \gamma_w \frac{k_g}{k_p}}$$

$$\phi_w = 0.00240 \left(\frac{D_t}{d_p}\right)^{1.58}$$

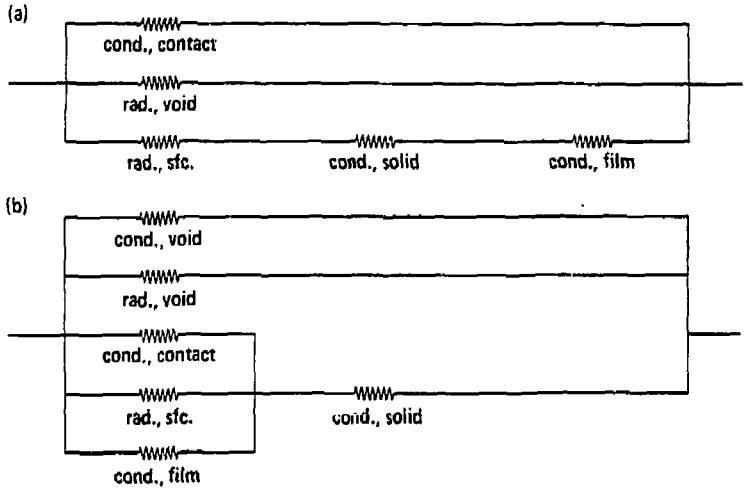

Figure 3.1-1. (a) Arrangement of thermal resistances postulated in the model of Yagi and Kunii (1957). (b) Arrangement of thermal resistances postulated in the model of Kunii and Smith (1960).

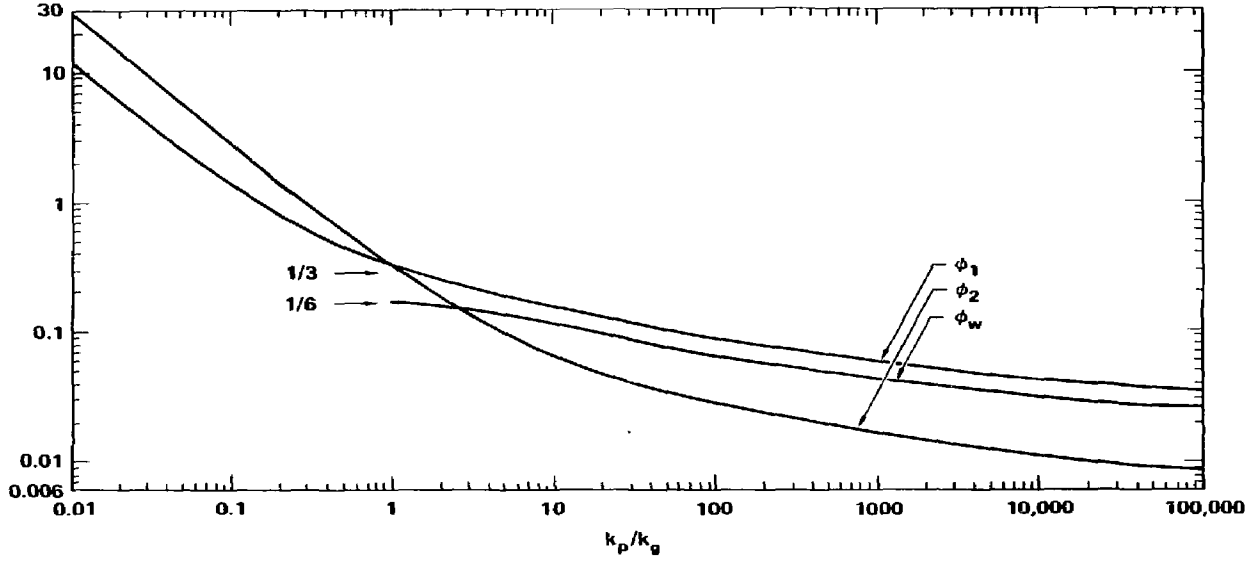

Figure 3.1-2. The parameters ϕ_1 and ϕ_2 derived by Kunii and Smith (1960). The parameter ϕ_w derived by Yagi, Kunii, and Wakao (1961).

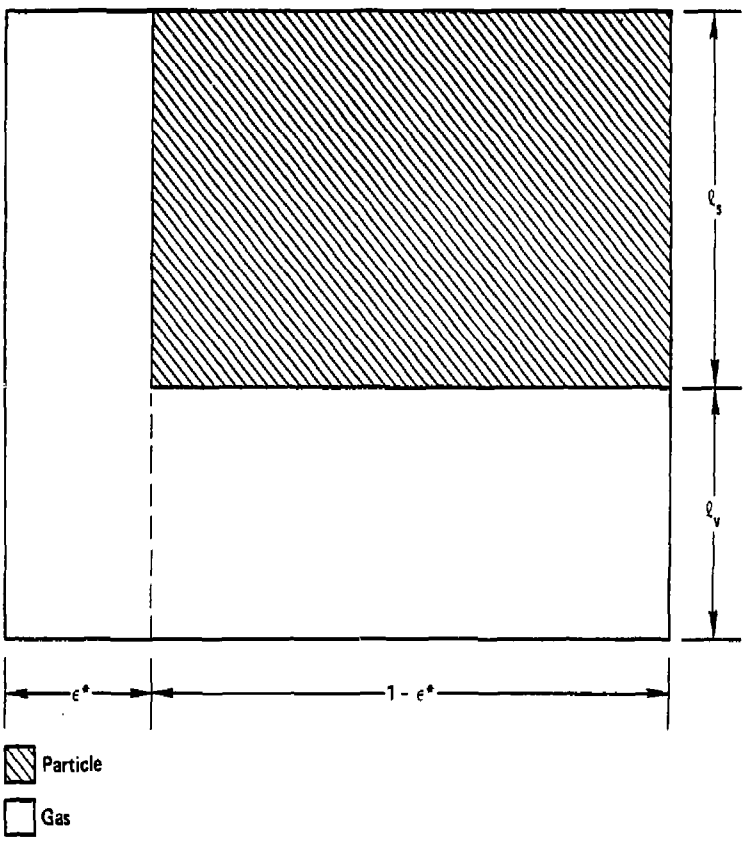

Figure 3.1-3. Heat transfer area fractions postulated in the model of Willhite, Kunii, and Smith (1962).

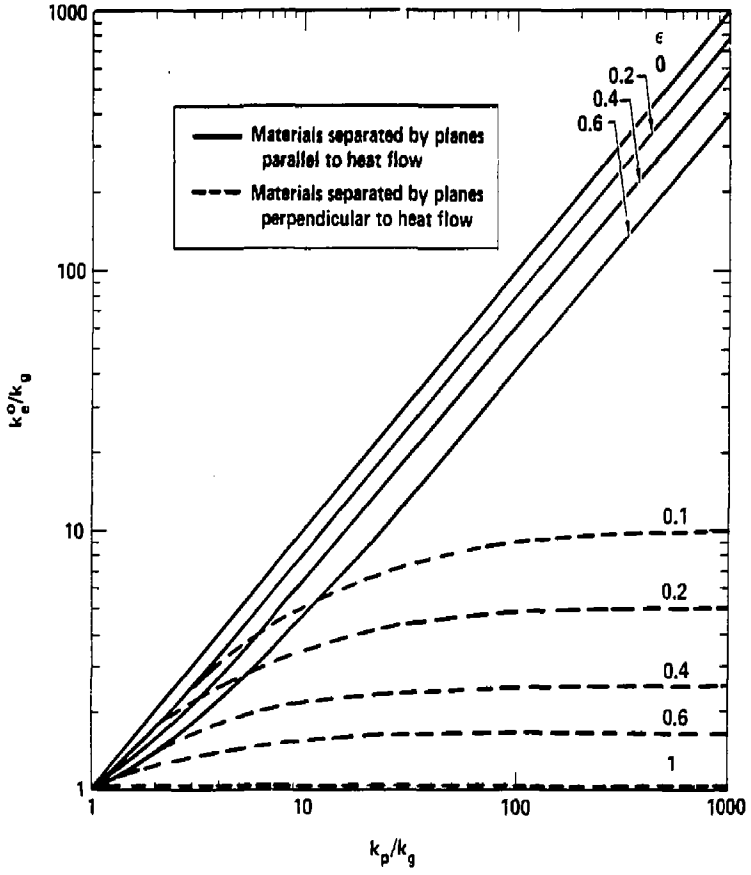

Figure 3.1-4. Minimum and maximum static effective thermal conductivities of two-phase systems derived by Deissler and Boegli (1951).

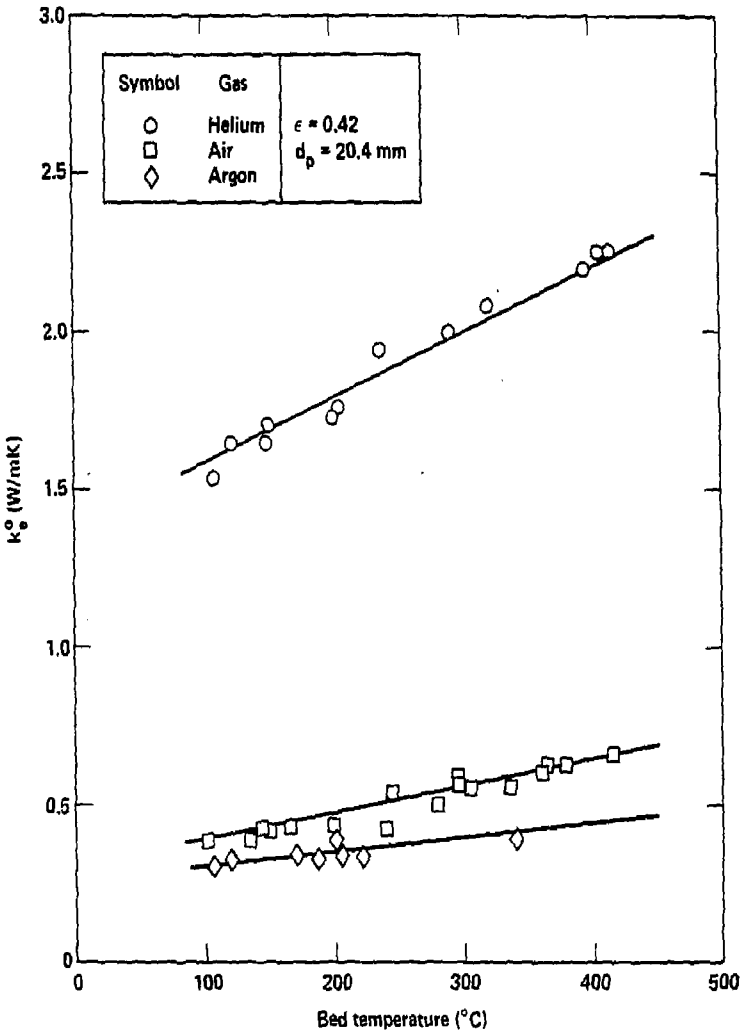

Figure 3.1-5. Static effective thermal conductivity of magnesium oxide powder reported by Deissler and Boegli (1951).

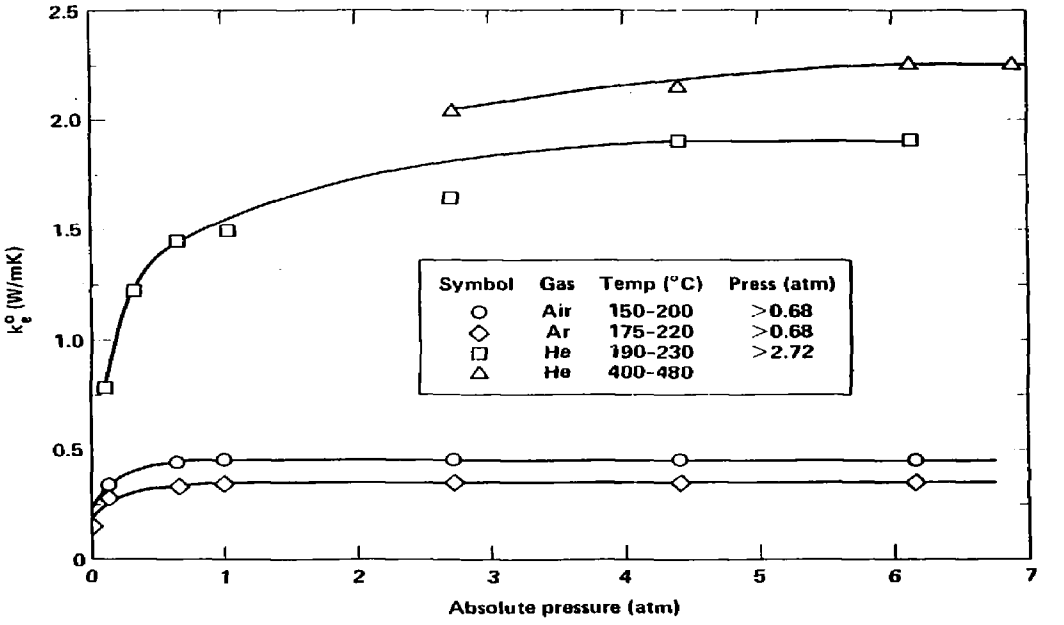

Figure 3.1-6. **Effect of gas pressure on static effective thermal conductivity of magnesium oxide powder reported by Deissler and Boegli (1951).**

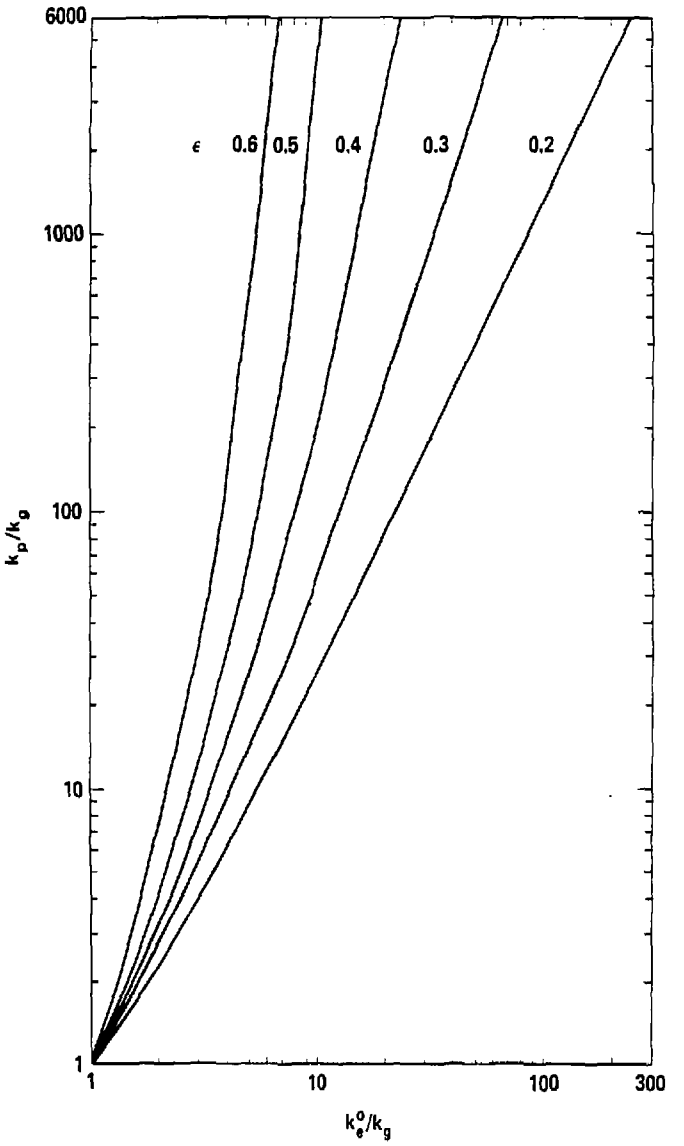

Figure 3.1-7. Static effective thermal conductivity correlation of Deissler and Eian (1952) reported by Schotte (1960).

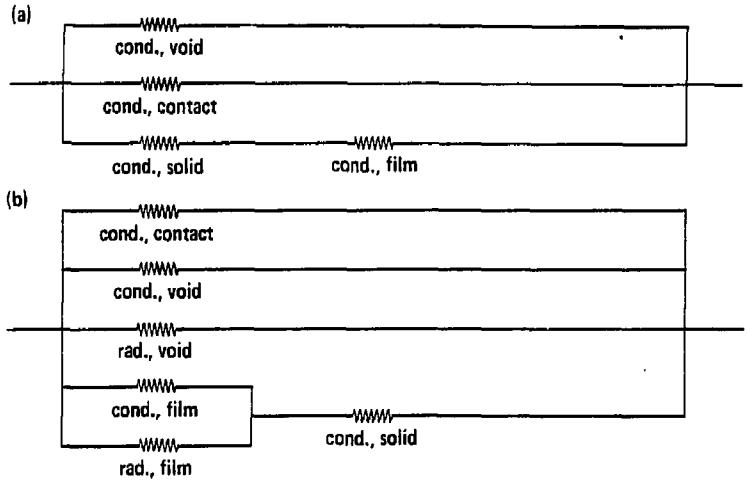

Figure 3.1-8. (a) Arrangement of thermal resistances postulated in the model of Masamune and Smith (1963). (b) Arrangement of thermal resistances postulated in the model of Imura and Takegoshi (1974).

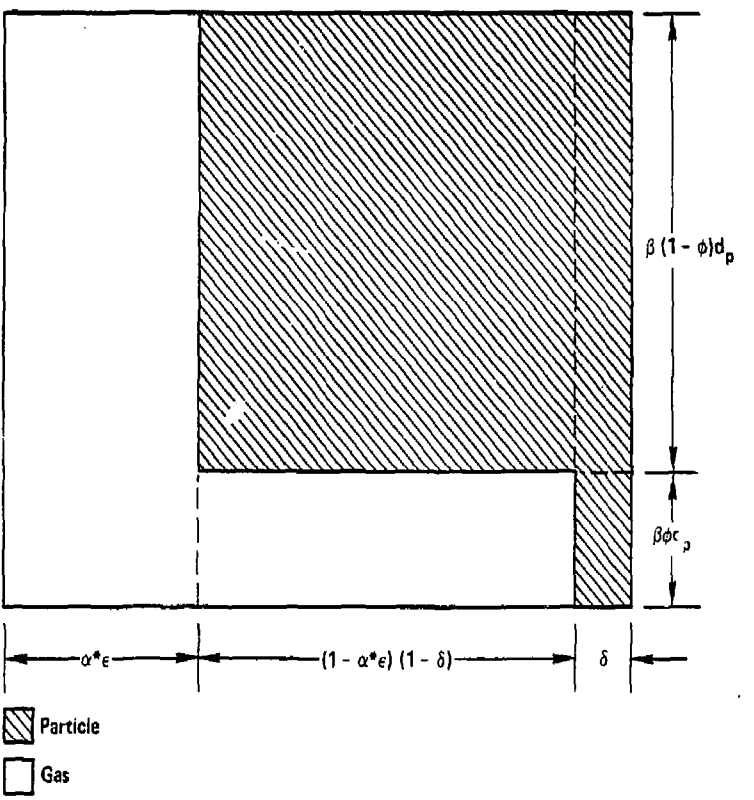

Figure 3.1-9. Heat transfer area fractions postulated in the model of Masamune and Smith (1963).

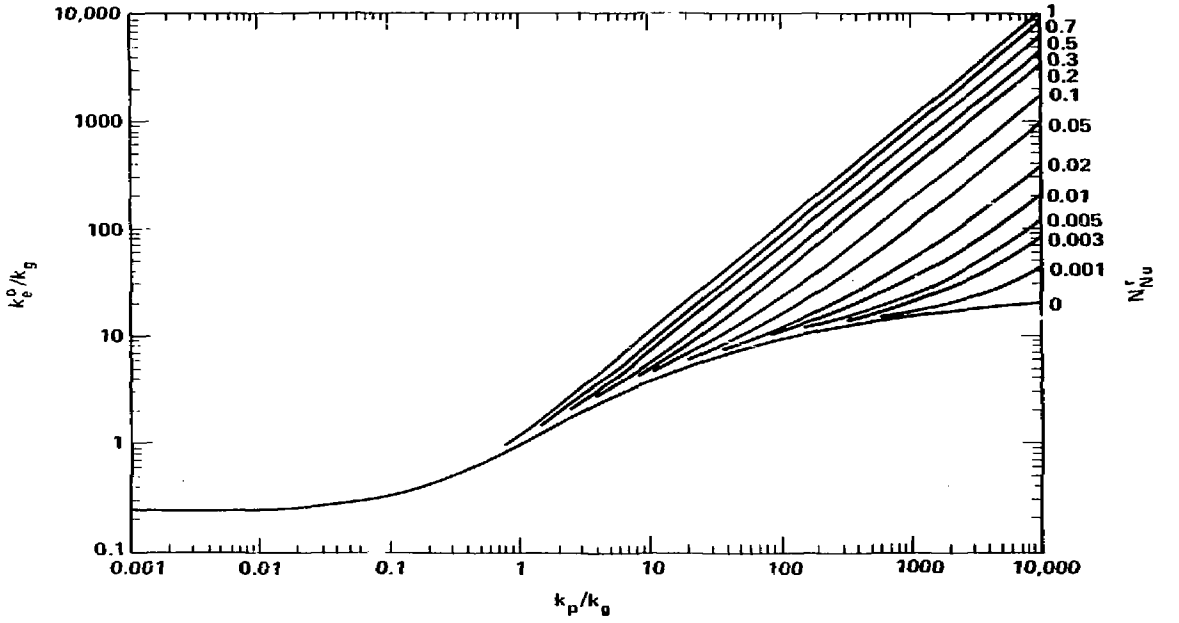

Figure 3.1-10. Static effective thermal conductivity by combined conduction and radiation for an orthorhombic lattice of spheres contacting only at a point as derived by Wakao and Kato (1969).

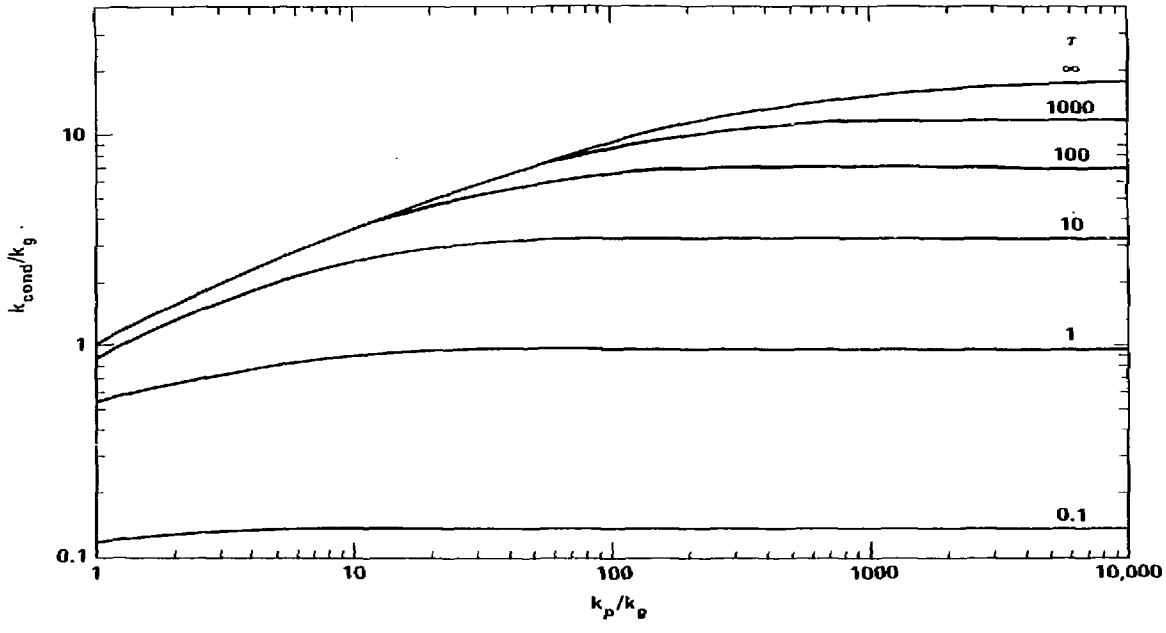

Figure 3.1–11. Pressure dependence of the gas–solid conduction contribution to the static effective thermal conductivity in the model of *Wakao and Vortmeyer (1971).*

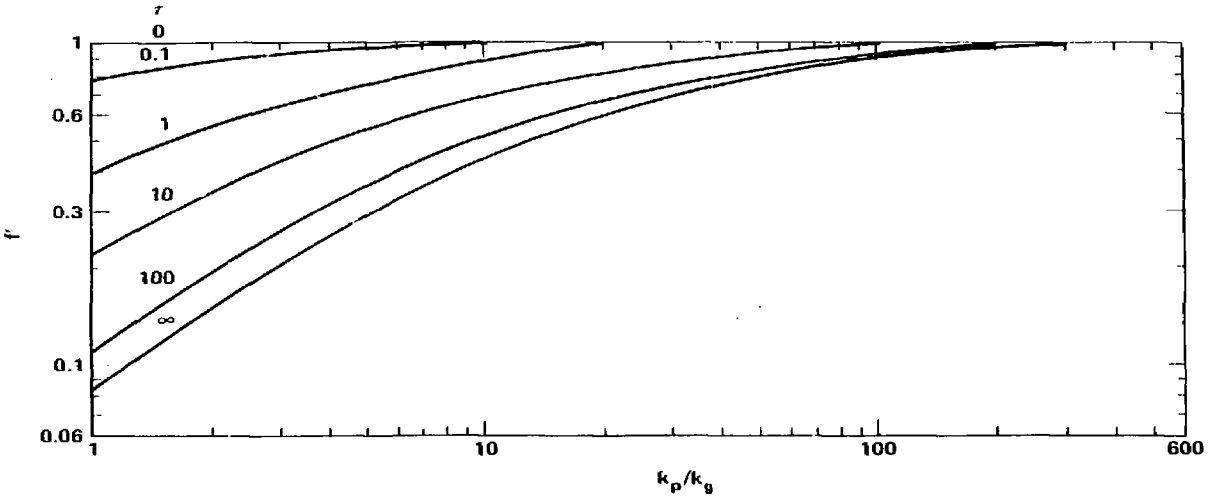

Figure 3.1-12. Correction factor f' accounting for pressure dependence of the radiant contribution to the static effective thermal conductivity in the model of Wakao and Vortmeyer (1971).

CHAPTER 4

FALLING BED HEAT TRANSFER

As was seen in Chapters 2 and 3, much work has been presented in the literature for stationary packed beds with either stagnant or flowing gas. Much less work, on the other hand, has been presented for packed particle beds falling through tubes. Only three experiments on this topic have been reported in the literature. The first two to be discussed were concerned with packed beds falling past flat plates immersed in the tubes; the heat transfer mechanism in these experiments was reported in terms of the average convective heat transfer coefficient between the respective plate surfaces and the surrounding granular material. These experiments will be reviewed in Section 4.1. The correlations presented are listed in Table 4.1-1. The most interesting experiment, so far as this investigation is concerned, is presented in Section 4.2. Comparisons between the effective thermal conductivity for both stationary and flowing packed beds were made. Also, experiments were conducted to observe the velocity profile in a falling bed; comparison to that obtained with fluid flow was made.

4.1 Falling Bed - Flat Plate Heat Transfer

As was mentioned above, the two investigations to be discussed here presented data for the convective heat transfer coefficient in packed particle beds falling past heated flat plates. The heat transfer

coefficient was treated as an average quantity over the surface of the plate and was defined in terms of the average local temperature difference.

Sullivan and Sabersky (1975) studied the convective heat transfer from a flat plate immersed in granular media flowing through a tube. The data were correlated in a form similar to an equation derived by Sullivan and Sabersky based upon a simplified model (Table 4.1-1). Here, χ was correlated for each experiment and was a function of k_g/k_p, L^o/d_p, and ε. The parameter χ was found to be between 0.01 and 0.06 for glass beads and between 0.037 and 0.062 for mustard seed.

Denloye and Botterill (1977) discovered that simultaneous countercurrent flow of gas upwards through a falling bed markedly influenced the flow behavior. The mean temperature difference between the heat transfer surface and the bed varied by less than 10% across the length of the surface which was centered in the middle of a rectangular tube. Therefore, the heat transfer coefficient was based upon the simple arithmetic average of the temperature difference. The heat transfer coefficient was correlated in term of the Archimedes number.

4.2 Comparison of Falling Bed Experimental Results to Known Physical Phenomena

The above experiments were quite interesting; however, they did not provide for the estimation of any local characteristics. Only the

average heat transfer coefficient for heat flow from the immersed plate was presented. Furthermore, all of the experiments discussed in Chapter 2 were for packed beds contained by a heat transfer barrier. Even for falling packed bed apparatus, this could be envisioned to be the more useful type of arrangement.

Only one experiment has been conducted in which the falling packed bed was heated by the tube through which it was flowing. The heat transfer parameters describing this system were compared to those which describe stationary packed bed systems. In addition, the flow characteristics of the falling packed bed were compared to the classical results for fluid flow in circular tubes. Such comparisons are useful in developing theoretical descriptions of these systems.

Brinn, Friedman, Gluckert, and Pigford (1948) measured the bulk density in both settled and stationary packed beds of Ottawa sand and crushed Ilmenite ore. They found that the bulk density of the Ottawa sand was approximately the same in both types of beds. For the Ilmenite sand, however, the bulk density was found to be slightly greater in the case of the moving bed. This was explained as an indication of closer packing of the smaller particles while in motion.

Experiments with falling beds demonstrated that the particles flowed with rod-like velocity profiles. The velocity was found to be uniform across the tube diameter except near the wall where it was found to be 15 to 20% lower.

Data for the effective thermal conductivity in both stationary and falling beds were obtained and compared. Theoretical curves for the temperature profile of a pseudofluid with rod-like flow and a constant wall temperature were used to calculate the effective thermal conductivities from the experimental data. It was found that k_e obtained in the falling bed and in the stationary bed with stagnant gas agreed to within 10%.

Such results are very important from the theoretical standpoint. They suggest that the models proposed in Chapter 3 for stationary beds with stagnant gas may be used to predict the effective thermal conductivity in a falling bed. Furthermore, these results suggest that the classical expressions for laminar fluid flow in tubes may be used to describe the system once the flat velocity profile has been accounted for. This is the basis for treatment of falling packed bed heat transfer that will be presented here in Chapter 5. The expressions that describe this type of fluid flow are derived in Appendix 2.

Table 4.1-1 Range of Validity and Specific Correlations Presented for the Convective Heat Transfer Coefficient in Falling Packed Beds Flowing Past Flat Plates

Sullivan and Sabersky (1975)	$2 \leq \frac{L^0 v_0 \rho_p c_{pp}}{k_p} \leq 4000$
	$\frac{h_L L^0}{k_p} = \frac{1}{X + \frac{\sqrt{\pi}}{2}\left(\frac{L^0 v_0 \rho_p c_{pp}}{k_p}\right)^{-1/2}}$
Denloye and Botterill (1977)	$10^3 \leq N_{Ar} \leq 10^6$
	$\frac{h_L d_p}{k_g} = 1.283(N_{Ar})^{0.162}$

CHAPTER 5

FALLING PARTICLE BED EXPERIMENTAL RESULTS

This chapter will discuss the experimental results obtained in this investigation on the heat transfer characteristics of gravity flowing particle beds. A heat transfer loop has been constructed through which glass microspheres have been allowed to flow by gravity at controlled rates through an electrically heated stainless steel tubular test section. It has been the aim of this investigation to determine experimentally the heat transfer coefficient and Nusselt number for flowing particle beds as functions of the average bed velocity, heat flux, channel geometry, and particle size. The effect of heat flux was studied in order to account for the radiative contribution. Such information is necessary for the design of moving particle bed type fusion reactor blankets and associated tritium recovery systems as discussed in Chapter 1.

The experimental equipment and procedure are described in Section 5.1. In Section 5.2 the experimental results are presented. Conclusions and recommendations for further research are discussed in Section 5.3

5.1 Experimental Equipment and Procedure

5.1.1 Experimental Equipment

Figure 5.1-1 is a schematic diagram of the heat transfer loop. Solid soda-lime glass particles of controlled size distribution

flowed by gravity from the upper storage tank through an entrance region 29 cm in length before entering the test section. The test section used was an electrically heated Type 321 stainless steel tube 54 cm in length. Several tubes with various diameters have been used. From the test section, the particles flowed through a 36 cm exit length of the same diameter into the lower collection tank. The particles were manufactured by Cataphote Division of Ferro Corporation and the characteristics of the three particle sizes studied are presented in Table 5.1-1.

The particle flow rate through the test section was controlled by means of a sliding cone valve assembly located at the lower end of the tube exit region. The particles were periodically collected in a stainless steel bucket over a measured period of time. The mass flow rate was then computed from the weight of the particles collected during this time.

The particles flowed continuously through the test section and were then cooled and returned to the upper storage tank via a counter flow shell and tube heat exchanger. This return was accomplished by a large suction pump located on the top of the upper storage tank and was aided by injection of high-pressure air into the shell side of the heat exchanger. The particle return heat exchanger and the upper storage tank inlet were lined with high strength glass to minimize erosion of the loop by the particles. A photograph of the loop is shown in Figure 5.1-2.

Each tube was heated by passing electric current from a 50 kW DC power supply through the tube's wall. The power input was controlled by a resistor bank placed in series with the tube resistance. The test section was thermally insulated from the outside by a cylindrical composite wall of which the outer layer was made of fiberglass. For the two smaller tubes this outer layer was 5.1 cm thick while it was 3.8 cm thick for the large tube. The inner layer of insulation for the two smaller tubes was made of high temperature, organic impregnated, fibrous glass 7.6 cm in diameter. For the large tube, the inner insulation material was composed of rigid, hydrous calcium silicate 10.2 cm in diameter.

The test section was electrically insulated from the entrance and exit regions and the support frame by mounting the ends of the tube in Aremcolox ceramic sleeves placed on horizontal asbestos-concrete boards. The sleeves allowed the test section to expand freely in the vertical direction when it was heated and were machined to the same inside diameter as that of the test section.

The wall temperature distribution along the flow direction was measured by means of Chromel-Alumel thermocouples spot welded onto the outer tube surface. A photograph of the test section with the thermocouples and composite wall exposed is presented in Figure 5.1-3. A thermocouple was also used to measure the particle inlet bulk temperature; these temperatures were recorded on a twenty channel continuously scanning Type K Honeywell chart recorder.

The power input to the test section was determined by measuring the voltage drop across the tube and the current through a shunt in series with the tube resistance. Standard volt meters were used in this regard. The wall temperature distribution, power input, and particle bulk inlet temperature were used to determine the local and average heat transfer coefficients for the test section.

For some of the experimental cases, the radial temperature distribution of the particles was also measured at the exit of the exit section just upstream of the flow control valve by means of a Chromel-Alumel thermocouple probe mounted on a micrometer assembly. The output of this probe was measured using a Fluke digital thermometer.

5.1.2 Experimental Procedure

The experiment was operated in a steady state mode by continuously circulating the particles through the loop. The experiment was conducted for different power levels, particle sizes, tube diameters, and flow rates. Table 5.1-2 lists the range of experimental variables examined in these experiments.

Initially, the complete inventory of glass particles was placed in the lower collection tank. The heat exchanger cooling water and air injection were first turned on. With the control valve closed, the glass particles were then pumped to the upper storage tank. Once the lower collection tank had been emptied, the suction pump was momentarily shut off to allow the tube above the control valve

to become packed with particles. The suction pump was once again started and the control valve was adjusted to the position corresponding to the highest desired flow rate. The particles were circulated around the loop without heating for approximately thirty minutes to establish steady state flow conditions. The resistor bank connected in series with the test section was adjusted to obtain approximately the desired power input to the tube. The power supply was turned on and its controls were used to obtain the desired heat flux. The particle radial exit temperature profile probe, when it was used, was placed at the tube wall. The exit temperature, the axial wall temperatures, and the power level were monitored until steady state conditions were reached. This required approximately one hour. At that time, all the wall temperatures, power input, and the particle bulk inlet temperature were recorded. The flow rate was measured by collecting the particles in the stainless steel container over a measured period of time. In experiments utilizing the radial exit temperature profile probe, the profile was measured by moving the micrometer-mounted probe at approximately 0.06 cm radial intervals across the entire tube diameter. The flow rate was again measured with the probe fully inserted.

At this point, preparations were made to conduct the experiment at the next lower flow rate. The control valve was constricted to obtain the required mass flow. Again, the temperatures and power were monitored until the new steady state conditions were reached.

This required a waiting period of about forty-five minutes. Experiments at lower mass flow rates followed. The total number of flow rates studied varied with each tube size, particle size, and power level.

The resistor bank was adjusted and the above data were collected for the other two power levels. The loop was thoroughly cleaned and all three power levels were repeated for the additional particle sizes. When all the data were collected, the test section was replaced with one of the other tubes and the tests were repeated.

5.2 Experimental Results

5.2.1 Data Reduction

The void fractions were obtained as follows. A known mass of particles was introduced into the known volume of each of the three tubes. Due to the small tubes involved, calculations were based upon ten, seven, and four times the normal volume of packing contained in the 9.53, 14.29 and 25.40 mm tubes respectively. The published density for solid soda-lime glass of 2.51 g/cm^3 gave the nonvoided volume and therefore the void fraction. The void fraction for each combination of particle size and tube studied is listed in Table 5.2-1. A similar method was used to obtain the bulk particle density; a known volume of material was collected and weighed in a graduated cylinder. The density was found to be 1.455, 1.469, and 1.485 g/cm^3 for the 608, 304, and 203 particles respectively. The results of Brinn, Friedman, Gluckert, and Pigford (1948) suggest

that these data collected for stationary beds are applicable to flow conditions also.

The method used in calculating the particle mass flow was discussed in the last section. In the experiments which utilized the radial exit temperature profile probe, the mass flow was found to be the same when the probe was in either the full in or full out position. The particle mass velocity used in the calculation of the pseudohomogeneous Peclet number was obtained in the usual fashion; the flow was treated as a continuum and G_0 was based upon the mass flow and the tube diameter. The superficial particle velocity was then based upon the particle mass velocity and the particle density. An outline of the experimental program with the various combinations of these experimental variables is presented in Table 5.2-2.

When using the micrometer-mounted radial exit temperature thermocouple probe, no mechanism was used to detect the actual radial position within the bed. Instead, temperatures were measured across the entire tube diameter. The minimum temperature detected was taken to occur on the axis of the packed tube and r/R was computed accordingly.

The test section has been divided along the flow direction using a finite difference scheme. Twenty-six nodes were utilized in the 14.3 mm tube cases as opposed to thirty-two nodes for the other two tubes. Half of these nodes were distributed along the tube wall; horizontally adjacent to these, the other half were located along the axis in the flowing packed bed. The following effects have been

accounted for: i) variation of specific heat capacity with particle bulk exit temperature; ii) variation of nodal tube length and diameter with local wall temperature; iii) variation of nodal tube resistance with temperature and its impact on the local heat flux values; and iv) radiation losses from the tube wall to the particles.

The data for the variation of the physical properties with temperature used in the above analyses were obtained from the literature and are discussed in Appendix 1. Analysis showed that neglecting ii) above led to a minimum error of 6% in computing the local heat flux; neglecting iii) above led to an error of up to 30% A one-dimensional heat balance demonstrated that the temperature differed by less than 1.5^{o}C between the inner and outer wall; further analysis was therefore based upon the measured outer wall temperature profiles. Computation showed that the air which was carried in the voids of the packed bed provided negligible heat capacity. Heat losses from the outside surface of the composite cylindrical insulation were found to be small and were, therefore, neglected.

An energy balance over each node of the test section using the known power input, particle flow rate, and bulk inlet temperature was used to calculate the bulk particle temperature profile.

A gray body formulation was used to compute the local radiative heat flux. The configuration factor between any given tube wall node and the adjacent particle node was taken to be unity so that:

$$q''_{ri} = e\sigma(t^4_{wi} - t^4_{pi}) \qquad (5.2\text{-}1)$$

The above formulation assumed the particle bed to behave as a black body. Siegel and Howell (1972) quote the range of emissivity for stainless steel as being between approximately 0.2 and 0.4. Analysis revealed that the radiative contribution to the total heat flux was less than 4% and was very insensitive to the exact value of the emissivity; because of this, an average value of 0.3 was used throughout. The local convective heat flux was obtained as the difference between the total and radiative contributions:

$$q''_{ci} = Q \frac{R_i}{R_{tot}} \frac{1}{\pi D_i L_i} - q''_{ri} \tag{5.2-2}$$

The average convective heat flux was based upon all but the end nodes:

$$q''_{c,ave} = \sum_i \frac{q''_{ci} \pi D_i L_i}{A} \tag{5.2-3}$$

The local and average convective heat transfer coefficients were based upon the local and logarithmic-mean temperature differences, respectively:

$$h_{loc,i} = \frac{q''_{ci}}{t_{wi} - t_{pi}} \tag{5.2-4}$$

$$\bar{h}_c = \frac{q''_{c,ave}}{\Delta t_{ln}} \tag{5.2-5}$$

The experimental data for the local convective heat transfer coefficient profiles were then compared to theory as follows. The results of Brinn, Friedman, Gluckert, and Pigford (1948) suggest that the effective thermal conductivity of any flowing packed bed is the same as k_e^o in a stationary packed bed of the same material and gas; the particle and gas conductivities, which were obtained from the literature, and the void fraction were thus used to obtain the theoretical static effective conductivity predicted by six of the models that were discussed in Chapter 3. The models studied were those proposed by Yagi and Kunii (1957), Kunii and Smith (1960), Willhite, Kunii, and Smith (1962), Krupiczka (1967), Specchia, Baldi, and Sicardi (1980), and by Specchia and Sicardi (1980). These theoretical conductivities were combined with the local heat transfer coefficient profiles to obtain six experimental Nusselt number profiles. Each of these were expressed in terms of the nondimensional axial positions given by:

$$x^+ = \left(\frac{x}{2R}\right)\left[N_{Re}\ N_{Pr}\right]^{-1} \qquad (5.2\text{-}6)$$

The average Nusselt and pseudohomogeneous Peclet numbers were also based upon these theoretical conductivities. These six experimental Nusselt number profiles were then compared to theory; the theory is discussed in detail in Appendix 2. The classical expression for the local Nusselt number in the thermally developing region of a circular tube containing fluid with a fully developed parabolic flow profile

and heated by a constant wall heat flux is given by:

$$N_{Nu}^{loc} = \left[\frac{1}{4.364} + \frac{1}{2} \sum_{n} c_n R_n(1) \exp(-2\beta_n^2 x^+) \right]^{-1} \qquad (5.2\text{-}7)$$

A similar expression for the local Nusselt number with a fully developed flat velocity profile is derived in Appendix 2 and is listed here as:

$$N_{Nu}^{loc} = \left[\frac{1}{8} + \frac{1}{2} \sum_{n} C_n J_0(\omega_n) \exp(-4\omega_n^2 x^+) \right]^{-1} \qquad (5.2\text{-}8)$$

The eigenvalues β_n and ω_n are tabulated in Appendix 2.

The goals of these comparisons were to: i) verify the validity of a flat velocity profile assumption in falling packed beds; ii) verify the assumption of equality of the static effective thermal conductivity of a stationary bed and the effective thermal conductivity of a falling particle bed; and iii) determine which of the models presents the best comparison between experiment and theory.

5.2.2 Results

Typical results showing the wall temperature distribution along the tube wall as a function of axial distance from the heated tube inlet and average bed velocity are given in Figure 5.2-1. These are the outside surface temperatures measured by the Chromel-Alumel thermocouples welded onto the tube wall. The wall temperature is shown to increase rapidly at first followed by a nearly linear

increase away from the tube inlet. Such results are very similar to the case of fluid flow through round tubes. The wall temperature is significantly reduced as the average bed velocity increases.

Dependence of the wall temperature distribution on particle size for the same heat flux, bulk velocity, and tube diameter is shown in Figure 5.2-2. Although the difference is small, a consistently lower wall temperature along the entire length of the heated tube is exhibited by the smaller particles. This difference disappears as the distance from tube inlet increases.

The axial wall temperature variation shown in Figure 5.2-3 is plotted as a function of tube size. The temperatures obtained with the two larger tubes are within experimental error of one another. The temperature profile for the smaller tube is consistently higher and cannot be attributed to experimental error. This suggests that the experimental conditions for this tube lay in the regime where the tube to particle diameter ratio begin to be of importance. Here, $D_t/d_p \approx 36.3$.

Dependence of the wall temperature distribution on wall heat flux with all other parameters held constant is presented in Figure 5.2-4. As expected, the wall temperatures increase rapidly with heat flux.

Typical results showing the axial bulk particle temperature distribution as a function of the average bed velocity are given in Figure 5.2-5. These are the temperatures that were obtained by computing a heat balance on each of the nodes in the system. The bulk temperature is shown to increase linearly with axial position

throughout the entire packed bed. As was the case for the axial wall temperature profile, the bulk particle temperatures are greatly reduced as the average velocity is increased.

In Figure 5.2-6, the axial bulk particle temperature variation for constant bed velocity, heat flux, and tube size is plotted for the three particle sizes studied. No dependence on the particle size is observed.

The dependence of the bulk particle temperature profile upon tube size as shown in Figure 5.2-7 is as expected. For the same heat flux and bulk particle velocity, the larger tubes, with higher mass flow rates, exhibit lower particle temperatures along the entire length of the falling bed.

Dependence of the axial particle temperature distribution on wall heat flux with all other parameters held constant is presented in Figure 5.2-8. Again as expected, the particle temperatures increase with heat flux.

Typical results showing the radial temperature distribution for the particles at the exit section exit for different values of the average bed velocity are given in Figure 5.2-9. These are the temperatures that were measured using the micrometer-mounted thermocouple probe assembly. The particle temperature is plotted as a function of the nondimensional radial distance away from the tube center line. These profiles are expected to be somewhat flatter than those at the heated test section exit, approximately 37 cm upstream from this position, because of radial heat conduction. Figure 5.2-9

again shows that the particle temperature decreases rapidly with increasing bed velocity. The radial profile becomes increasingly flattened as the average velocity is increased.

Figure 5.2-10 shows the effect of particle size on the radial temperature profile. The same center line temperature is demonstrated. Near the wall,the larger particles attain a higher temperature. This discrepancy with Figure 5.2-2 is likely due to the method chosen to detect the tube center line. If the actual radial positions of either of the curves were displaced in the direction of the other, the curves would align with one another.

The local heat transfer coefficient was found to increase slightly with heat flux, and therefore temperature, when the particle size, tube size, and average velocity remain the same. Radiation was found, therefore, to be an important contribution. An attempt was made to account for the radiant contribution and compute the convective local heat transfer coefficient by Equation (5.2-4). In Figure 5.2-11, values of the local heat transfer coefficient along the tube wall are compared for different heat fluxes when an emissivity of 0.3 was assumed. Heat flux is found to no longer be a contributing variable when radiation is accounted for in this fashion. Figures 5.2-12 through 5.2-15 deal also with this purely convective contribution.

Typical results showing the local convective heat transfer coefficient along the tube wall as a function of axial distance from the tube inlet and average bed velocity are shown in Figure 5.2-12.

The local heat transfer coefficient is shown to decrease with axial distance to an asymptotic value and is quite sensitive to the average velocity. Again, these results are very similar to those obtained with fluid flow in tubes. These coefficients are quite low varying between 200 and 800 W/cm^2K and increase with the average bed velocity.

Figure 5.2-13 shows the effect of particle size on the local heat transfer coefficient. The smallest size particles have a slightly higher value of h_{loc} than the other particles shown.

The local convective heat transfer variation presented in Figure 5.2-14 is plotted as a function of tube size. The asymptotic value approached decreases as the tube diameter is increased. This suggests that nondimensionalizing the heat transfer coefficient in terms of a Nusselt number based upon the tube diameter may bring all the data to a single, universal curve.

Experiments were conducted on the 2.48 cm tube in order to demonstrate reproducibility of the data. Figure 5.2-15 compares the local convective heat transfer coefficient profiles obtained from two independent experiments in which all experimental variables were held constant. Excellent reproducibility is demonstrated along the entire length of the packed bed.

Typical results from the Nusselt number profile calculations are presented in Figure 5.2-16, 5.2-17, and 5.2-18. The plotted symbols are the Nusselt numbers based upon the experimental heat transfer coefficients and each of the six theoretical conductivities studied.

The results based upon the conductivities presented by Specchia, Baldi, and Sicardi (1980) and by Specchia and Sicardi (1980) differed little. A single symbol was used to represent the results for the Nusselt number variations based upon either of these two conductivities.

It is immediately apparent from these figures that the Nusselt number variations approximate that predicted by theory based upon a flat velocity profile assumption (solid line) more closely than by theory based upon a parabolic velocity profile assumption (dashed line). This was the case in one hundred twenty-eight of the one hundred thirty experiments. The other two agreed with neither flow assumption and are suspected to be caused by error in experimentation.

A thorough analysis of the data showed that only three of the models studied gave satisfactory results (Yagi and Kunii (1957), Specchia, Baldi, and Sicardi (1980), Specchia and Sicardi (1980)). Additional analysis showed that the experimental Nusselt number variation based upon the conductivity of Yagi and Kunii (1957) compared well with the theoretical profile in all of these one hundred twenty-eight cases. The experimental profiles based upon the model of Yagi and Kunii approach the asymptotic value of 8 for the Nusselt number while those based upon the models of Specchia et. al. consistently underestimate the Nusselt number along the entire length. An attempt was made to compute experimental Nusselt number profiles based upon the arithmetic average of the six theoretical conductivities. The results obtained did not compare with theory as

well as the above method using the model of Yagi and Kunii.

Figures 5.2-16, 5.2-17, and 5.2-18 are replotted as dimensional quantities in Figures 5.2-19, 5.2-20, and 5.2-21. The results are the same; the difference here is that the experimental profiles are purely experimental and the theoretical profiles were obtained purely from theory.

5.3 Conclusions and Recommendations

Table 5.2-2 lists the various combinations of tube size, particle size, heat flux, and average bed velocity investigated in this study. A total of 130 experiments have been obtained. One set of six experiments was repeated to examine the reproducibility of the data. Excellent reproducibility was demonstrated. High rates of flow were difficult to obtain in cases tested with the largest tube. It was not possible, therefore, to collect data for this tube at the highest heat flux; a heat flux of half the maximum studied for the other tubes was analyzed instead. Radial exit temperature profiles were obtained in the 52 cases indicated. The radiant heat flux was satisfactorily accounted for by Equation (5.2-1).

The axial wall temperature, axial bulk particle temperature, and local heat transfer coefficient profiles were demonstrated to be similar to those obtained for fluid flow in circular tubes heated by a constant wall heat flux. The temperature profiles increased linearly. The local heat transfer coefficients decreased in an asymptotic fashion; they were quite low, being between 200 and 800

W/m^2K. The wall heat flux was computed to vary by less than six per cent from inlet to exit in all the cases studied.

Good comparison was observed between the experimental Nusselt number profiles and theoretical Nusselt number profiles based upon a flat velocity profile assumption. The best comparison was obtained when the experimental Nusselt number was based upon the theoretical conductivity proposed by Yagi and Kunii (1957). The range of nondimensional axial distance covered by these one hundred thirty experiments was up to $x^+ = 0.05$. The theoretical description of the Nusselt number variation in the thermal entrance region of a circular tube with an applied constant wall heat flux and a "fluid" with a flat velocity profile is presented in Section A2.2.

These "experimental" Nusselt number profiles were based upon the obtained experimental local heat transfer coefficient profiles, but incorporated effective conductivities determined by theory obtained from the literature. The first recommendation for further research, therefore, is to obtain data for the effective thermal conductivity of a falling packed bed. The Nusselt number computed from such data would then be purely experimental. These experiments should be undertaken with the same particles and tubes studied here since the regime where particle-to-tube diameter ratio becomes important has been approached upon in some of the cases studied.

In all of the experiments, good comparison between experiment and theory was most difficult to obtain along the first few centimeters from the tube inlet. With such low heat transfer coefficients, the

conduction resistance through the tube may not have been negligible so that conduction losses near the ends of the test section may have been important. Before additional experiments are conducted, alterations should be made to eliminate this source of error.

No correlation for the average heat transfer coefficient or average Nusselt number has been presented here. This is because of the narrow ranges of experimental parameters studied. The Peclet number varied over only one and one half orders of magnitude. This variation is due largely to the variation of tube diameter and bulk velocity studied. The particle and gas characteristics were not studied. Additional experiments should be carried out incorporating various particles and gases so that the effect of particle physical properties and gas Prandtl number can be analyzed. Furthermore, the range of bulk particle velocity studied should be increased so that the widest possible range for the Peclet number may be considered. Finally, any useful correlation for the average Nusselt number must also consider the effect of the particle-to-tube diameter ratio.

Table 5.1-1 Characteristics of the Three Particle Sizes Used in This Investigation

Material: Soda-Lime Glass

Manufacturer's Description: Class IV, Type A, Non-Waterproof UNI-SPHERES

Manufacturer's Size Number	Size Distribution (μm)
203	590-840
304	420-590
608	177-250

UNI-SPHERES were quoted by the manufacturer to be spherical in shape, containing not more than 15% irregularly shaped particles, reasonably free of sharp particles, and 80% in the size range specified above.

Table 5.2-2 Range of Experimental Variables Studied in the Flowing Particle Bed Experiments

Tube Size (mm)	Particle Size Range (μm) 177-250	420-590	590-840	Heat Flux (W/cm^2)
	Bulk Particle Velocity Range (cm/s)			
7.75	(4) 4.4-11.6 (3) 7.7-13.3 (3) 7.6-11.8	(4) 3.0-10.9 (3) 6.2-12.3 (3) 5.8-10.9	(4) 2.1-10.7 (3) 4.7-10.4 (3) 5.5-11.5	2.55 3.35 4.20
13.8	(9) 3.5-11.8+ (8) 4.4-13.9+ (8) 4.9-15.3+	(9) 3.7-13.3+ (9) 2.4-14.3+ (9) 3.7-15.1+		2.55 3.35 4.20
24.8	(7) 1.3-7.2 (12) 1.8-6.6*	(6) 1.3-3.7 (6) 1.1-3.7 (5) 1.8-3.8	(5) 0.9-3.0 (4) 1.8-3.6 (3) 2.2-3.5	2.10 2.55 3.35

(#) Number of data points collected in the indicated range of velocity.

* Entire range of data repeated to demonstrate reproducibility.

+ Radial exit temperature profiles collected.

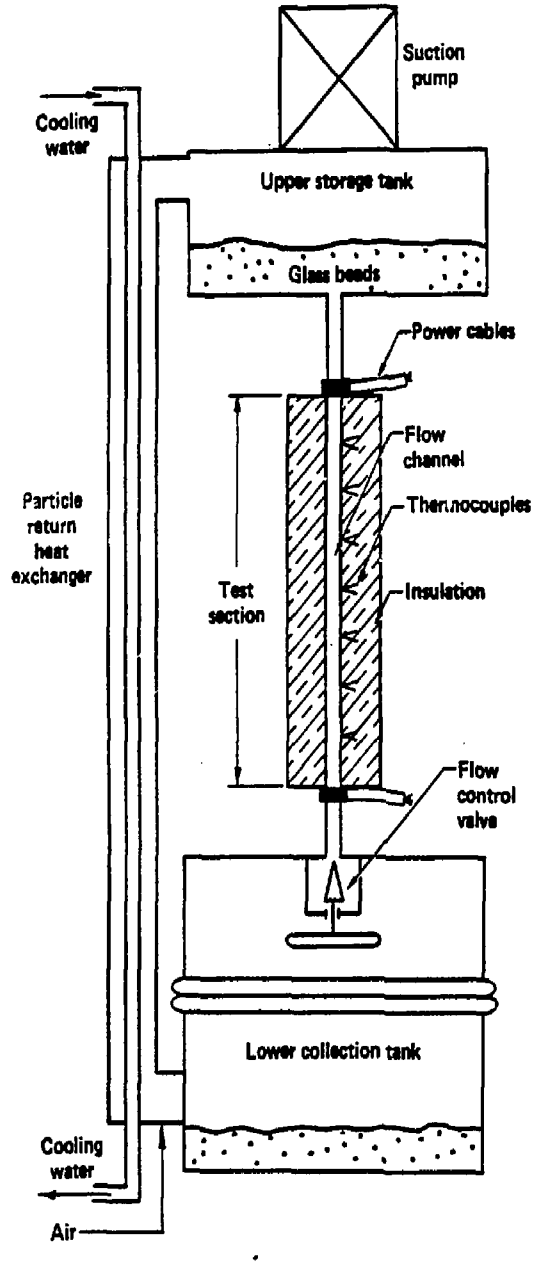

Figure 5.1-1. Schematic diagram of the falling bed test loop.

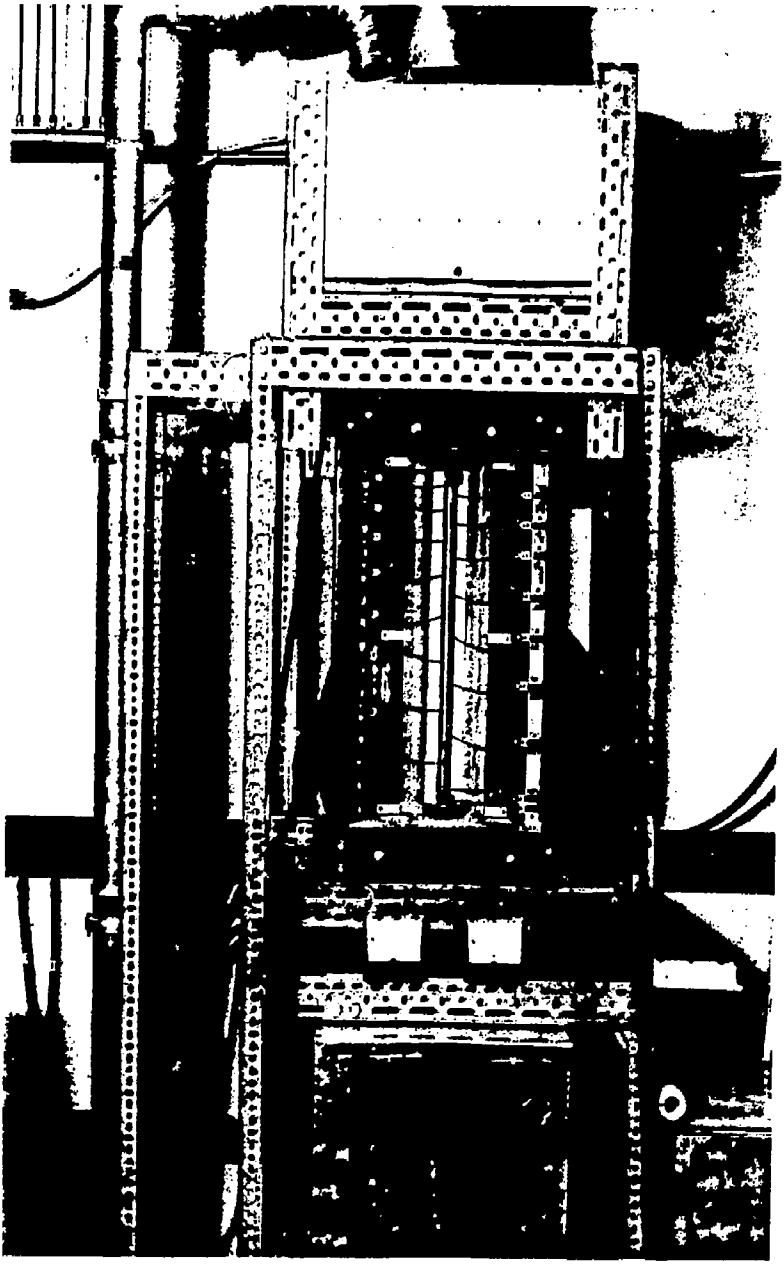

Figure 5.1-2. Photograph of the flowing bed test loop with exposed test section.

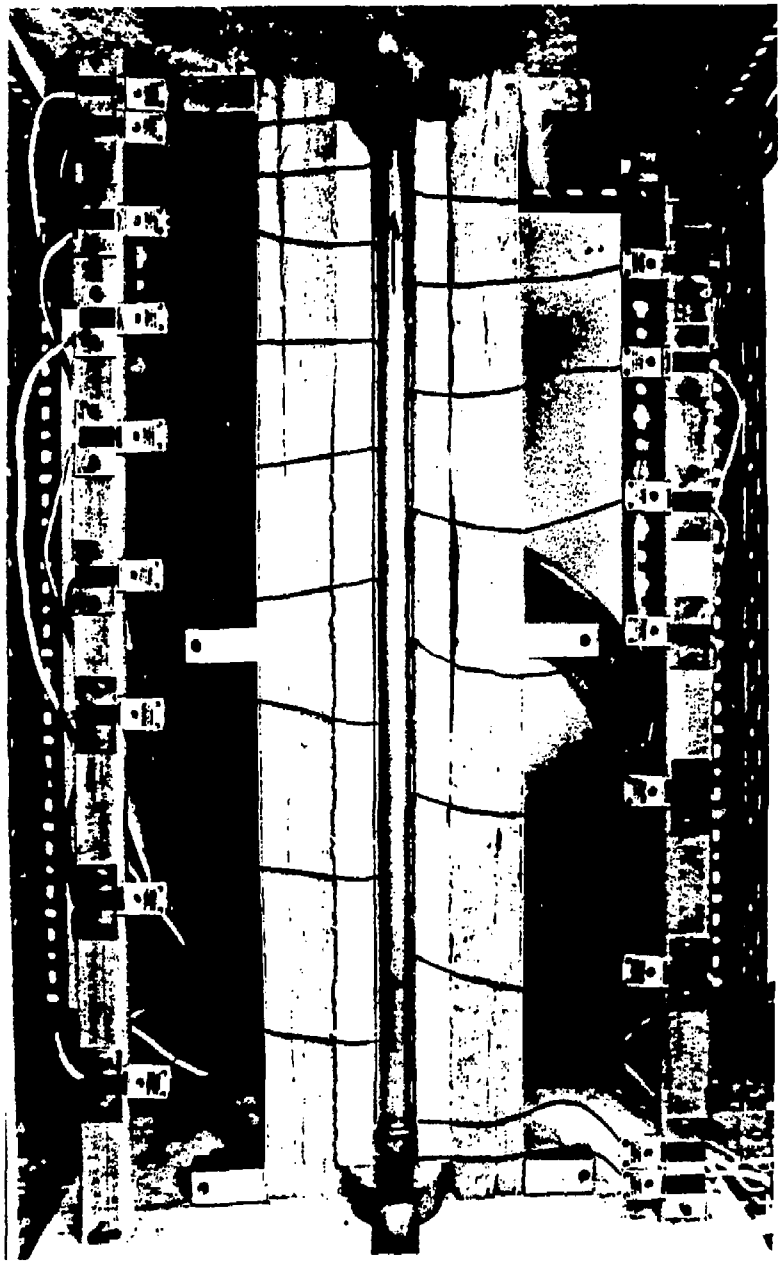

Figure 5.1-3. Photograph of the test section showing the surface thermocouples and outer insulation.

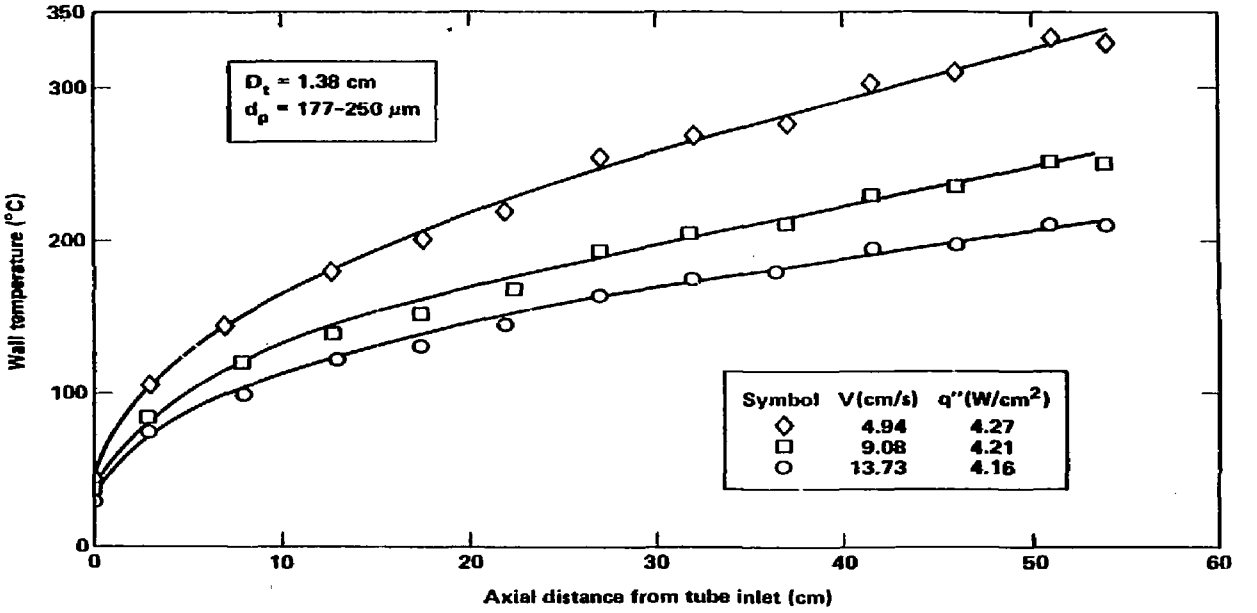

Figure 5.2-1. Axial wall temperature variation as function of bed velocity.

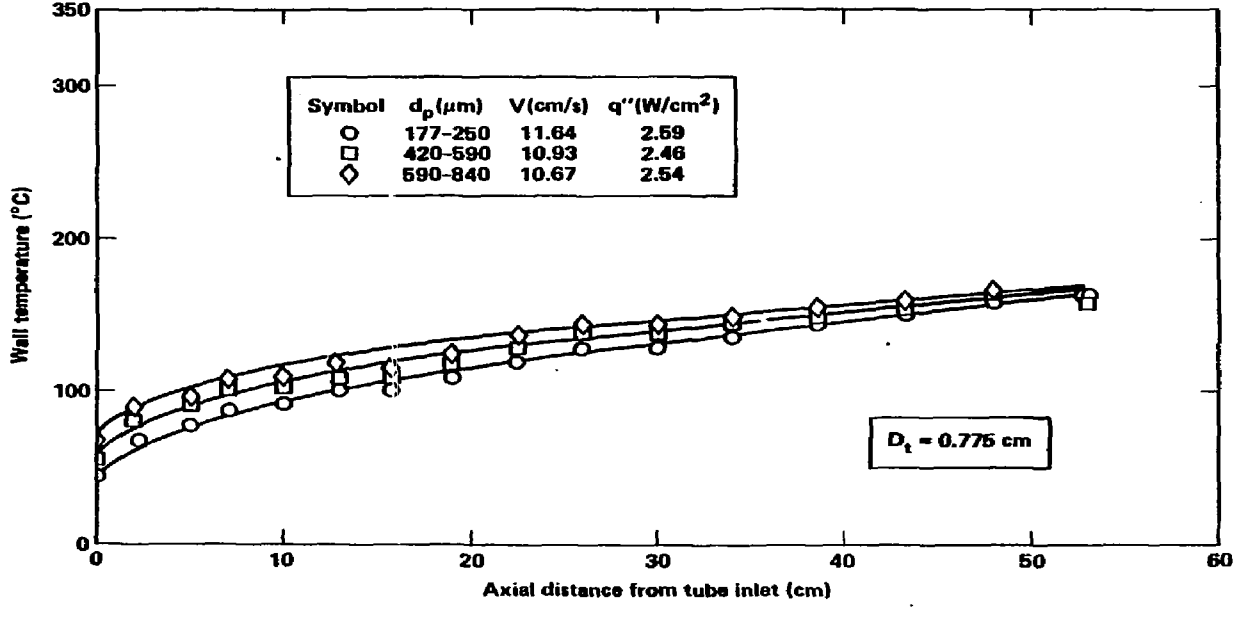

Figure 5.2-2. Axial wall temperature variation as function of particle size.

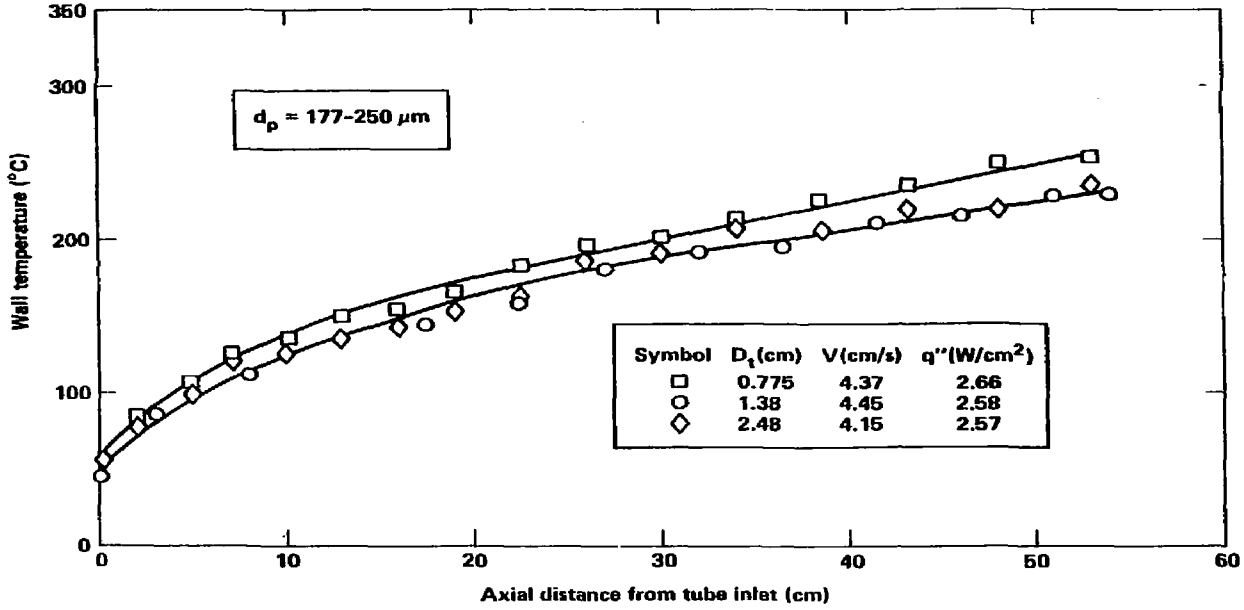

Figure 6.2-3. Axial wall temperature variation as function of tube size.

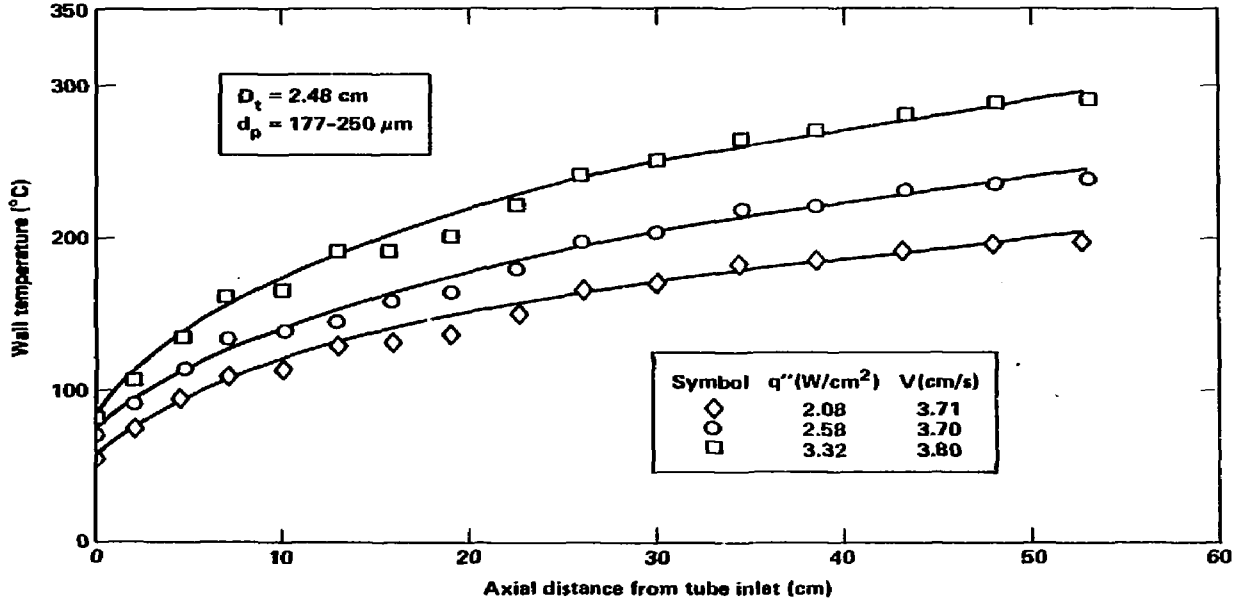

Figure 5.2-4. Axial wall temperature variation as function of heat flux.

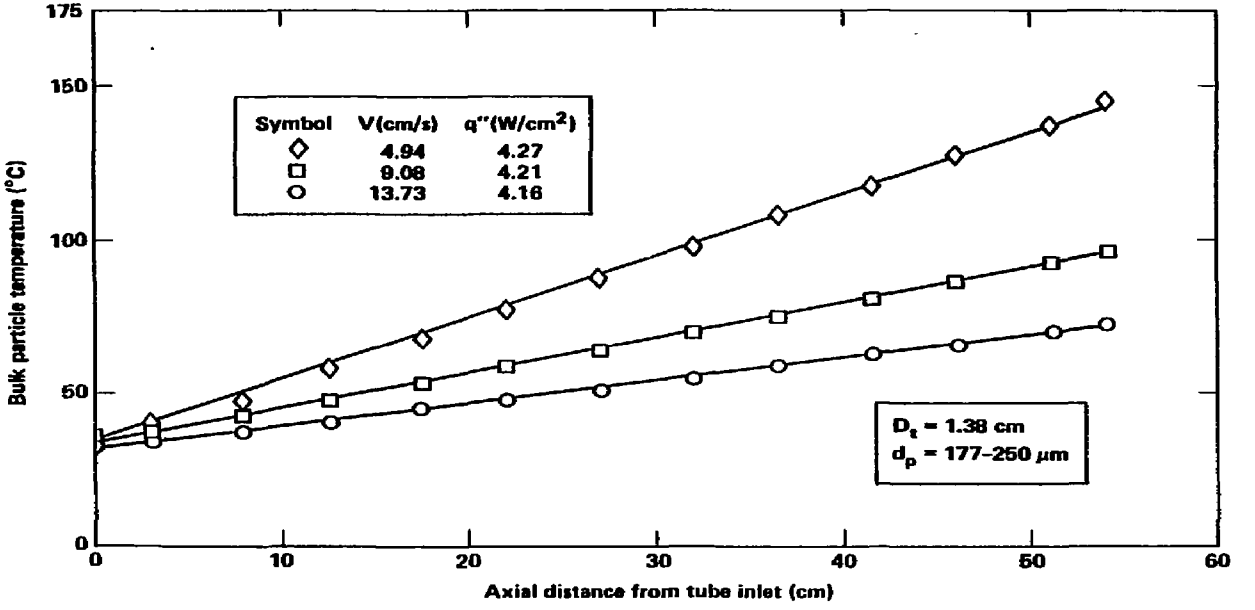

Figure 5.2-5. Axial bulk particle temperature variation as function of bed velocity.

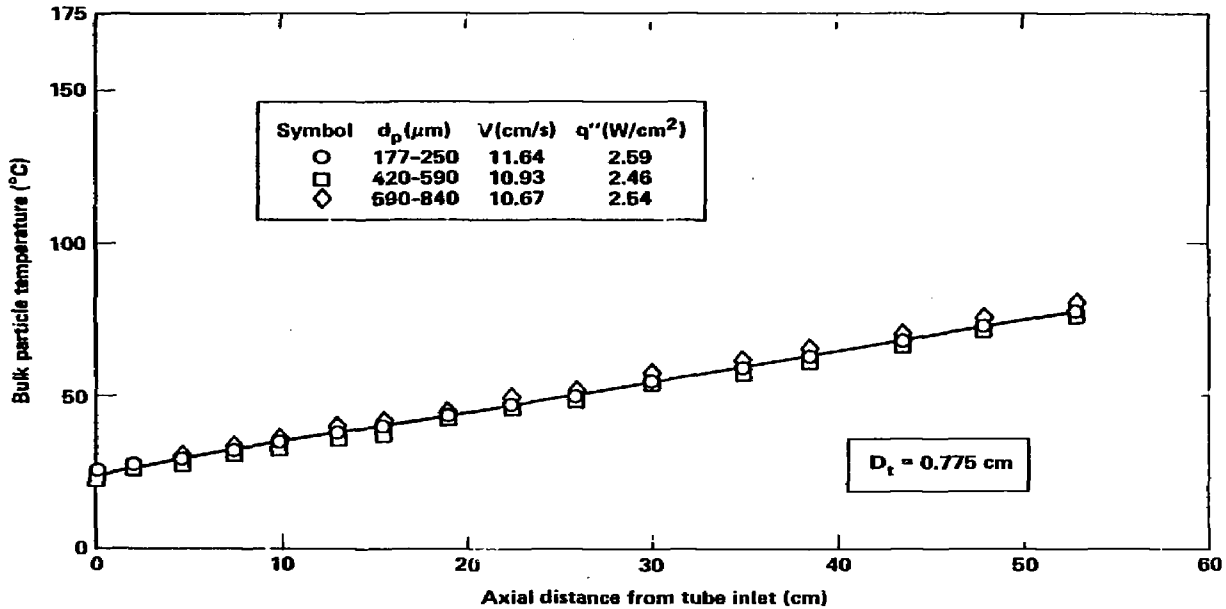

Figure 5.2-6. Axial bulk particle temperature variation as function of particle size.

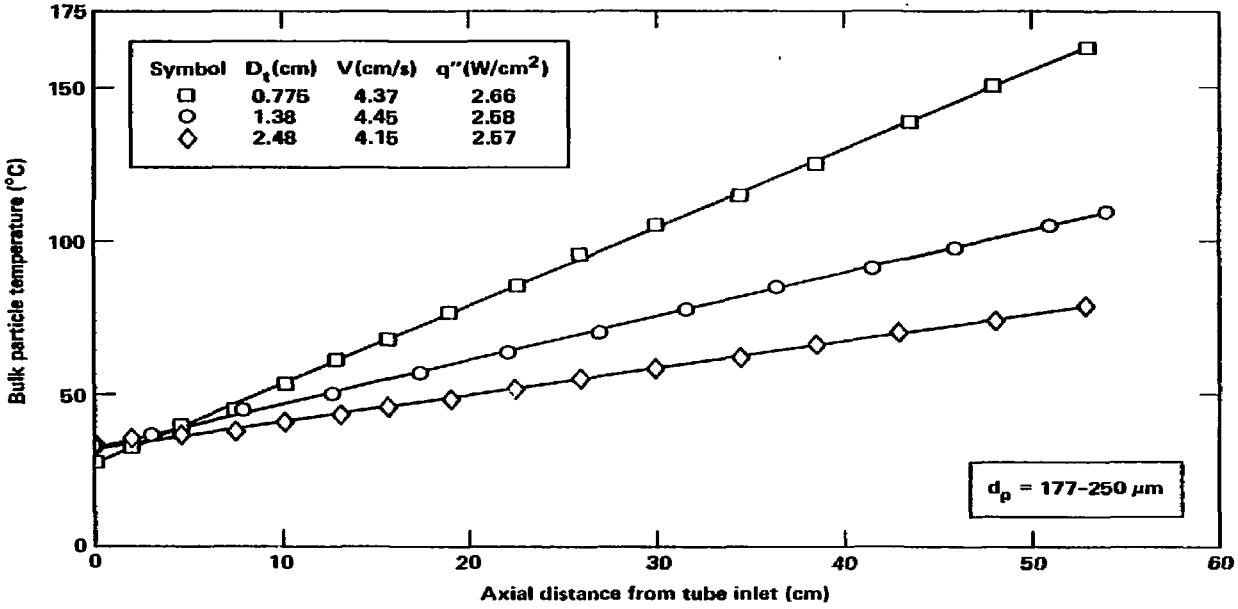

Figure 5.2-7. Axial bulk particle temperature variation as function of tube size.

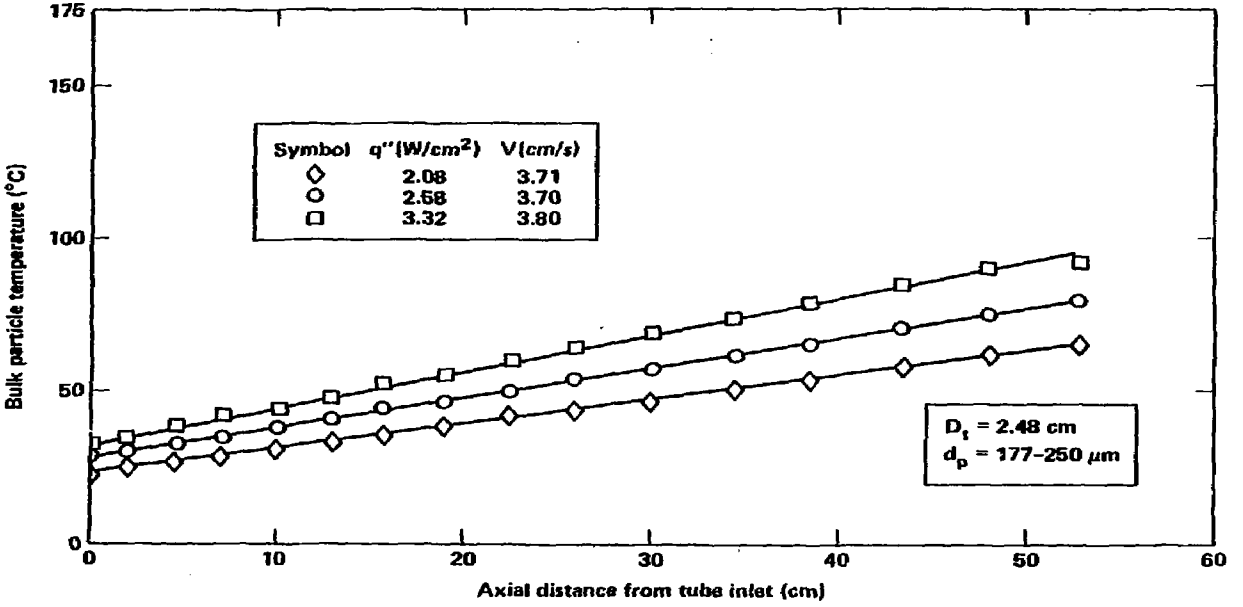

Figure 5.2-8. Axial bulk particle temperature variation as function of heat flux.

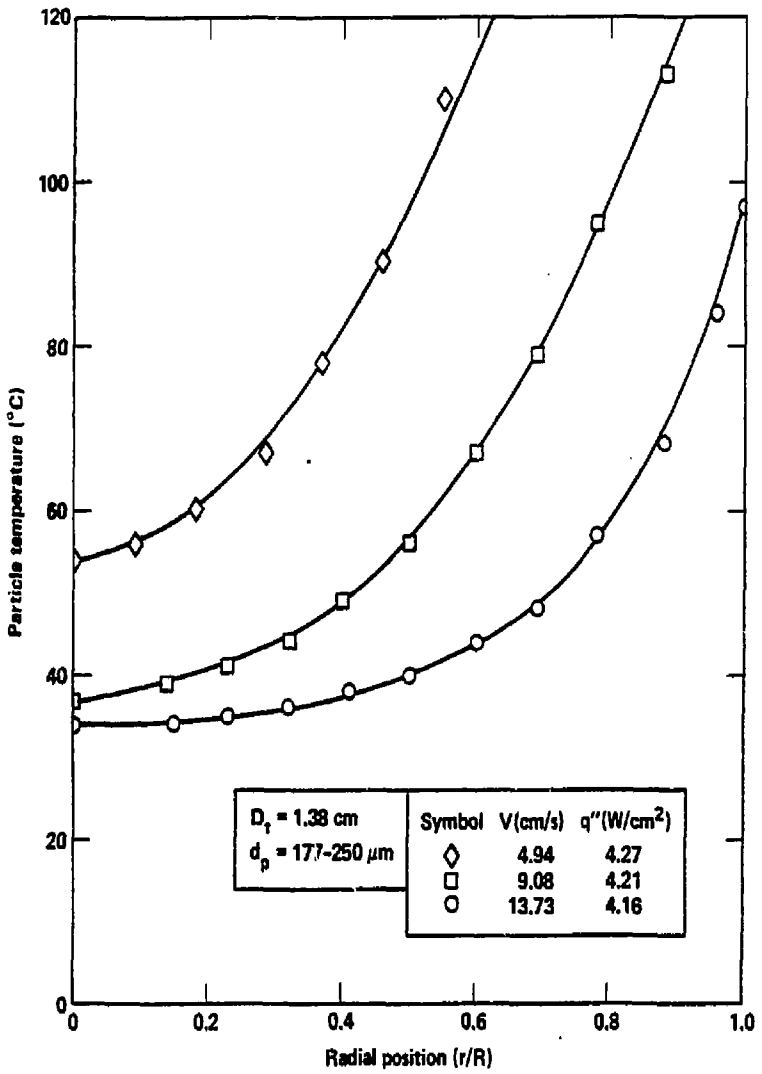

Figure 5.2-9. Particle radial exit temperature profile as function of bed velocity.

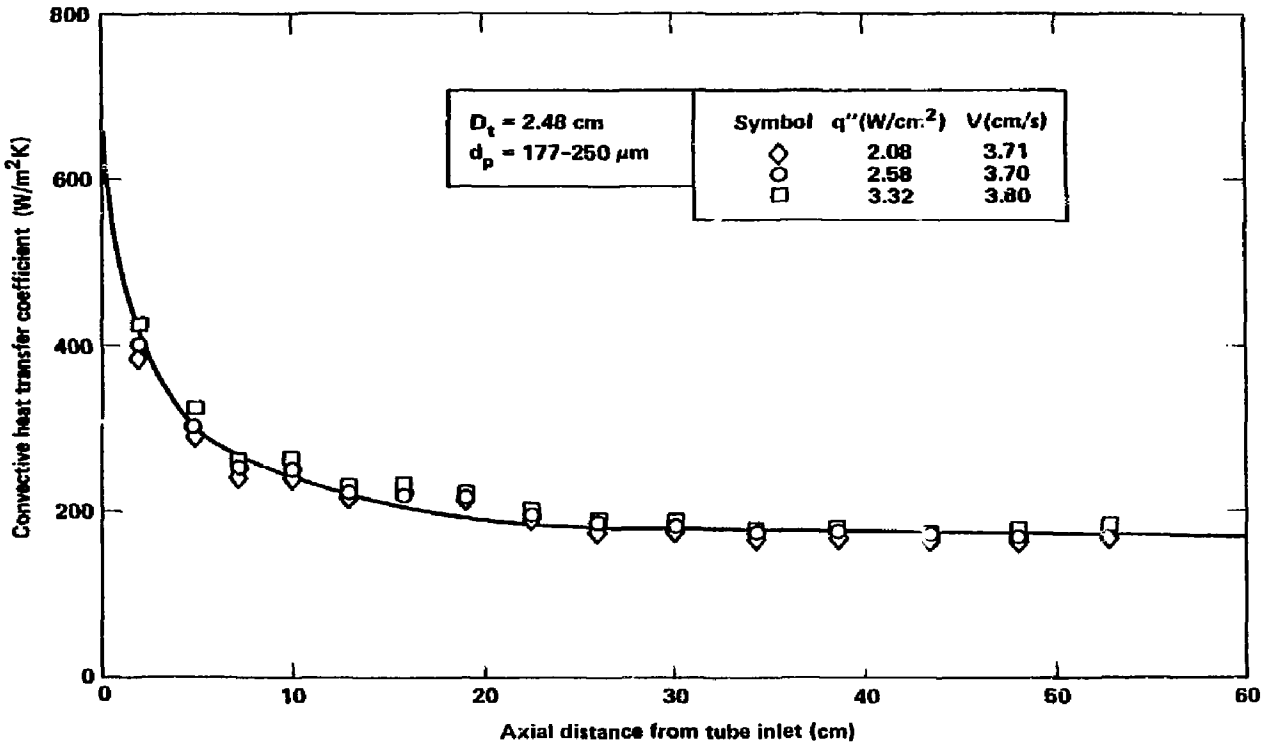

Figure 5.2-11. Local heat transfer coefficient variation as function of heat flux.

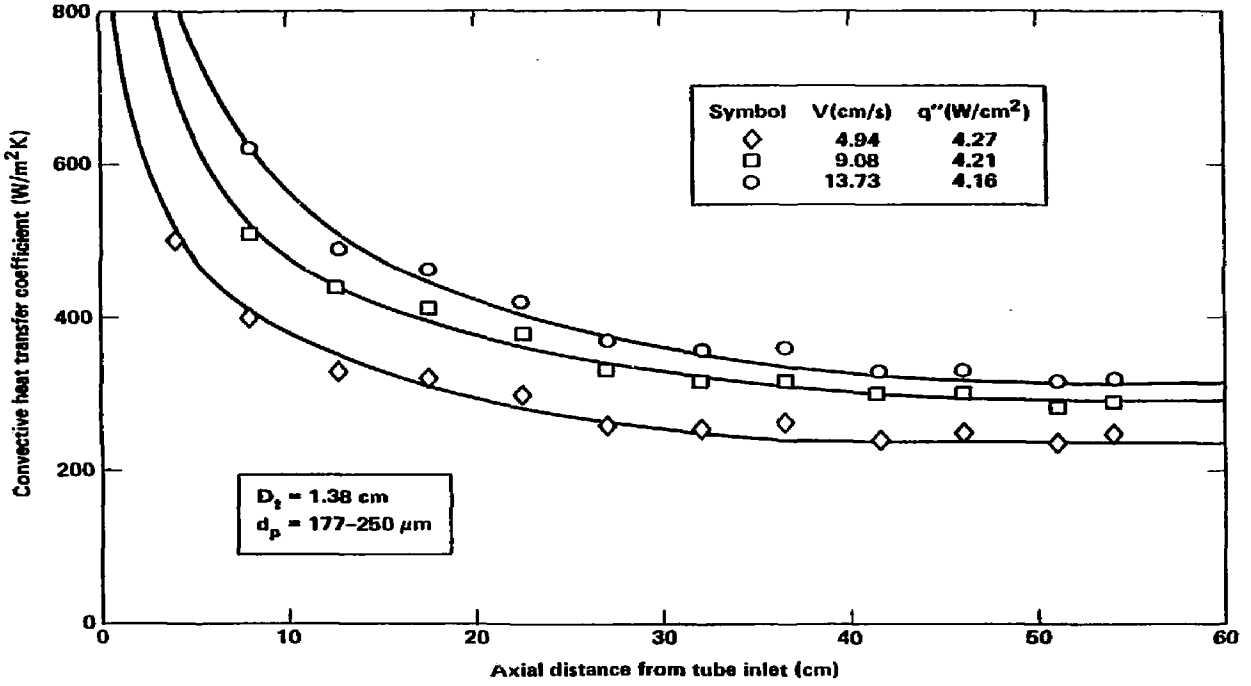

Figure 5.2-12. Local heat transfer coefficient variation as function of bed velocity.

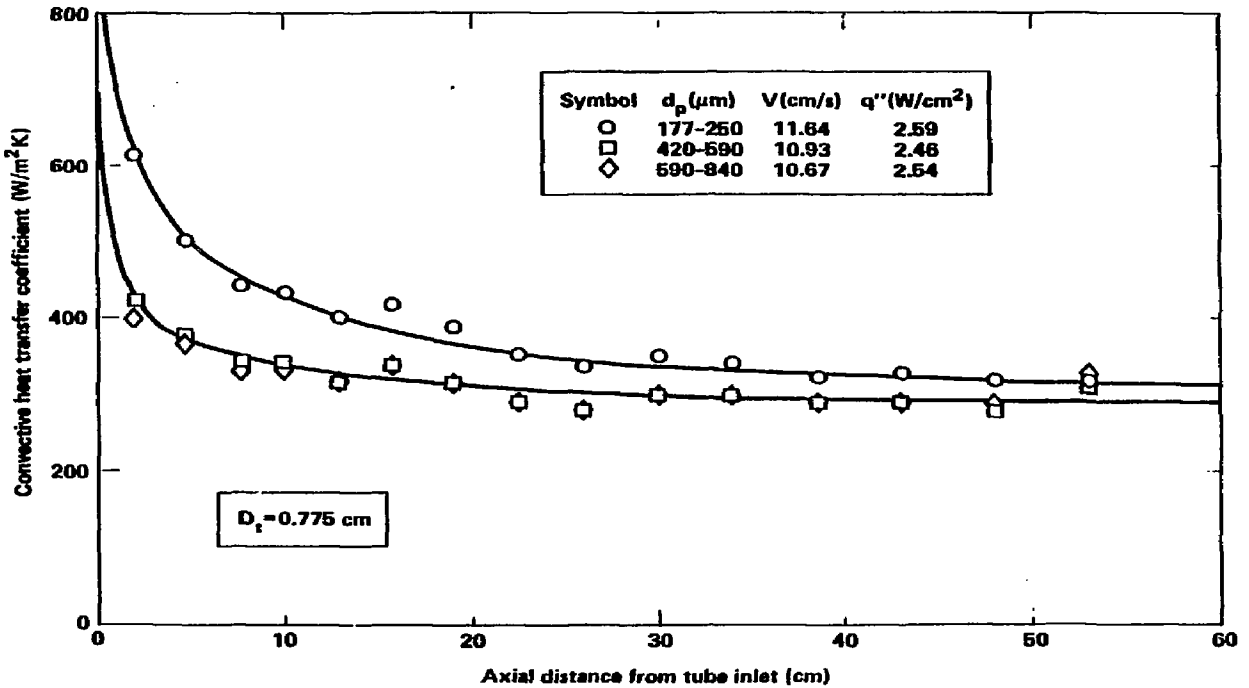

Figure 5.2-13. Local heat transfer coefficient variation as function of particle size.

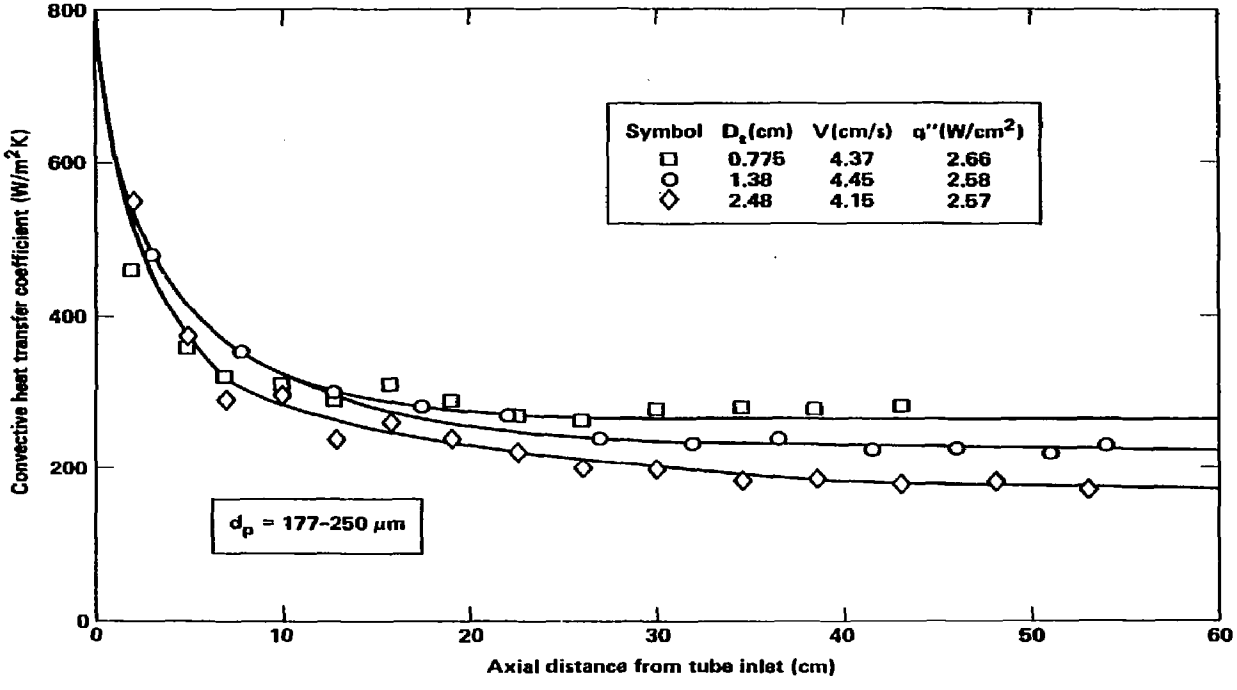

Figure 5.2-14. Local heat transfer coefficient variation as function of tube size.

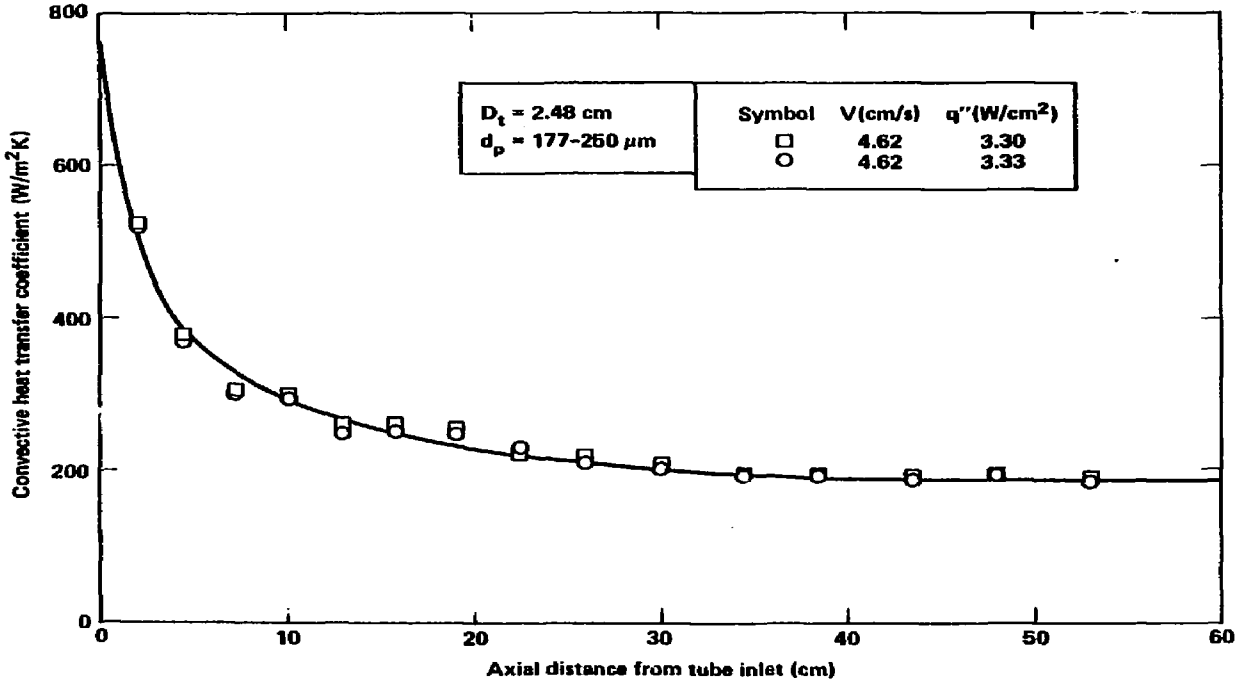

Figure 5.2-15. Local heat transfer coefficient variation demonstrating reproducible data.

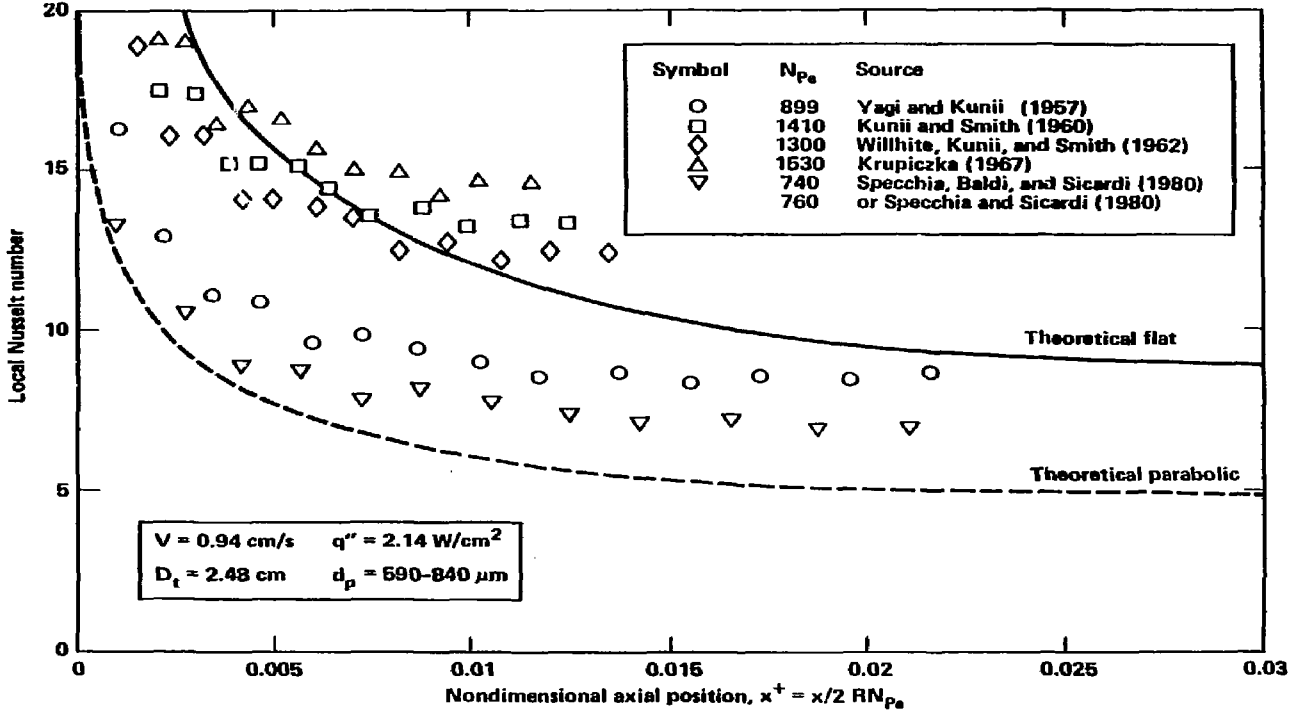

Figure 5.2-16. Local Nusselt number versus nondimensional distance from inlet for the six models analyzed.

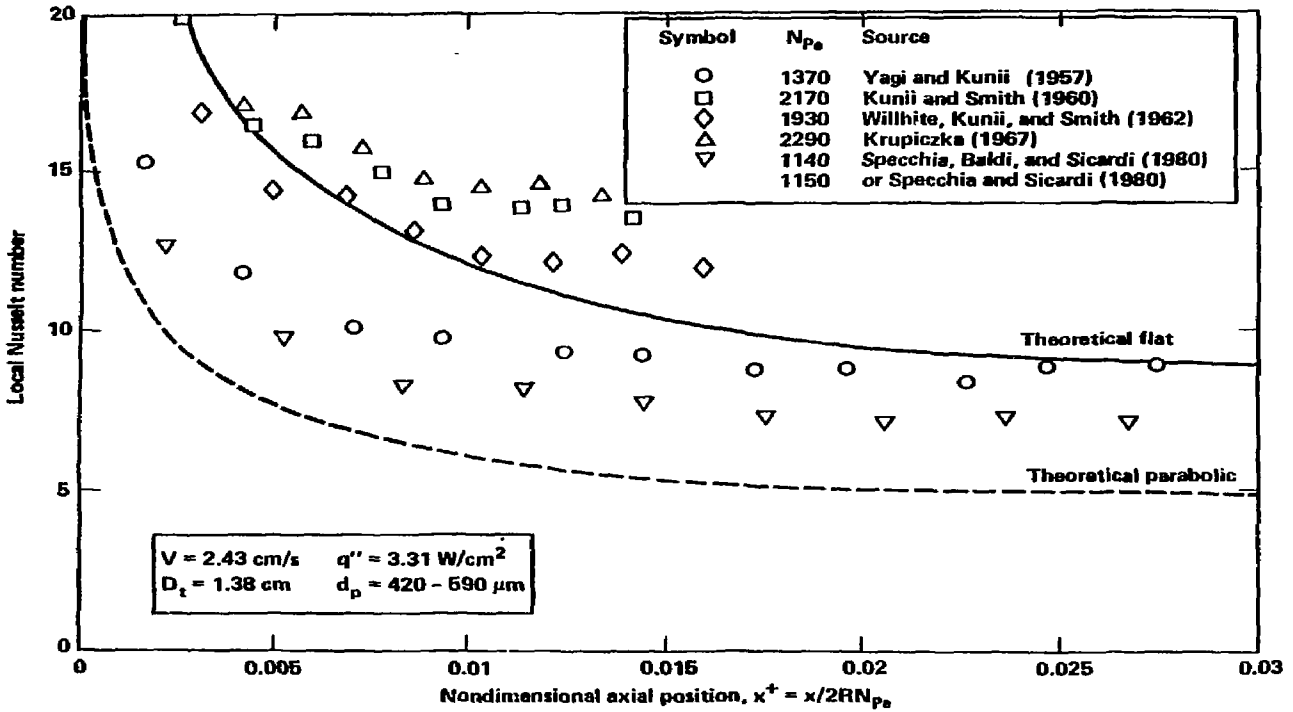

Figure 5.2–17. Local Nusselt number versus nondimensional distance from inlet for the six models analyzed.

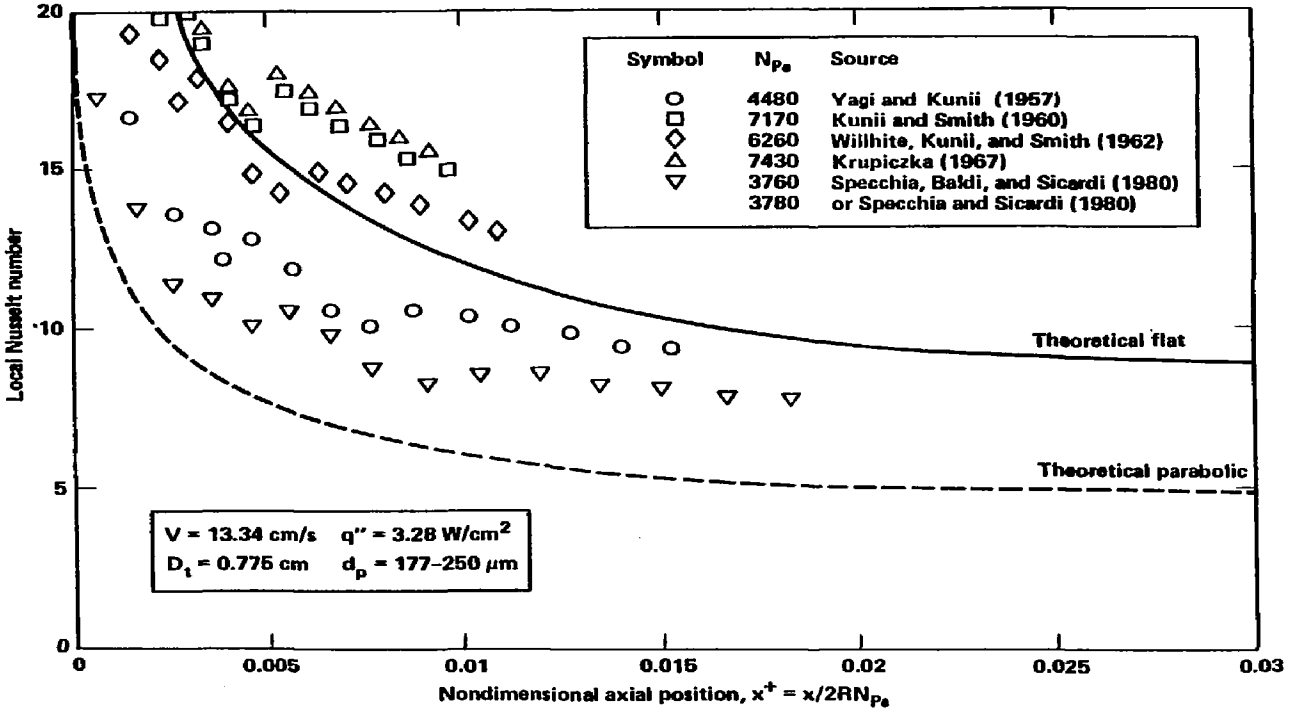

Figure 6.2-18. Local Nusselt number versus nondimensional distance from inlet for the six models analyzed.

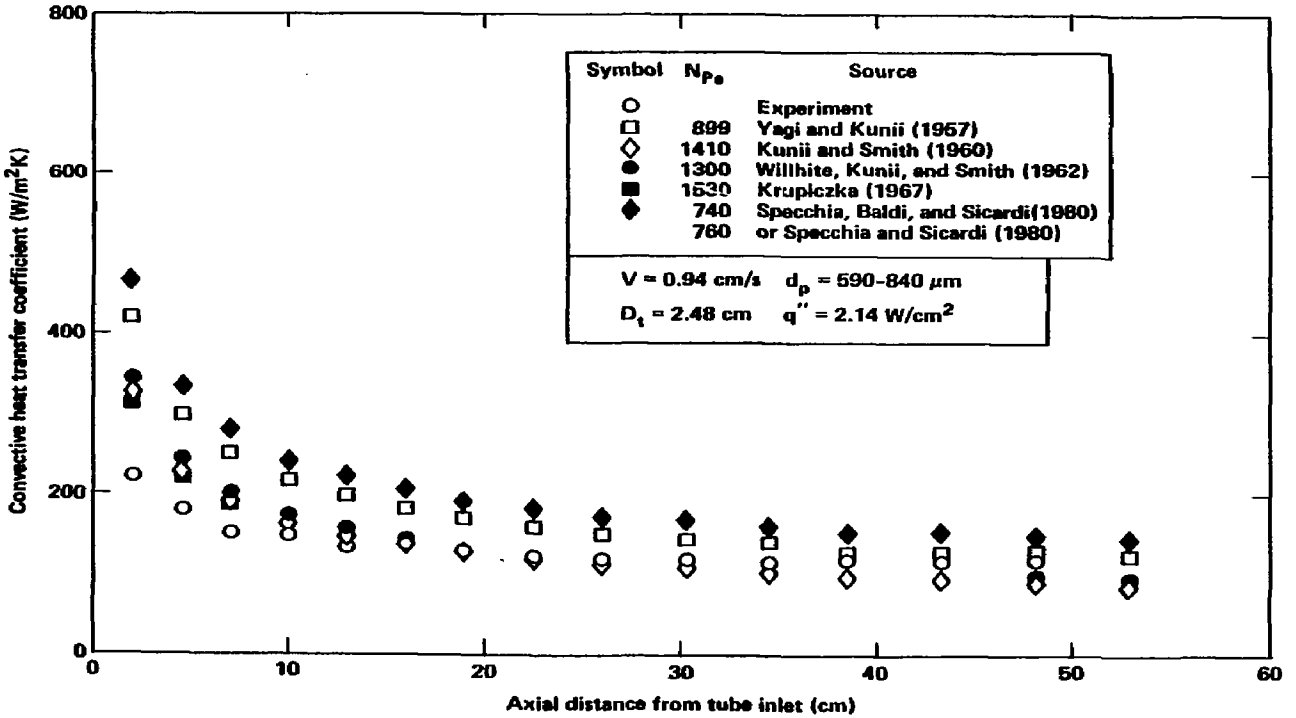

Figure 5.2-19. Experimental and theoretical-flat heat transfer coefficient profiles.

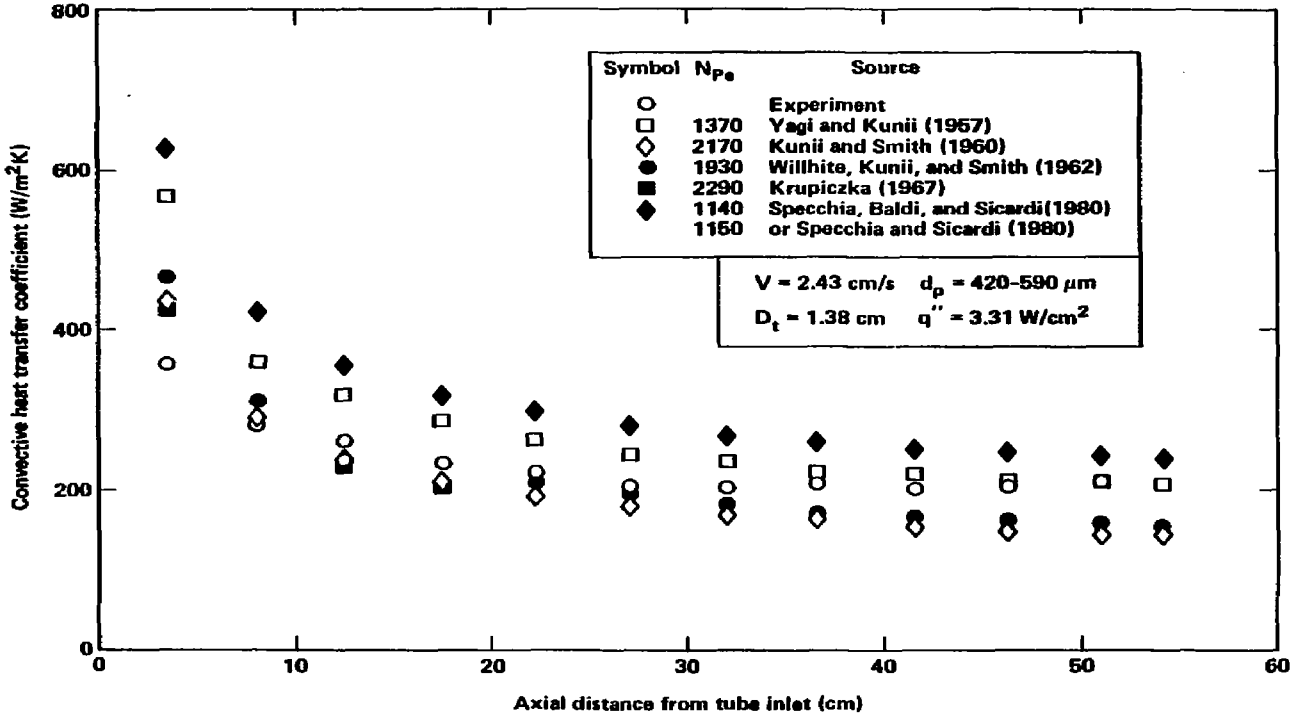

Figure 5.2-20. Experimental and theoretical-flat heat transfer coefficient profiles.

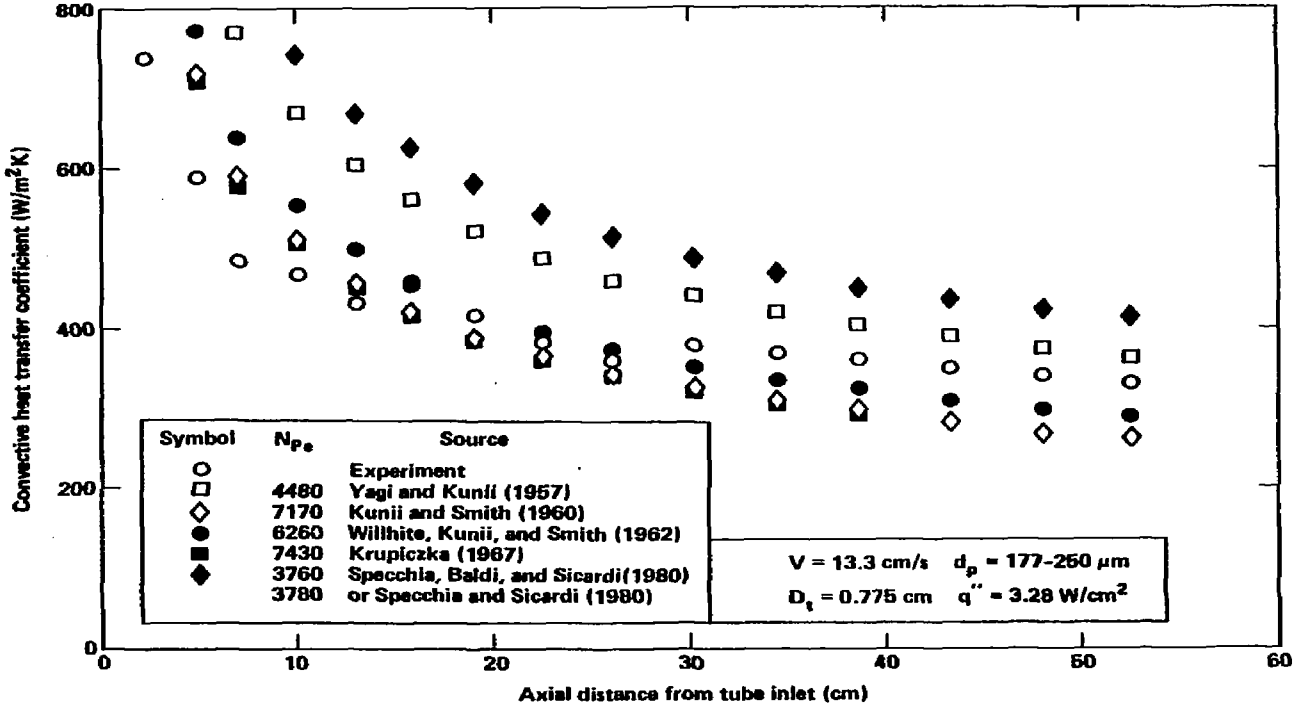

Figure 5.2-21. Experimental and theoretical-flat heat transfer coefficient profiles.

CHAPTER 6

STATIONARY PARTICLE BED EXPERIMENTAL RESULTS

This chapter will discuss the experimental results obtained in this investigation on the heat transfer characteristics of a stationary packed particle bed of glass microspheres. An annular packed bed has been constructed in which heat was applied through the outer wall by electric heating of a stainless steel tube. Cooling occurred at the inner wall of the annular bed by flowing air through the central tube. A gas stream (air) was also allowed to flow through the packed bed. It has been the aim of this investigation to experimentally determine the overall effective thermal conductivity k_o for the packed bed as a function of the superficial gas velocity through the bed, inner tube coolant gas velocity, heat flux, and particle size. The effects of heat flux and coolant gas velocity were studied in order to account for the radiative contribution. Such information is necessary for the design of stationary particle bed type fusion reactor blankets as discussed in Chapter 1.

The experimental equipment and procedure are described in Section 6.1. In Section 6.2 the experimental results are presented. Conclusions and recommendations for further research are discussed in Section 6.3.

6.1 Experimental Equipment and Procedure

6.1.1 Experimental Equipment

Figure 6.1-1 is a schematic diagram of the apparatus. Solid soda-lime glass particles were constrained between the two tube walls in the radial direction and between two porous bronze plates in the axial direction. The particles used in the falling bed experiments discussed in the last chapter were used in these experiments also. The outer tube had an inside diameter of 50.19 mm and was 0.30 mm thick; the inner tube had an outside diameter of 12.70 mm and was 0.51 mm thick. Both were made of Type 321 stainless steel.

Electric current from a 50 kW DC power supply was passed through the wall of the outer tube. The power input was controlled by a resistor bank placed in series with the tube resistance. The power input to the test section was determined by measuring the voltage drop across the outer tube and the current through a shunt connected in series with the tube resistance. Standard voltmeters were used in this regard.

The upper and lower end plugs and porous plates were electrically insulated from the outer tube by an annular section of phenolic. The inner tube was mounted directly on the end plugs and bronze plates and was therefore also electrically isolated. The outer tube was electrically isolated from the support frame by mounting the flanges, which were welded to the tube wall, on horizontal asbestos-concrete boards. The entire apparatus hung

from the upper flange which was rigidly fastened to the upper board. The lower flange was not rigidly fixed to the lower board to allow for thermal expansion of the tube when it was heated. The outer tube was thermally insulated from the outside by an inner layer of 5.1 cm thick rigid, hydrous calcium silicate followed by an outer layer of 2.5 cm thick fiber glass and a 1.6 cm thick aluminum shroud. The end plugs were thermally insulated by layers of fiber glass. Not pictured in Figure 6.1-1 were Swagelok tube fittings that clamped onto the outer tube and threaded into the phenolic insulators. It was through these fittings that gas leakage from the packed bed was to be prevented.

The outer wall temperature distribution along the flow direction was measured by means of Chromel-Alumel thermocouples spot welded onto the tube's outer surface. The inner wall axial temperature profile was obtained by the following method. Holes were first drilled at desired positions in the tube wall. Chromel-Alumel thermocouples were then threaded inside the tube and extracted through these small holes; the thermocouples were soldered in place with high temperature silver solder. Finally, the solder joints were filed to obtain a smooth tube surface.

The temperature profile of the packed bed was measured by sixteen Chromel-Alumel thermocouple probes inserted through the outer tube wall and into the packing material. Fourteen of these probes were situated at positions such that four axial and four radial temperature profiles could be obtained simultaneously. The

four horizontal planes containing these thermocouples were located at 4.1, 11.1, 18.1, and 25.1 cm above the inlet to the heated test section. The other two thermocouple probes, located at 4.1 and 18.1 cm from the inlet, were mounted on micrometer assemblies; the radial temperature profile in these planes could therefore be measured in great detail.

One wire from each of the two micrometer-mounted thermocouples was connected to the positive pole of an ohmmeter; the inner tube wall was electrically connected to the negative pole. The location of the tube wall could thus be detected by the change in resistance indicated on the ohmmeter.

In order to position the stationary thermocouple probes clear plexiglass discs, one face of each scribed with rings located at the radial positions of the probes, were mounted onto the outer tube prior to installation of the inner tube and end plugs. The correct positions of these probes were thus obtained by visually aligning the scribe marks with their corresponding probes.

The two micrometer-mounted probes and the two stationary probes located next to the inner tube wall at a radial position of r/R = 0.316 were made with a sheath thickness of 1.6 mm to avoid possible bending (recall that R = 25.1 mm and the inner wall was located at r/R = 0.253). The stationary probes located at r/R = 0.506 and 0.759 (four each) where the possibility of bending was less pronounced were made with thinner sheaths 0.8 mm in diameter in order to minimize the disruption of the flow pattern near the

sheath. The final set of four thermocouples located near the outer wall at r/R = 0.886, where flow disruptions were minimal, were also made with the thicker sheath diameter.

A thermocouple probe was located along the axis of the inner tube to measure the exit temperature of the inner air. Thermocouples were also located in the lower end plug and at the top of the inner tube to measure the outer and inner air bulk inlet temperatures respectively. The outer surface temperature of the composite wall of insulation was measured by means of a thermocouple attached to the shroud in the midplane of the test section. Another thermocouple was placed nearby to measure the local ambient temperature; from these temperatures, the heat losses could be estimated. Finally, thermocouples were located at the inlet of each of the two rotameters to verify that the air had been cooled to ambient temperature, which was where the rotameters were calibrated. All of these temperatures were recorded on a forty channel Monitor Labs 9300 data logger. A photograph of the test section with the thermocouples and insulation exposed is presented in Figure 6.1-2.

A schematic of the cooling system is presented in Figure 6.1-3. Compressed air from a supply line was first passed through a filter to remove oils and particulates. The air was then divided into two streams, each of which was regulated to desired conditions before entering the test apparatus.

The coolant air, hereafter called the inner air, flowed downward through the inner tube and exited at the bottom of the test section.

The heated inner air was then cooled to room temperature by flowing through a coil immersed in a water bath. The volumetric flow rate of the air was then measured by a rotameter previously calibrated against a wet test meter at atmospheric pressure and room temperatue. The inner air finally exited to the atmosphere.

The air supplied by the second regulator, hereafter called the outer air, formed the stream that flowed through the voids in the packing of the bed. The outer air first flowed into the annular region of the lower end plug. This allowed the pressure to be constant on the lower side of the porous bronze plate which held the bed in place and served as a flow distributor. The air then flowed upward through the pores of this plate and into the packing. The packed bed consisted of three sections. The first 17.1 cm served as an unheated entrance region; the air thus exited this region with a fully developed velocity profile. The next 29.2 cm consisted of the test section which coincided with the heated outer wall. Another 17.1 cm of packing followed. The outer air flowed through another porous plate, into an upper annular region, and exited the test apparatus. Finally, another cooling coil immersed in the water bath cooled the outer air to room temperature before its flow rate was measured by a rotameter which was also calibrated at ambient temperature. The outer air was then released into the atmosphere. A photograph of the entire experimental apparatus is presented in Figure 6.1-4.

6.1.2 Experimental Procedure

The experiment was operated in a steady state mode. Experiments were conducted for different power levels, particle sizes, inner and outer air flow rates. The experimental variables are listed in Table 6.1-1.

Initially, the two regulators were adjusted to obtain approximately the desired flow. Valves on the two rotameters were used to obtain the correct flow rate. The highest rates to be tested for both air streams were first used. The resistor bank connected in series with the test section was adjusted to obtain approximately the desired power input to the tube. The power supply was turned on and its controls were used to obtain the desired heat flux. The power, air flow rates, and all temperatures were monitored until steady state conditions were reached; this required approximately five hours. At that time, all temperatures, power input, and inner and outer air velocities were recorded. The data for radial temperature profiles obtained by the two micrometer-probe assemblies were then recorded one at a time. The Swagelok fittings connected to these probes were first loosened, the probe was moved to the desired positions, and the Swageloks were then tightened in the new positions. In this manner, all air leaks which were found to affect the measured temperature were eliminated. A waiting period of a few seconds was required to bring the temperature reading to its new value. When the complete profile had been recorded, the probe was withdrawn to its full out position.

At this point, preparations were made to conduct the experiment at a lower outer air velocity. The regulator and rotameter valve were constricted to obtain the required flow rate. Again, the power, air flow rates, and temperatures were monitored until the new steady state conditions were reached. This required a waiting period of an additional two hours. Experiments at other flow rates followed. In this manner, six experiments were conducted with the various combinations of inner and outer air flow rates for each particle size and power level.

The resistor bank was adjusted and the above data were collected for the other power level. The apparatus was next partially disassembled, thoroughly cleaned, repacked with different size particles, and reassembled. Both power levels were repeated for each of the two additional particle sizes.

Originally it was intended to collect data with all three particle sizes at three separate power levels, however, the Swagelok tube fittings at both ends of the bed were found to leak as the system heated up at the beginning of each day's tests. At the two lower power levels this leakage was stopped by coating the tube fitting with Devcon aluminum based epoxy. As the bed heated up the epoxy was somewhat pliable allowing for thermal expansion. When the bed cooled the epoxy cracked. It was therefore necessary to obtain as many experiments as possible each time the bed was heated because new epoxy had to be applied at the beginning of each day's tests. At the highest power level large enough temperature fluctuations

were found to occur, as the inner and outer air flow rates were varied, that the epoxy cracked even as the power was still being applied. Experiments were thus conducted only at the two lower levels. Prior to applying new epoxy at the beginning of each day's tests the old epoxy had to be removed using a hand held propane torch. After several sets of experiments had been collected, the phenolic had been burned to a sufficient extent that gas leakage could no longer be stopped. At that point experimentation was concluded. Of the experiments collected two are not reported here as other problems occurred which cast doubt upon their reliability. In one of these, thermal expansion caused the bed particles to grind against the upper porous plate decreasing gas flow there; the plate had to be cleaned before additional exerimentation could proceed. A total of twenty-eight experiments are thus reported here.

6.2 Experimental Results

6.2.1 Data Reduction

The void fractions in the three packings studied were obtained as follows. A known mass of particles was introduced into the known volume of the annular region. The published density for solid soda-lime glass of 2.51 g/cm^3 gave the nonvoided volume and therefore the void fraction. This resulted in void fractions of 0.419, 0.395, and 0.385 for the 608, 304, and 203 particles respectively.

The data for the variation of the physical properties with temperature used in the following analyses were obtained from the literature and are discussed in Appendix 1. The inner and outer air velocities were calculated from the measured volumetric flow velocities and the flow cross sectional areas. The Reynolds number was based upon the inner air velocity and the coolant tube diameter. The outer air velocity was calculated in the usual fashion and based upon the empty annular area. The modified Reynolds number was calculated from this velocity and the average particle size. An outline of the experimental program with the various combinations of these experimental variables is presented in Table 6.2-1.

The experimental conditions were utilized in order to calculate the theoretical static effective conductivities predicted by six of the models that were discussed in Chapter 3. The models studied were those proposed by Yagi and Kunii (1957), Kunii and Smith (1960), Willhite, Kunii, and Smith (1962), Krupiczka (1967), Specchia, Baloi, and Sicardi (1980), and by Specchia and Sicardi (1980). Similarly, the effective conductivities predicted by eight of the correlations discussed in Chapter 2 were calculated. The correlations studied were those of Bunnell, Irvin, Olson, and Smith (1949), Schertz and Bischoff (1969), Quinton and Storrow (1956), Plautz and Johnstone (1955), Coberly and Marshall (1951), Campbell and Huntington (1952), Calderbank and Pogorski (1957), and Phillips, Leavitt, and Yoon (1960).

Initially, an attempt was made to present data for k_e and h_w in the annular packed bed. However, an energy balance could not be verified even when accounting for the heat losses from the shroud to the surrounding ambient air. Furthermore, no consistent temperature discontinuity between the wall and the bed was observed; this was true for both the heated outer and cooled inner walls. It was therefore decided to present data for the overall effective conductivity inasmuch as k_o depended upon the temperature profile but not the heat flow.

The nondimensional temperature profile based upon the assumptions valid for the experimental conditions is derived in detail in Appendix 3 and is listed here as:

$$\frac{t - t_R'}{t_R - t_R'} = 1 - \frac{\partial t}{\partial z}\frac{R^2 G_o c_p}{4k_o(t_R - t_R')}(1 - \xi^2) - \left\{1 - \frac{\partial t}{\partial z}\frac{R^2 G_o c_p}{4k_o(t_R - t_R')}\left[1 - \left(\frac{R'}{R}\right)^2\right]\right\}\frac{\ln \xi}{\ln (R'/R)} \qquad (6.2\text{-}1)$$

The experimental temperature profiles obtained by the micrometer-mounted thermocouple probe located in the axial plane 18.1 cm above the inlet were plotted as nondimensional profiles and curve fitted in order to compare them with Equation (6.2-1). The reader is reminded that Equation (6.2-1) is valid over the cross section of the annulus in any axial plane beyond the thermal entrance region and was based upon the assumption of a constant axial temperature

gradient in the packed bed. Except for the portion of the packed bed located beyond the plane 18.1 cm above the inlet, the axial temperature profiles were found to be quite linear with approximately constant slope across the bed cross section. The axial temperature gradient was thus calculated with the temperatures obtained by the stationary thermocouple probes lying in the axial planes 11.1 and 18.1 cm above the inlet. As was mentioned above, it was this section that lay just prior to the plane in which k_0 was calculated. Three separate values for the temperature gradient were calculated at the radial positons of $r/R = 0.506$, 0.759, and 0.886. Since these three values differed only slightly, their average was utilized. The stationary thermocouple probes located at a radial position of $r/R = 0.316$ were not used in this calculation since the micrometer-mounted probe was located in the plane 18.1 cm above the inlet. Discrepencies between the two types of probes were observed; other inconsistencies suggested that data obtained from these stationary probes were unreliable.

An iterative scheme was utilized in order to obtain the overall conductivity from the data utilizing Equation (6.2-1). Of the six models studied for the static effective conductivity, the model of Krupiczka (1967) consistently predicted the lowest value. It was thus this value that was used as a first approximation for k_0. With this approximation the theoretical nondimensional temperature profile could be computed from Equation (6.2-1). The error between the experimentally observed and theoretically predicted nondimensional

temperature profiles was then computed as the sum of the squares of the difference between the two profiles at each of the radial positions experimentally studied. The assumed overall conductivity was then increased by 1% and the entire process was iterated so that the overall effective conductivity corresponding to the minimum error was obtained. In this method the true error-minimized overall effective thermal conductivity was computed for each set of experimental data. The overall conductivity was also nondimensionalized with respect to the gas conductivity in the axial plane containing the micrometer-mounted thermocouple probe.

The theoretical nondimensional temperature profiles calculated above, corresponding to the error-minimized overall conductivity, along with t_R and t_R' were utilized to compute the theoretical temperature profiles in the same plane. This allowed comparison with the experimentally obtained temperature profiles. Similarly, the effective conductivity predicted by the eight correlations discussed above were utilized to compute theoretical temperature profiles via Equation (6.2-1).

The goals of these comparisons were to: i) verify that the error-minimized temperature profiles approximated those of the experimental data; ii) verify whether temperature profiles based upon the correlations, none of which were valid in the range of modified Reynolds number studied, could approximate those of the experimental data; and iii) determine whether correlations for k_e and k_0 both of which were utilized in ii) above, produced significant differences here.

6.2.2 Results

Figures 6.2-1, 6.2-2, and 6.2-3 show typical results for the axial temperature profiles. These temperature profiles were obtained by the stationary thermocouple probes located at three radial positions within the bed as well as thermocouples spot welded onto the inner and outer walls. Within the bed it can be seen that the temperature increased approximately linearly with axial position except near the top of the bed where the end effects mentioned above occurred. The gradient was found to be indepencent of radial position. The approximation of constant axial temperature gradient utilized to derive Equation (6.2-1) was thus found to be valid.

Typical radial temperature profiles obtained by the micrometer-mounted thermocouple probe located in the axial plane 4.1 cm above the inlet are presented in Figure 6.2-4. The temperature profiles at that elevation were similar in all of the cases studied. The profiles were found to be relatively flat near the inner wall with small negative radial temperature gradient indicating outward heat flow from the hot coolant in the central tube near its exit.

Typical nondimensional radial temperature profiles obtained by the micrometer-mounted thermocouple probe located in the axial plane 18.1 cm above the inlet are presented in Figures 6.2-5, 6.2-6, and 6.2-7. Results for the error-minimized theoretical profiles are also presented. Three different observations become immediately apparent. Profiles like Figure 6.2-5 are very similar in form to the theoretical profile predicted by Equation (6.2-1). Other profiles

like Figure 6.2-6 were found to be S-shaped in nature with a nearly constant increase in temperature across the middle of the annulus; the two-dimensional one-parameter method does not match the experimental data of the type presented in Figure 6.2-6 as well as for profiles of the type reproduced in Figure 6.2-5. Finally, some of the experimental data produced temperature profiles that were flat over large distances adjacent to the outer wall; an example is presented in Figure 6.2-7. These profiles are clearly in error. They were a result of slippage of the probe or air leakage through the guide tube through which the thermocouple probe penetrated the outer wall. Analysis showed that unrealistically high values of k_0 would be needed to fit such temperature profiles.

In Figures 6.2-8, 6.2-9, and 6.2-10 typical results for the experimentally observed radial temperature profiles and error-minimized radial temperature profiles are reproduced. These are again the profiles obtained by the micrometer-mounted thermocouple probe located in the plane 18.1 cm above the inlet. Plotted for comparison are the temperature profiles predicted by Equation (6.2-1) incorporating the effective conductivities proposed by the correlations of five of the authors discussed in Section 6.2.1. No agreement between the experimental and calculated temperature profiles was found when the effective conductivities predicted by Bunnell, Irvin, Olson and Smith (1949), Quinton and Storrow (1956), or Phillips, Leavitt, and Yoon (1960) were utilized. Analysis showed that no single correlation provided consistent agreement between experiment and theory. It is

interesting to note that even though Equation (6.2-1) was derived based upon the two-dimensional, one-parameter method better comparison between experiment and theory was obtained when using the correlations for the effective conductivity based upon the two-dimensional, two-parameter method. In fourteen of the twenty-eight experiments, however, none of the eight correlations provided satisfactory comparison.

Results obtained for the error-minimized overall effective conductivity in each of the twenty-eight experiments are presented in Table 6.2-2. Also presented for comparison are the modified Reynolds numbers for each case. Note that in five experiments the nondimensionalized overall conductivity is designated by an asterisk. These were the experiments which demonstrated nondimensional radial temperature profiles corresponding to the type depicted in Figure 6.2-7. As was discussed above, the flattened profiles near the outer wall caused disagreement between the experimental and theoretical curves unless unrealistically high values for the overall conductivities were assumed.

It was not possible to correlate the overall effective conductivity with modified Reynolds number in either the usual linear fashion or any other consistent function. In fact, it can be seen in Table 6.2-2 that different experiments conducted in the same packed bed at the same modified Reynolds number did not necessarily yield the same overall conductivities. Since the bed had not been

dissassembled or repacked these discrepancies cannot be attributed to the packing characteristics of the bed. Neither can these discrepancies be attributed to an additive contribution due to radiation effects which were not considered in the derivation of Equation (6.2-1). The overall conductivity consistently decreased as heating, either increasing power level or decreasing inner air velocity, was increased; in none of the tests did the temperature exceed 250°C.

Other less likely explanations for the discrepancies discussed above were also analyzed. These included: i) the variations of the physical properties, which were required by Equation 6.2-1, with temperature across the bed cross section; and ii) variations in the method used to calculate the axial temperature gradient. No appreciable differences from the results presented in Table 6.2-2 were observed.

The two remaining possibilities are: i) slippage of the micrometer probe so that the data for the radial temperatures were not always obtained at the radial positions recorded; and ii) the two-dimensional one-parameter method does not describe well the heat transfer in a packed bed at low modified Reynolds number. Although the former is a possibility it is not likely. In order to describe satisfactorily temperature profiles of the type depicted in Figure 6.2-7 the radial positions recorded would have to have been in error by up to 0.48 cm. Explanation in terms of a two-dimensional, two-parameter method is much more likely; the S-shaped profiles could

better be explained in terms of a constant effective thermal conductivity across the bed and wall heat transfer coefficients effective in the narrow regions near either wall. No attempt was made to obtain data for k_e or h_w because of the heat balance problems discussed above.

6.3 Conclusions and Recommendations

Table 6.2-1 lists the various combinations of particle size, heat flux, coolant flow velocity and purge gas velocity investigated in this study. A total of twenty-eight experiments have been obtained. Data were difficult to obtain in cases tested with large temperature fluctuations. It was not possible, therefore, to collect data at power levels above 150W. Radiant heat transfer was found to be insignificant in the packed bed which never exceeded 250^{o}C.

The axial temperature profiles within the bed were found to be linear with a constant slope across the bed cross section. With this observation the radial temperature profile was derived in terms of k_o based upon the two-dimensional one-parameter method. Derivation of this temperature profile is presented in Section A3.1. The experimental radial temperature profiles were found to be similar to the theoretically predicted profile as was presented in Equation (6.2-1).

An iteration procedure and an error minimization scheme were utilized in order to obtain k_o from a comparison of the experimental profile and Equation (6.2-1). The results were

presented in Table 6.2-2.

No correlation for k_0 could be presented. The most likely cause for the inconsistent dependence of the overall conductivity on N_{Re}' is that the two-dimensional, one-parameter method was not applicable for this packed bed at low modified Reynolds numbers. The first recommendation for further research, therefore, is to obtain data for the effective thermal conductivity and wall heat transfer coefficient in the packed bed. This would require that modifications be incorporated so that a heat balance could be obtained. To this end, the outer air exit temperature must be measured. Restricting studies to packed beds with fine particles would be very useful. In such beds the velocity profile has been demonstrated to be quite flat; insertion of a thermocouple probe into the exit plane approximately one half the distance across the annulus would give results for the bulk exit temperature that would not be in serious error. More accurate values for the exit temperature would require more extensive modification of the existing system. A micrometer-mounted thermocouple probe could be inserted into the exit plane; simple numerical integration with a flat velocity profile would yield the exit temperature. Extensive modification of the existing apparatus would be required should larger particle sizes be pursued. The velocity profile in such systems would make numerical integration complicated. Instead, the bulk exit temperature should be measured in a mixing section that should be located immediately above the heated section. The present apparatus has a 17.1 cm calming section

between the exit from the heated section and the mixing section.

The particle and gas characteristics were not studied. Additional experiments should be carried out incorporating various particles and gases so that the effect of particle physical properties and gas Prandtl number can be analyzed. Finally, any useful correlation for k_e or h_w must also consider the effect of the particle-to-tube diameter ratio. In the literature k_e and h_w were generally tabulated for each particular value of d_p/D_t. Data in this form is generally not useful when making theoretical predictions of the type discussed in Section 6.2.

Table 6.1-1 Experimental Variables for the Stationary Particle Bed Experiment

Particle Size Range
- 177-250 μm
- 420-590 μm
- 590-840 μm

Power Level
- 100, 150 W

Heat Flux
- 0.217, 0.326 w/cm^2

Inner Air Velocity
- 200, 500 cm/s

Reynolds Number
- 1340-3630

Outer Air Velocity
- 10, 20, 30 cm/s

Modified Reynolds Number
- 1.00-11.70

Table 6.2-1 Combinations of Experimental Variables Stucied in the Stationary Packed Bed experiments

Inner Air	Particle Size Range (μm)						Power
Superficial	177-250		420-590		590-840		Level
Velocity (cm/s)	Outer Air Velocity (cm/s)						(W)
	200	500	200	500	200	500	
10	X	X	X	X	X	X	100
			X	X		X	150
20	X	X	X	X	X	X	100
				X	X	X	150
30	X	X	X	X	X	X	100
			X	X	X	X	150

Table 6.2-2 Results Obtained for N'_{Re} and k_o/k_g in the Stationary Packed Bed Experiments

Particle size Range (μm)	Inner Air Superficial Velocity (cm/s)						Outer Air Velocity (cm/s)	Power Level (W)
	10		20		30			
	N'_{Re}	$\frac{k_o}{k_g}$	N'_{Re}	$\frac{k_o}{k_g}$	N'_{Re}	$\frac{k_o}{k_g}$		
177-250	0.999	36.9	2.185	14.2	3.457	14.9	200	100
	1.027	*	2.187	20.7	3.453	15.1	500	
420-590	2.477	33.6	5.204	15.1	8.286	16.0	200	100
	2.579	50.2	5.250	16.7	8.300	14.7	500	
	2.367	9.8			8.195	7.9	200	150
	2.397	13.9	5.154	9.3	8.200	8.1	500	
590-840	3.139	*	7.310	51.8	11.685	23.8	200	100
	3.300	*	7.298	140	11.704	*	500	
			6.543	45.4	10.660	18.7	200	150
	2.922	*	6.741	21.2	10.805	32.4	500	

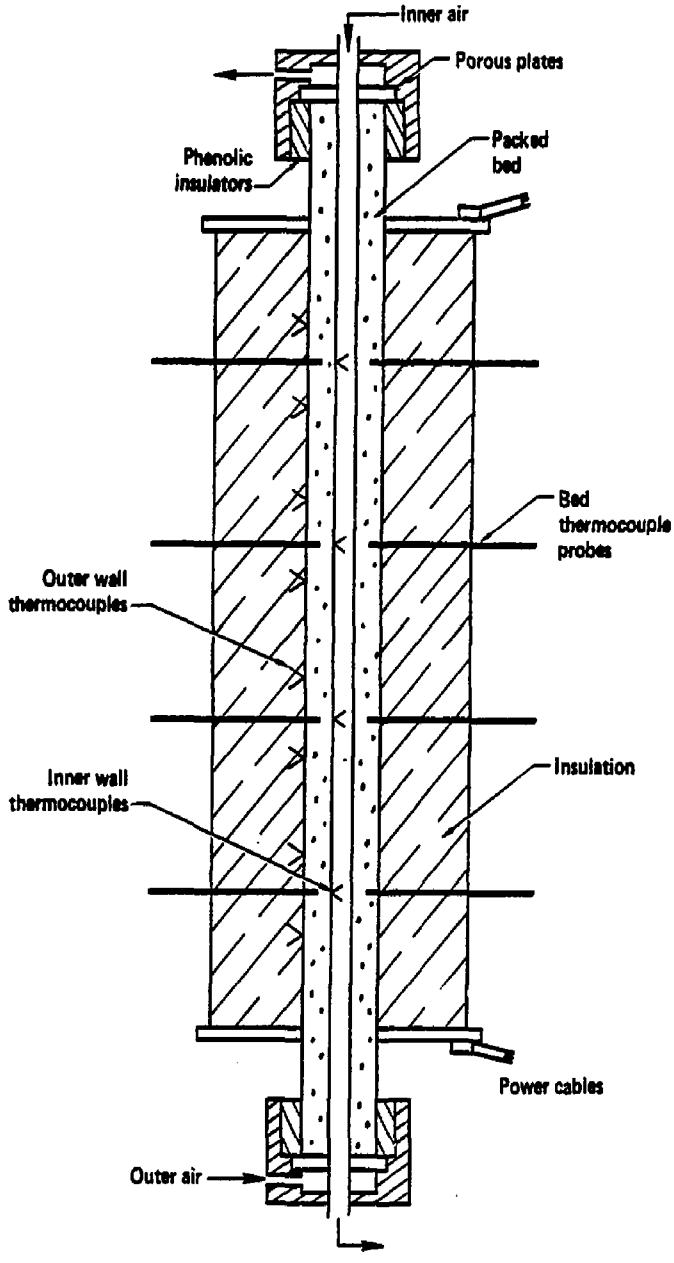

Figure 6.1-1. Schematic of the stationary bed test apparatus.

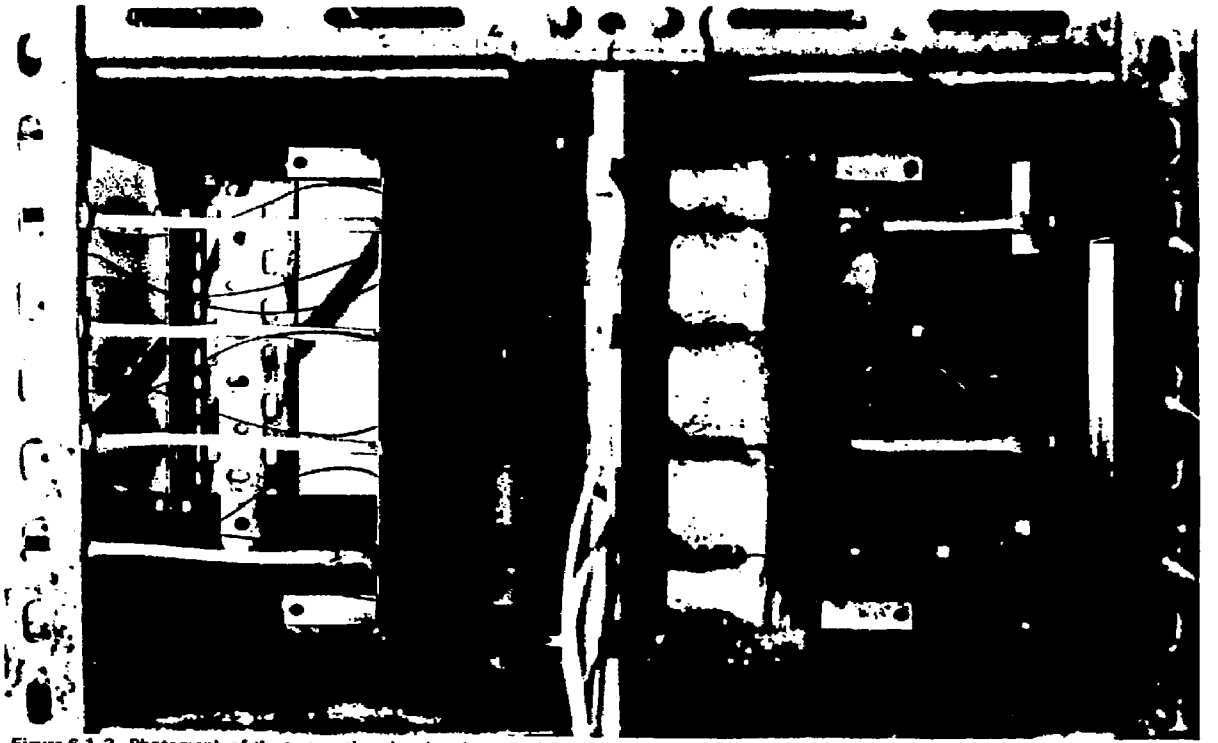

Figure 6.1-2. Photograph of the test section showing the outer insulation, the surface thermocouples, the stationary and micrometer mounted thermocouple probes.

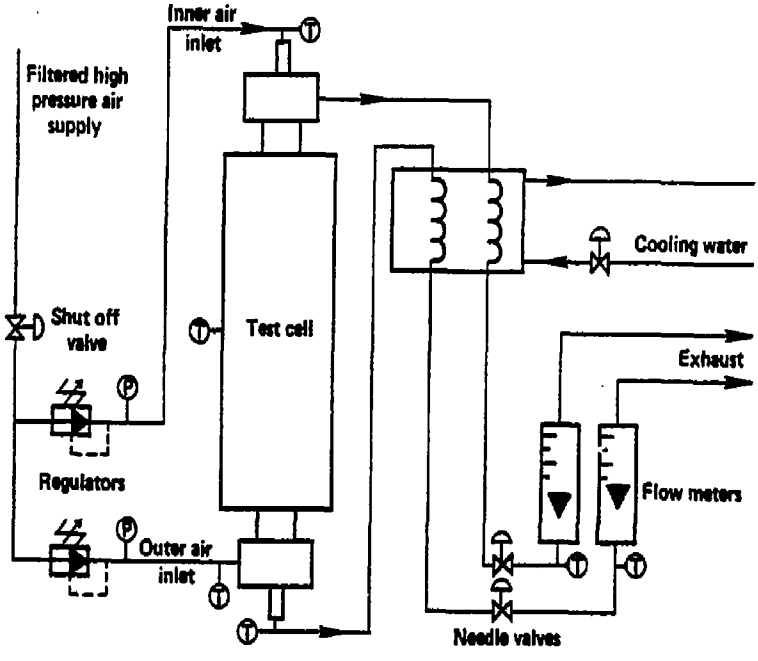

Figure 6.1-3. Stationary bed experiment cooling system.

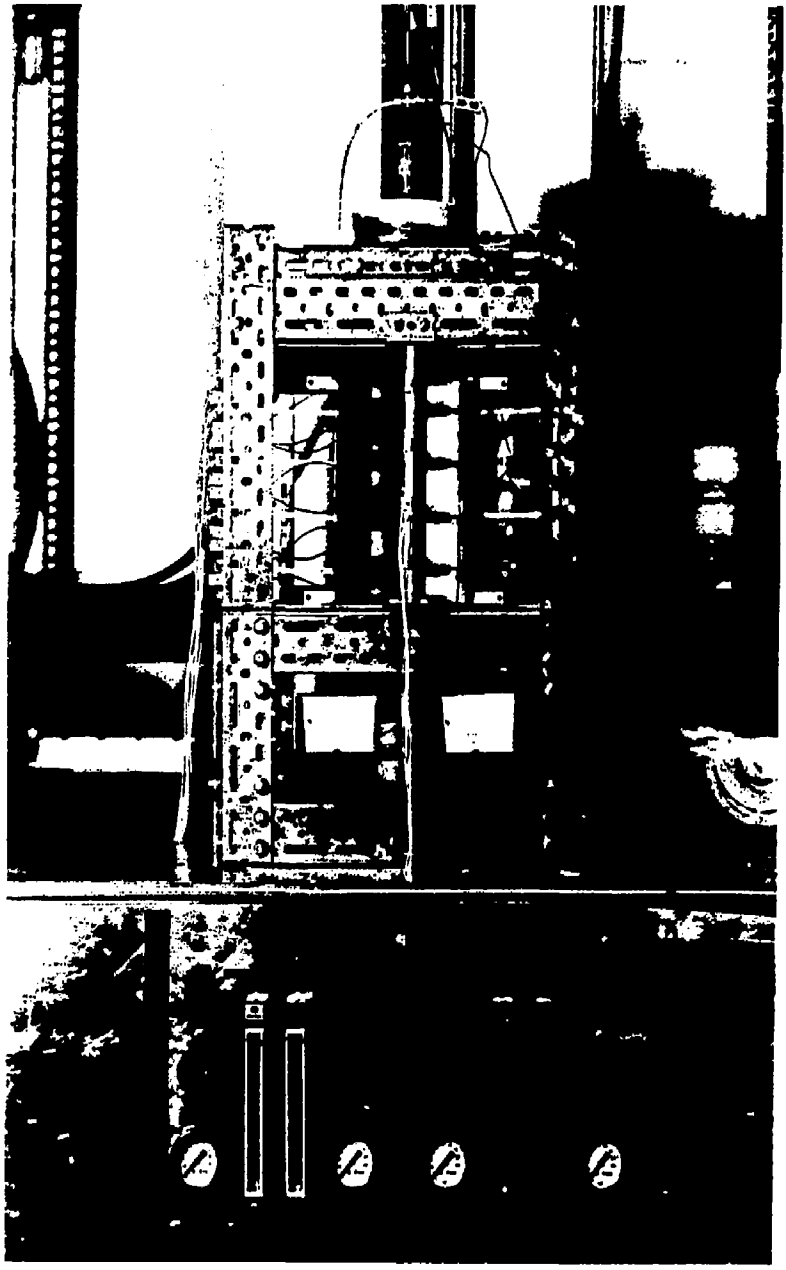

Figure 6.1-4. Photograph of the stationary bed experiment with exposed test section.

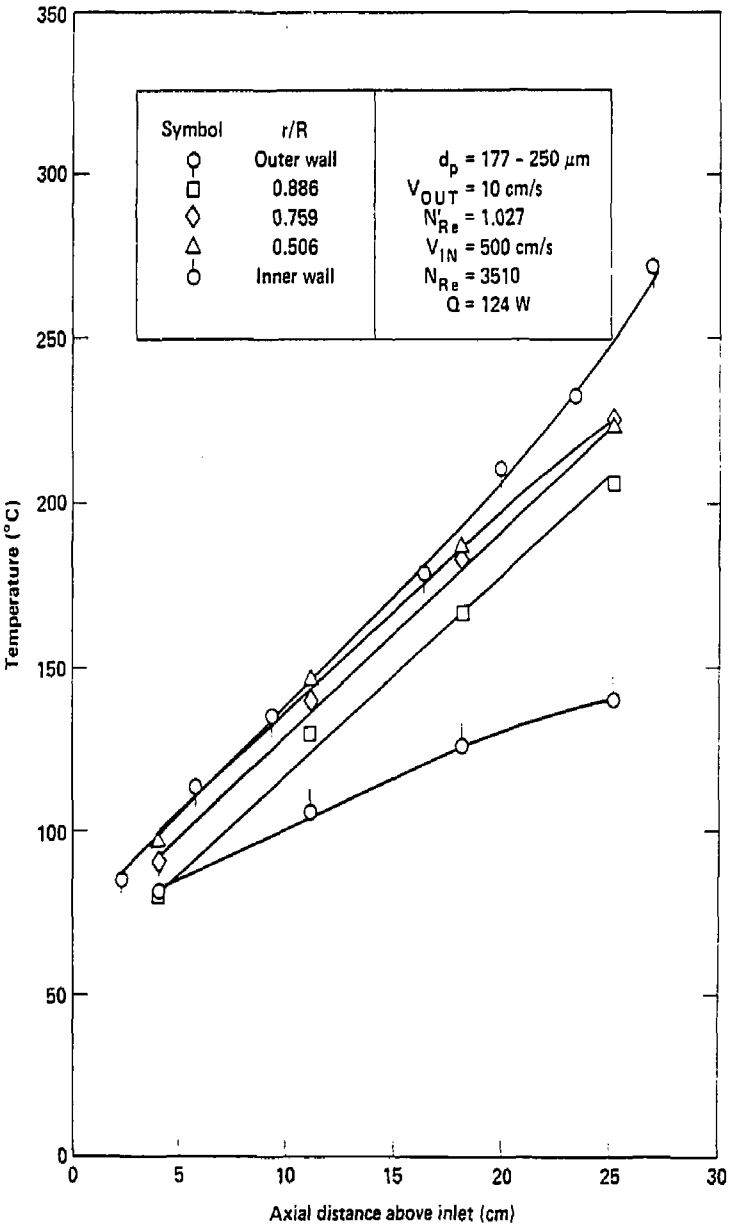

Figure 6.2-1 Packed bed axial temperature profiles as functions of radial position.

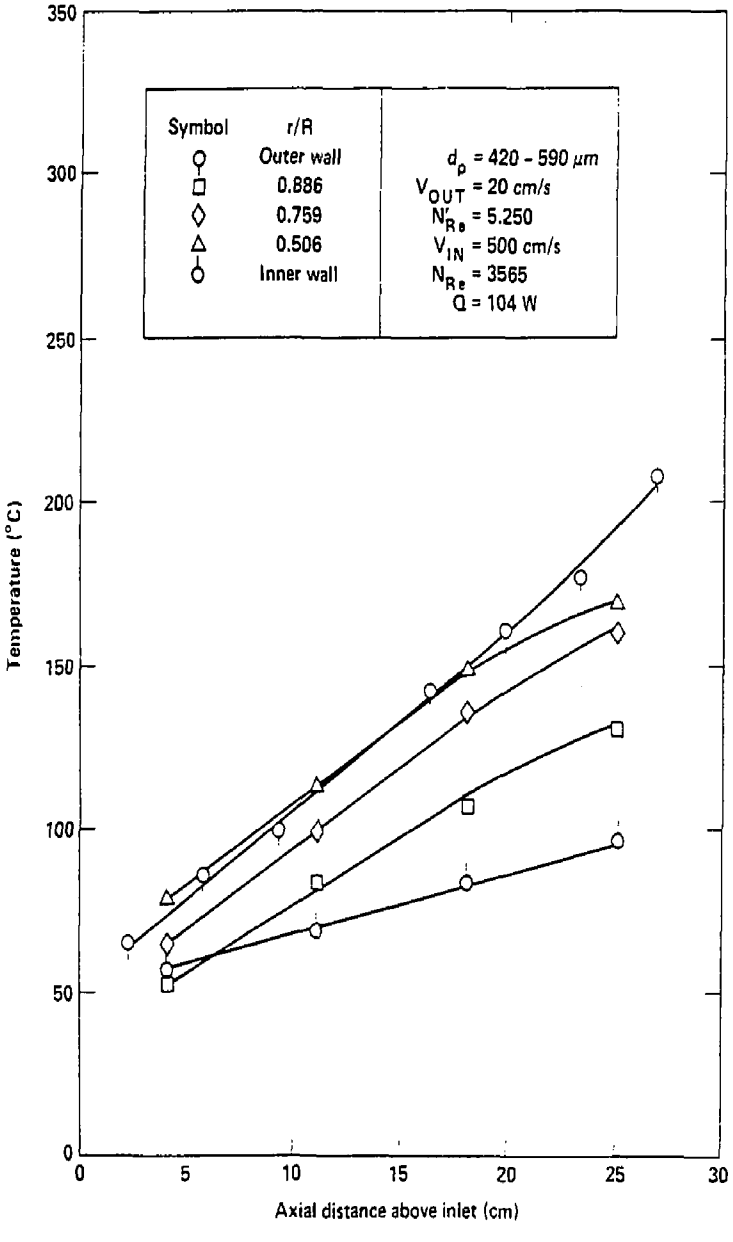

Figure 6.2-2 Packed bed axial temperature profiles as functions of radial position.

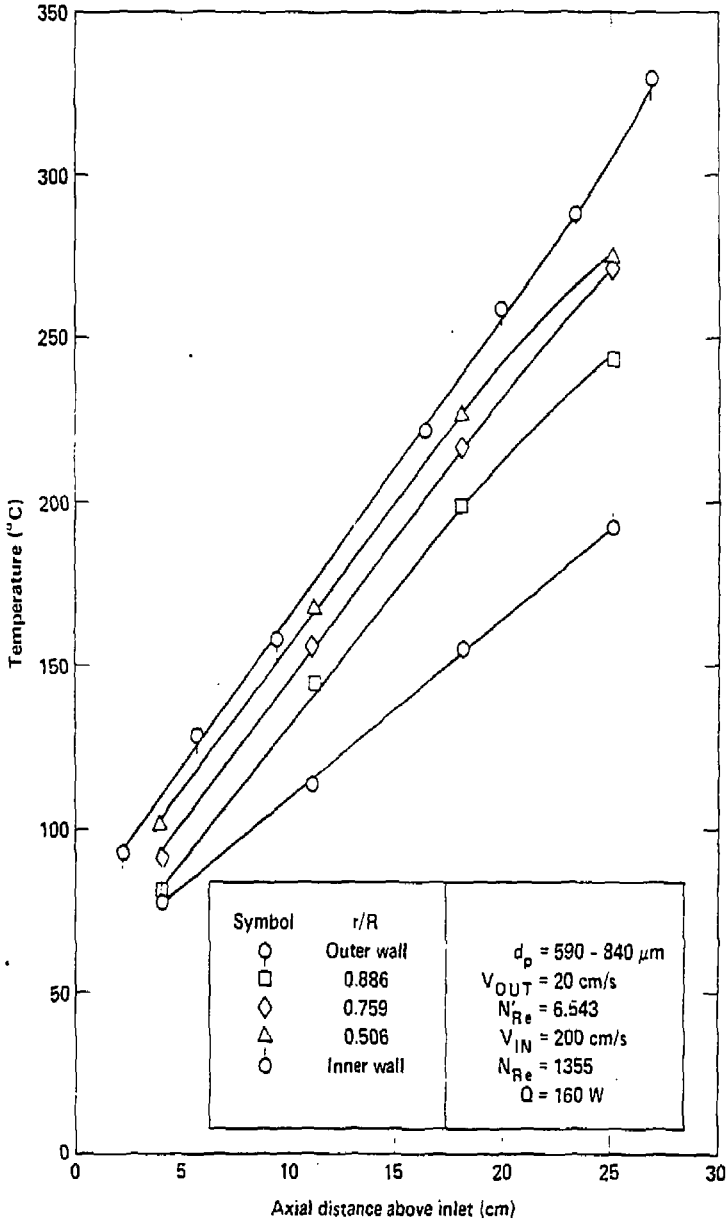

Figure 6.2-3 Packed bed axial temperature profiles as functions of radial position.

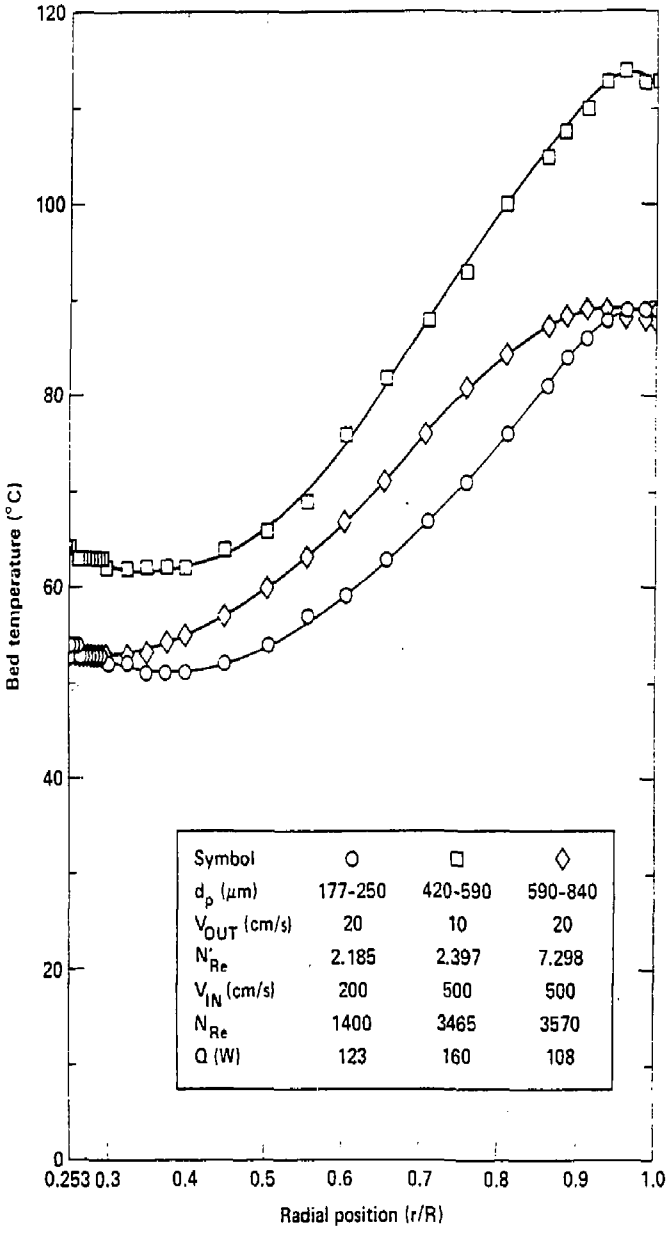

Figure 6.2-4 Radial temperature profile in the plane 4.1 cm above the inlet.

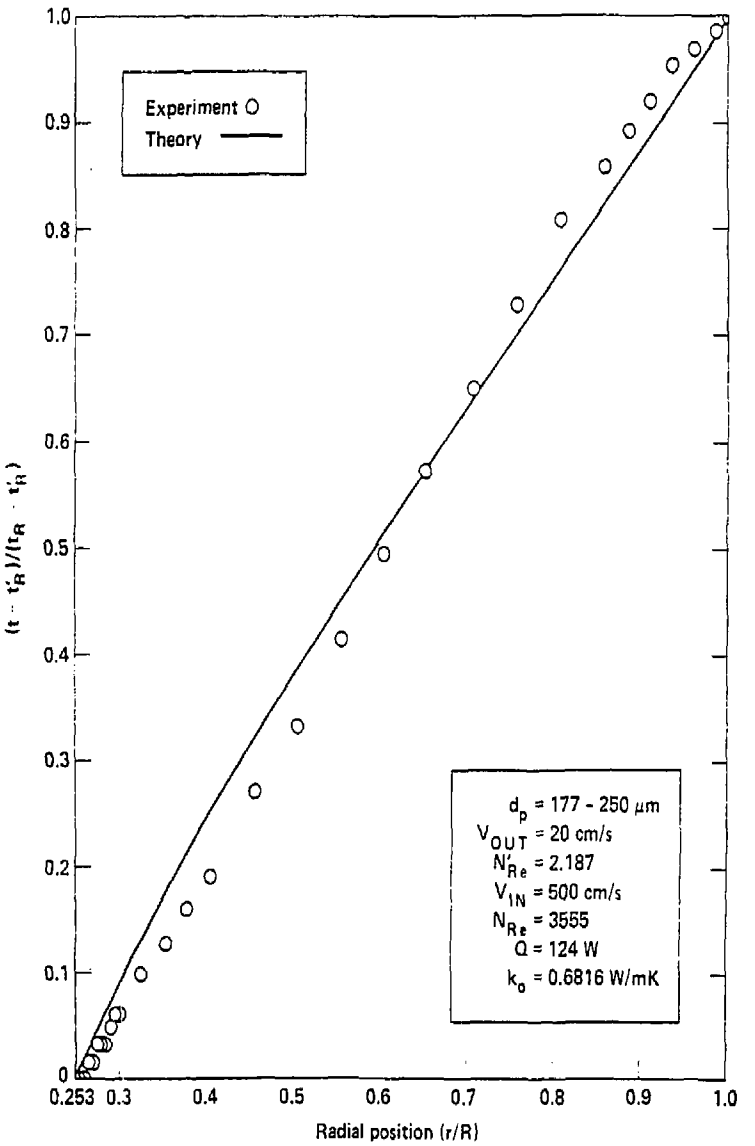

Figure 6.2-5 Experimental and error-minimized theoretical nondimensional temperature profiles in the plane 18.1 cm above the inlet.

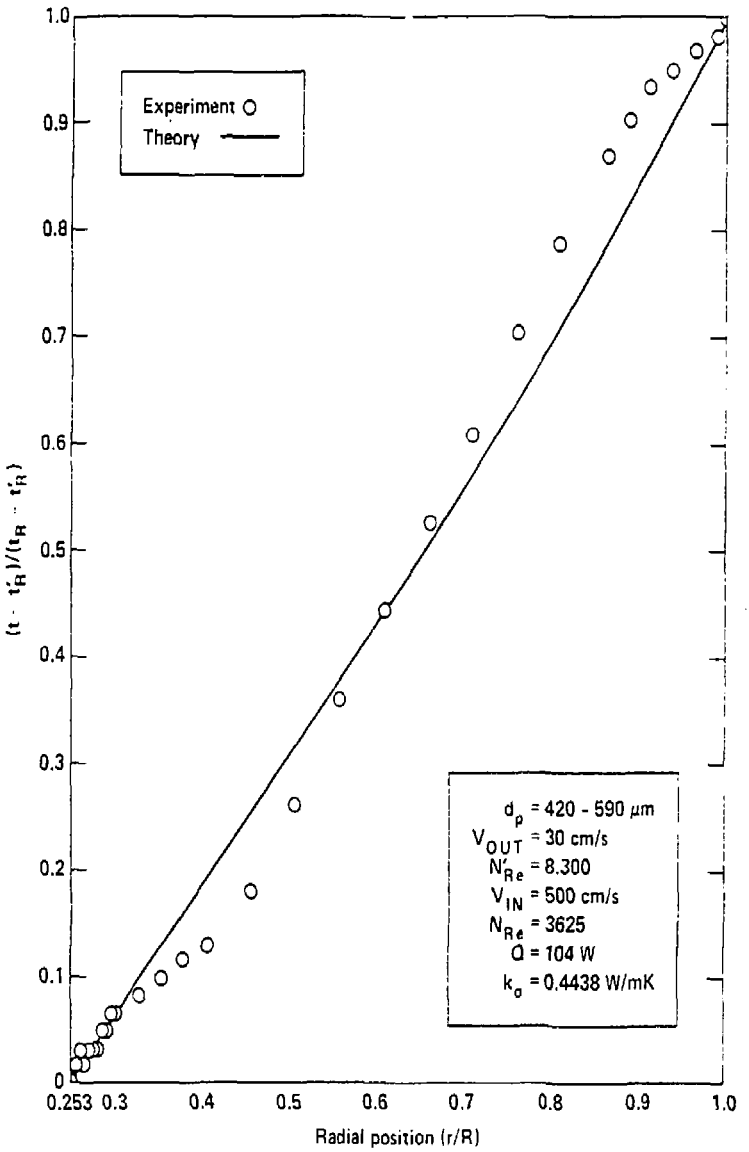

Figure 6.2-6 Experimental and error-minimized theoretical nondimensional temperature profiles in the plane 18.1 cm above the inlet.

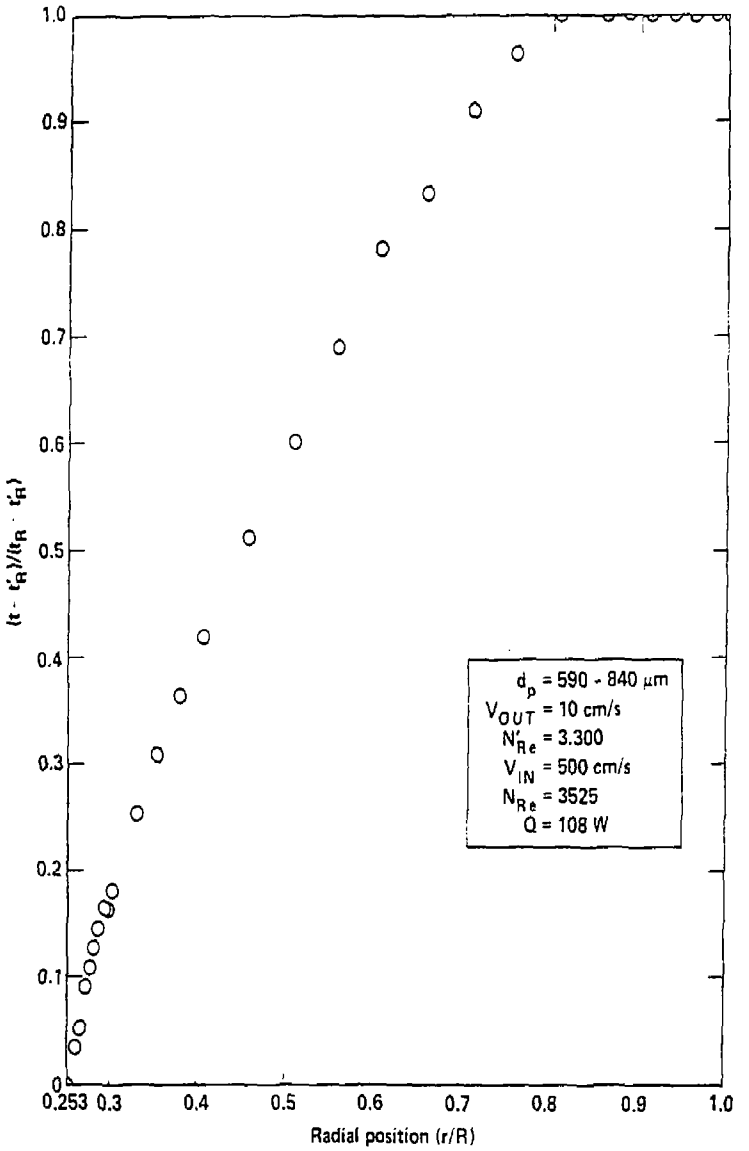

Figure 6.2-7 Experimental nondimensional temperature profile in the plane 18.1 cm above the inlet.

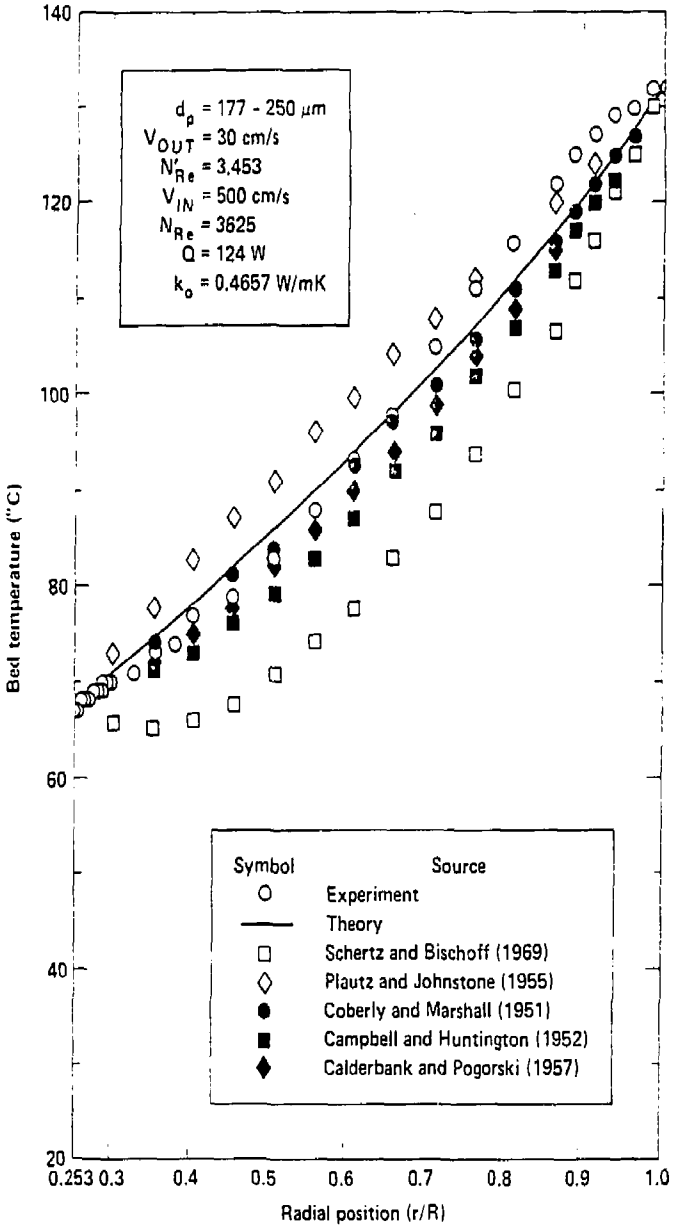

Figure 6.2-8 Radial temperature profiles in the plane 18.1 cm above the inlet.

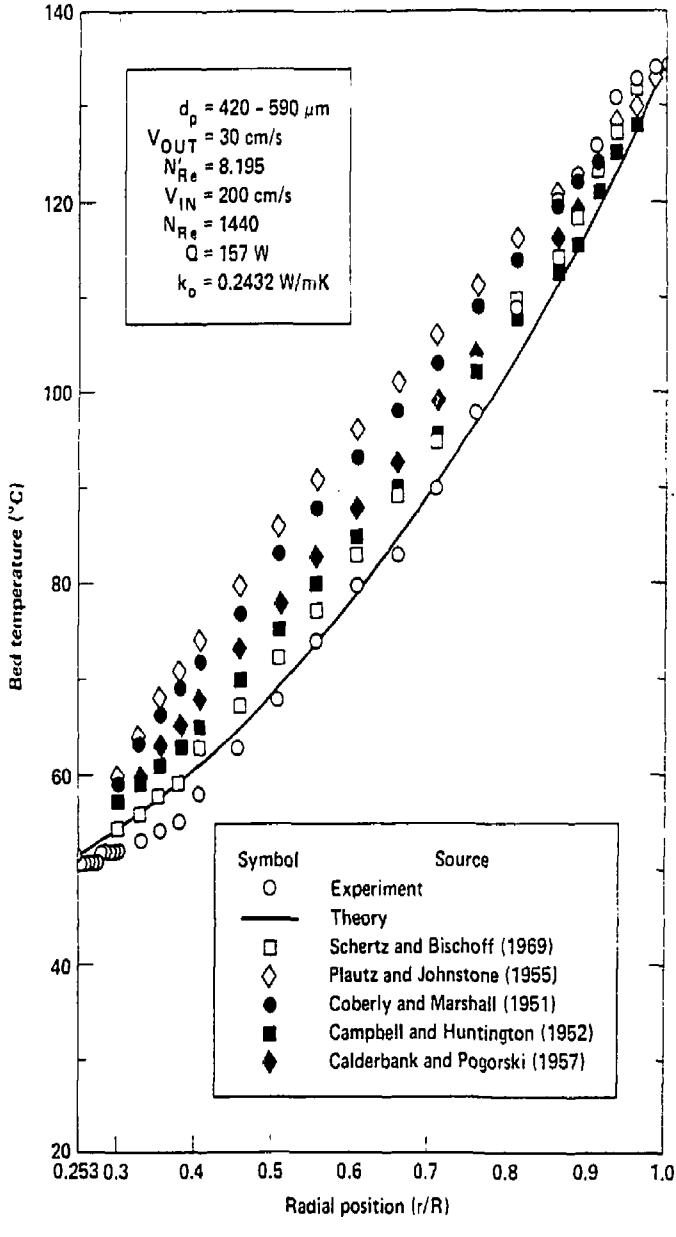

Figure 6.2-9 Radial temperature profiles in the plane 18.1 cm above the inlet.

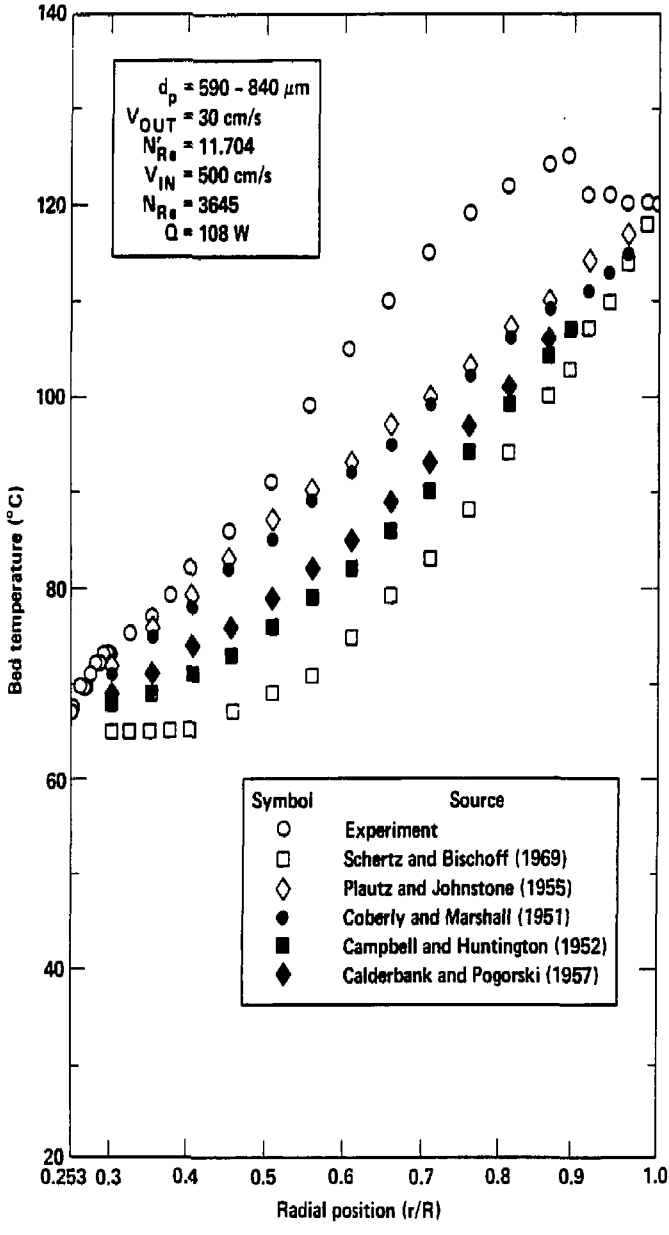

Figure 6.2-10 Radial temperature profiles in the plane 18.1 cm above the inlet.

NOMENCLATURE

a	function of d_p/D_t presented by Colburn (1931)
a_1	function of r/R presented in correlation of Irvin, Olson, and Smith (1951)
a'	parameter in correlation of Baumeister and Bennett (1958)
A	wall surface area in packed bed
A_m	normalization coefficient presented by Sellars, Tribus, and Klein (1956)
A'	parameter in model of Krupiczka (1967)
b	thickness of annular ring in annular packed bed
b'	parameter in correlation of Baumeister and Bennett (1958)
b^*	distance over which conduction takes place in model of Schotte (1960)
B'	parameter in model of Krupiczka (1967)
c_1	constant in correlation of Hanratty (1954)
c_2	constant in correlation of Schertz and Bischoff (1969)
c_3	constant in correlation of Votruba, Hlavacek, and Marek (1972)
c_n	normalization coefficient presented by Siegel, Sparrow, and Hallman (1958)
C_n	normalization coefficient for thermally developing region with flat velocity profile
c_p	specific heat of gas
c_{pp}	specific heat of particle
d_e	equivalent diameter of particle with rough

$$\text{surface} = \frac{4\varepsilon}{S + 0.75A}$$

d_g mean diameter of gas molecule

d_o diameter of sphere with same external surface area as particle

d_p diameter of spherical particle

D_e equivalent diameter of annular ring = 2b

D_i tube nodal inside diameter

D_o equivalent diameter defined by Votruba, Hlavacek, and Marek (1972) $= \dfrac{(4/6)\, D_t \varepsilon}{1 + (1 - \varepsilon)(D_t/d_p)}$

D_t diameter of tube

e emissivity of particle

f combined friction factor for packed bed

f_1 parameter in Figure 2.1-2

f' parameter in model of Wakao and Vortmeyer (1971)

g 9.8 m/s^2

G local superficial gas velocity based on empty tube area

G_o average superficial gas velocity based on empty tube area

h_c average convective heat transfer coefficient for falling bed

$h_{loc,i}$ local heat transfer coefficient for node i

h_L heat transfer coefficient between flat plate and falling bed

h_o overall heat transfer coefficient

h_p heat transfer coefficient for conduction through points of contact

h_{pg} heat transfer coefficient between particle and gas

h_r radiant heat transfer coefficient

h_{rs} heat transfer coefficient due to radiation between particle surfaces

h_{rv} heat transfer coefficient due to radiation between voids

h_w wall heat transfer coefficient

h_w^o stagnant contribution to h_w

h_w^t eddy contribution to h_w

h_w^* heat transfer coefficient of the boundary layer on the wall

h' heat transfer coefficient between particle surface and fluid or other particles

j_H j-factor for heat transfer $= \frac{h_{pg}}{c_p G_o}\left(\frac{c_p \mu_g}{k_g}\right)^{2/3}$

j_{Ho} asymptotic value of j_H according to Glaser and Thodos (1958)

k_B Boltzmann constant = 1.380×10^{-23} J/K

$k_{contact}$ additive term in model of Wakao and Vortmeyer (1971)

k_c' thermal conductivity for molecular conduction in the void space

k_e effective thermal conductivity

k_e^d dynamic contribution to conduction

k_e^o stagnant contribution to k_e

k_e^t eddy contribution to k_e

k_e^v k_e^o under vacuum conditions

k_e^* apparent conductivity $= \dfrac{k_g\, 0.9(1 - \varepsilon)}{\phi + (2/3)(k_g/k_p)}$

k_{er} radial effective thermal conductivity

k_{ew} effective thermal conductivity in the near-wall region

k_{ew}^o stagnant contribution to k_{ew}

k_{ez} axial effective thermal conductivity

k_{ez}^o static contribution to k_{ez}

k_g thermal conductivity of gas at average bed temperature

k_g' thermal conductivity of gas which varies with pressure

k_o overall effective thermal conductivity

k_o^g overall effective thermal conductivity for gas

k_o^o stagnant contribution to k_o

k_o^p overall effective thermal conductivity for particles

k_p thermal conductivity of particle

k_p' thermal conductivity for conduction through the points of contact

k_r' thermal conductivity for radiation in the void space

k_{rad}^∞ additive term in model of Wakao and Vortmeyer (1971)

k_{series}' thermal conductivity for heat flow through particle

k_{td}' thermal conductivity for turbulent diffusion in the void space

k_w thermal conductivity of gas at wall temperature

k_w^o $= 2\, k_{ew}^o$

ℓ_p average length between two neighboring particles in the direction of heat flow

ℓ_s	effective length of solid relating to conduction
ℓ_s^*	ℓ_s in the near-wall region
ℓ_v	effective thickness of fluid film in void relating to conduction
ℓ_v^*	ℓ_v in the near-wall region
ln x	natural logarithm of x
log x	ordinary logarithm of x
L	length of packed bed
L^o	length of flat plate in falling bed experiments
L_i	tube nodal length
m	$= k_e/h_w R$
m'	$= 0.55 \left(\frac{L}{D_t}\right)^{0.165}$
n	number of contact points
N	$= 1/\beta\ d_p$
N_{Ar}	Archimedes number $= d_p^3 g \rho_g (\rho_p - \rho_g)/\mu_g^2$
N'_{Gz}	modified Graetz number $= 1/\varepsilon\tau$
N_{Nu}	particle-gas Nusselt number $= h_{pg} d_p/k_g$
N_{Nu}^{loc}	local Nusselt number in a cylindrical tube
N_{Nu}^r	radiation Nusselt number $= h_r d_p/k_p$
N'_{Pe}	modified Peclet number $= d_p c_p G_o/k_e^t$
N_{Pem}	Peclet number for mass transfer
N_{Pr}	gas Prandtl number $= c_p \mu_g/k_g$
N_{Re}	Reynolds number $= D_t G_o/\mu_g$
N'_{Re}	modified Reynolds number $= d_p G_o/\mu_g$

p	absolute pressure
p_b	absolute breakaway pressure
p_o	atmospheric pressure
Δp	pressure drop through packed bed
q''	average wall heat flux
$q''_{c,ave}$	total convective heat flux
q''_{ci}	nodal convective heat flux
q''_o	constant wall heat flux
q''_{ri}	nodal radiative heat flux
Q	heat flow from wall to packed bed
r	radial distance from center line
r_H	hydraulic radius which varies with $r = \frac{\epsilon d_p}{6(1 - \epsilon)}$
R	bed radius = $D_t/2$
R_i	tube nodal electrical resistance
$R_n(r)$	eigenfunction presented by Siegel, Sparrow, and Hallman (1958)
R_{tot}	total tube electrical resistance
S	surface area of particle/unit volume of bed
S_p	surface area of equivalent particle
t	temperature of packed bed assuming $t_p = t_g$
t_a	average temperature in any given plane
t_e	average temperature in exit plane
t_{fd}	fully developed temperature profile in flowing packed bed
t_g	temperature of gas

t_i	average temperature in inlet plane
Δt_{ln}	terminal logarithmic mean temperature difference between wall and bed
t_L	radial temperature profile at some axial position L
t_m	mean temperature of packed bed with respect to radial position
t_o	constant inlet temperature of fluid
t_p	temperature of particle
t_{pi}	bulk particle temperature for node
t_R	extrapolated temperature of bed at inside surface of tube wall
t_w	temperature of tube wall
t_{wi}	wall temperature for node i
t'	$t \text{ @ } r = R - d_p/2$
t^+	difference temperature profile in thermal entrance region
T	$= t - t_w$
T_a	average temperature of packed bed
u	velocity at a given position
u_o	velocity at center line of tube
v_o	average velocity of flowing packed bed
V	average velocity across a given cross section
x	distance from inlet to heated section
x^+	$= (x/2R) [N_{Re} N_{Pr}]^{-1}$
z	axial distance from lowest point in heated bed

Greek Nomenclature

α	mass velocity of fluid flowing in direction of heat transfer/G_o = $\phi + \gamma/(k_g + k_p)$ in Willhite-Kunii-Smith model
α_e	effective thermal diffusivity
α_i	roots of $J_0(\alpha_i) = 0$
α_T	thermal coefficient of linear expansion
α_v	coefficient in Equation (2.3-5)
α_w	mass velocity of fluid flowing in direction of heat transfer near tube wall/G_o
$(\alpha\beta)$	parameter indicating eddy contribution to k_e = $1/N'_{Pe}$
α'	accomodation coefficient
α^*	fraction of voided space due to conduction in Masamune-Smith model
β	= ℓ_p/d_p
β_1	= $k_e/G_o c_p R^2$
β_n	eigenvalue presented by Siegel, Sparrow, and Hallman (1958)
β'	= $k_e/\rho_g c_p R^2$
γ	= ℓ_s/d_p
γ_m	eigenvalue presented by Sellars, Tribus, and Klein (1956)
γ_w	= ℓ_s^*/d_p
γ'	= c_p/c_v

δ	fraction of space not devoted to void conduction that is due solely to conduction through the points of contact in Masamune-Smith model
δ_1	fraction of effective area for heat transfer due to conduction through points of contact in Yagi-Kunii model
δ'	coefficient in correlation of Yagi, Kunii, and Wakao (1960)
δ^*	area fraction in model of Imura and Takegoshi (1974)
ϵ	void fraction
ϵ_1	void fraction for most loose packed state
ϵ_2	void fraction for most close packed state
ϵ_0	ϵ in central core of bed
ϵ_w	ϵ in near-wall region
ϵ'	area fraction in model of Imura and Takegoshi (1974)
ϵ^*	void fraction correction used by Willhite, Kunii, and Smith (1962)
Θ	time since initiation of transient
λ_1	eigenvalue presented by Kwong and Smith (1957)
λ_i	eigenvalue presented by Hougen and Piret (1951)
λ_n	eigenvalue presented by Coberly and Marshall (1951)
λ_o	mean free path of gas at atmospheric pressure
Λ	contact area/projected area of particle
μ	viscosity of gas at r_H
μ_g	viscosity of gas at average bed temperature
μ_o	viscosity of gas at room temperature

μ_w viscosity of gas at wall temperature

ξ $= r/R$

ρ_g density of gas

ρ_p density of particle

σ Steffan-Boltzman constant $= 5.729 \times 10^{-8}$ W/m^2K^4

τ $= 4Lk_o/c_pG_oD\dot{t}$

τ' $= \dfrac{(d_p/\lambda_o)(p/p_o)}{2(2-\alpha')/\alpha'}$

ϕ $= \ell_v/d_p$

ϕ_1 ϕ for most loose packed state

ϕ_2 ϕ for most close packed state

ϕ_m $= \ell_v^*/d_p$

ϕ' shape factor proposed by Glaser and Thodos (1958)

χ correlational parameter of Sullivan and Sabersky (1975)

ω_n eigenvalue for thermal developing region with flat velocity profile

REFERENCES

Abramowitz, M., and I. A. Stegun (Eds.), Handbook of Mathematical Functions, p. 409, Dover, New York (1965)

Agnew, J. B., and O. E. Potter, "Heat Transfer Properties of Packed Tubes of Small Diameter," Trans. Inst. Chem. Eng., 48(1), T15-T20 (1970)

Argo, W. B., and J. M. Smith, "Heat Transfer in Packed Beds. Prediction of Radial Rates in Gas-Solid Beds," Chem. Eng. Prog., 49(8), 433-451 (1953)

Baddour, R. F., and C. Y. Yoon, "Local Radial Effective Conductivity and the Wall Effect in Packed Beds," Chem. Eng. Prog. Sym. Series, (32), 35-50 (1961)

Baumeister, E. B., and C. O. Bennett, "Fluid-Particle Heat Transfer in Packed Beds," AIChE J., 4(1), 69-74 (1958)

Benenati, R. F., and C. B. Brosilow, "Void Fraction Distribution in Beds of Spheres," AIChE J., 8(3), 359-361 (1962)

Bernard, R. A., and R. H. Wilhelm, "Turbulent Diffusion in Fixed Beds of Packed Solids," Chem. Eng. Prog., 46(5), 233-244 (1950)

Bhattacharyya, D., and D. C. T. Pei, "Heat Transfer in Fixed Bed Gas-Solid Systems," Chem. Eng. Sci., 30(3), 293-300 (1975)

Bischoff, K. B., "Axial Thermal Conductivities in Packed Beds," Can. J. Chem. Eng., 40(4), 161-163 (1962)

Brinn, M. S., S. J. Friedman, F. A. Gluckert, and R. L. Pigford, "Heat Transfer to Granular Materials. Settled Beds Moving Downward Through Vertical Tubes," Ind. Eng. Chem., 40(6), 1050-1061 (1948)

Bunnell, D. G., H. B. Irvin, R. W. Olson, and J. M. Smith, "Effective Thermal Conductivities in Gas-Solid Systems," Ind. Eng. Chem., 41(9), 1977-1981 (1949)

Calderbank, P. H., and L. A. Pogorski, "Heat Transfer in Packed Beds," Trans. Inst. Chem. Eng., 35, 195-207 (1957)

Campbell, J. M., and R. L. Huntington, "Heat Transfer and Pressure Drop in Fixed Beds of Spherical and Cylindrical Solids. Part II. Heat Transfer and Temperature Gradients," Petrol. Ref., 31(2), 123-131 (1952)

Carlson, G. A., B. Arfin, W. L. Barr, B. M. Boghosian, J. L. Erickson, J. H. Fink, G. W. Hamilton, B. G. Logan, J. O. Myall, and W. S. Neef, Jr., "Tandem Mirror with Thermal Barriers," UCRL-52836 (1979)

Chu, Y. C., and J. A. Storrow, "Heat Transfer to Air Flowing Through Packed Tubes," Chem. Eng. Sci., 1(5), 230-237 (1952)

Coberly, C. A., and W. R. Marshall, Jr., "Temperature Gradients in Gas Streams Flowing Through Fixed Granular Beds," Chem. Eng. Prog., 47(3), 141-150 (1951)

Colburn, A. P., "Heat Transfer and Pressure Drop in Empty, Baffled, and Packed Tubes. I-Heat Transfer in Packed Tubes," Ind. Eng. Chem., 23(8), 910-913 (1931)

Conn, R. W., S. I., Abdel-Khalik, G. A. Moses, et al., "SOLASE, A Conceptual Laser Fusion Reactor Design," UWFDM-220 (1977)

Cybulski, A., M. J. Van Dalen, J. W. Verkerk, and P. J. Van Den Berg, "Gas-Particle Heat Transfer Coefficients in Packed Beds at Low Reynolds Numbers," Chem. Eng. Sci., 30(9), 1015-1018 (1975)

Damköhler, G., Der Chemie Ingenieur "Eucken Jakob", 3, Part I, 441 (1937)

De Wasch, A. P., and G. F. Froment, "Heat Transfer in Packed Beds," Chem. Eng. Sci., 27(3), 567-576 (1972)

Deissler, R. G., and C. S. Eian, "Investigation of Effective Thermal Conductivities of Powders," NACA RM E52C05 (1952)

Deissler, R. G., and J. S. Boegli, "An Investigation of Effective Thermal Conductivities of Powders in Various Gases," Trans. ASME, 80(7), 1417-1425 (1958)

Denloye, A. O. O., and J. S. M. Botterill, "Heat Transfer in Flowing Packed Beds," Chem. Eng. Sci., 32(5), 461-465 (1977)

Dietz, P. W., "Effective Thermal Conductivity of Packed Beds," Ind. Eng. Chem. Fund., 18(3), 283-286 (1979)

Dixon, A. G., D. L. Cresswell, and W. R. Patterson, ACS Sym. Series 65, Chem. Reaction Eng. - Houston, p. 237 (1978)

Gamson, B. W., G. Thodos, and O. A. Hougen, "Heat, Mass and Momemtum Transfer in the Flow of Gases Through Granular Solids," Trans. AIChE, 39(1), 1-35 (1943)

Gelperin, J. J., and A. M. Kagan, "Study of Heat Transfer in Gas Flow in Tubes Packed with Granular Materials," Proc. 3rd Int. Ht. Trns. Conf., 4, 308-321 (1966)

Glaser, M. B., and G. Thodos, "Heat and Momemtum Transfer in the Flow of Gases Through Packed Beds," AIChE J., 4(1), 63-68 (1958)

Gunn, D. J., and M. Khalid, "Thermal Dispersion and Wall Heat Transfer in Packed Beds," Chem. Eng. Sci., 30(2), 261-267 (1975)

Gupta, S. N., R. B. Chaube, and S. N. Upadhyay, "Fluid-Particle Heat Transfer in Fixed and Fluidized Beds," Chem. Eng. Sci., 29(3), 839-843 (1974)

Hall, R. E., and J. M. Smith, "Design of Gas-Solid Catalytic Reactors," Chem. Eng. Prog., 45(7), 459-470 (1949)

Hanratty, T. J., "Nature of Wall Heat Transfer Coefficient in Packed Beds," Chem. Eng. Sci., 3(5), 209-214 (1954)

Hill, F. B., and R. H. Wilhelm, "Radiative and Conductive Heat Transfer in a Quiescent Gas-Solid Bed of Particles: Theory and Experiment," AIChE J., 5(4), 486-496 (1959)

Hougen, J. O., and E. L. Piret, "Effective Thermal Conductivity of Granular Solids Through Which Gases are Flowing," Chem. Eng. Prog., 47(6), 295-303 (1951)

Imura, S., and E. Takegoshi, "Effect of Gas Pressure on the Effective Thermal Conductivity of Packed Beds," Ht. Trans. Jap. Res., 3(4), 13-26 (1974)

Irvin, H. B., R. W. Olson, and J. M. Smith, "Design of Fixed-Bed Catalytic Reactors. Part II," Chem. Eng. Prog., 47(6), 287-294 (1951)

Kennard, E. H., Kinetic Theory of Gases, p. 311, McGraw-Hill, New York (1938)

Krupiczka, R., "Analysis of Thermal Conductivity in Granular Materials," Int. Chem. Eng., 7(1), 122-144 (1967)

Kulkarni, B. D., and L. K. Doraiswamy, "Estimation of Effective Transport Properties in Packed Bed Reactors," Catal. Rev. Sci. Eng., 22(3), 431-483 (1980)

Kunii, D., and J. M. Smith, "Heat Transfer Characteristics of Porous Rocks," AIChE J., 6(1), 71-98 (1960).

Kunii, D., and J. M. Smith, "Heat Transfer Characteristics of Porous Rocks: II. Thermal Conductivities of Unconsolidated Particles with Flowing Fluids," AIChE J., 7(1), 29-34 (1961)

Kunii, D., and M. Suzuki, "Heat Transfer Between Wall Surface and Packed Solids," Proc. 3rd Int. Ht. Trns. Conf., 4, 344-352 (1966)

Kunii, D., M. Suzuki, and N. Ono, "Heat Transfer From Wall Sufrace to Packed Beds at High Reynolds Number," J. Chem. Eng. Japan, 1(1), 21-26 (1968)

Kwong, S. S., and J. M. Smith, "Radial Heat Transfer in Packed Beds," Ind. Eng. Chem., 49(5), 894-903 (1957)

Leva, M., "Heat Transfer to Gases Through Packed Tubes. General Correlations for Smooth Spherical Particles," Ind. Eng. Chem., 39(7), 857-862 (1947)

Leva, M., and M. Grummer, "Heat Transfer to Gases Through Packed Tubes, Effect of Particle Characteristics," Ind. Eng. Chem., 40(3), 415-419 (1948)

Leva, M., M. Weintraub, M. Grummer, and E. L. Clark, "Cooling of Gases Through Packed Tubes," Ind. Eng. Chem., 40(4), 747-752 (1948)

Leva, M., "Packed-Tube Heat Transfer," Ind. Eng. Chem., 42(12), 2498-2501 (150)

Masamune, S., and J. M. Smith, "Thermal Conductivity of Beds of Spherical Particles," Ind. Eng. Chem. Fund., 2(2), 136-143 (1963)

McConnachie, J. T. L., and G. Thodos, "Transfer Processes in the Flow of Gases Through Packed and Distended Beds of Spheres," AIChE J., 9(1), 60-64 (1963)

Molino, D. F., and J. O. Hougen, "Thermal Conductivity of Granular Solids Through Which Gases are Flowing," Chem. Eng. Prog., 48(3), 147-149 (1952)

Morales, M., C. W. Spinn, and J. M. Smith, "Velocities and Effective Thermal Conductivities in Packed Beds," Ind. Eng. Chem., 43(1), 225-232 (1951)

Ofuchi, K., and D. Kunii, "Heat-Transfer Characteristics of Packed Beds with Stagnant Fluids," Int. J. Heat Mass Trns., 8(5) 749-757 (1965)

Phillips, B. D., F. W. Leavitt, and C. Y. Yoon, "Heat Transfer with Molecular Sieve Adsorbent. 1. Effective Thermal Conductivity," Chem. Eng. Prog. Sym. Series, (30), 219-228 (1960)

Plautz, D. A., and H. F. Johnstone, "Heat and Mass Transfer in Packed Beds," AIChE J., 1(2), 193-199 (1955)

Quinton, J. H., and J. A. Storrow, "Heat Transfer to Air Flowing Through Packed Tubes," Chem. Eng. Sci., 5(6), 245-257 (1956)

Ranz, W. E., "Friction and Transfer Coefficients for Single Particles and Packed Beds," Chem. Eng. Prog., 48(5), 247-253 (1952)

Roblee, L. H. S., R. M. Baird, and J. W. Tierney, "Radial Porosity Variation in Packed Beds," AIChE J., 4(4), 460-464 (1958)

Schertz, W. W. and K. B. Bischoff, "Thermal and Material Transport in Nonisothermal Packed Beds," AIChE J., 15(4), 597-604 (1969)

Schotte, W., "Thermal Conductivity of Packed Beds," AIChE J., 6(1), 63-67 (1960)

Schuler, R. W., V. P. Stallings, and J. M. Smith, "Heat and Mass Transfer in Fixed-Bed Reactors," Chem. Eng. Prog. Sym. Series, (4), 19-30 (1952)

Schwartz, C. E., and J. M. Smith, "Flow Distribution in Packed Beds," Ind. Eng. Chem., 45(6), 1209-1218 (1953)

Sellars, J. R., M. Tribus, and J. S. Klein, "Heat Transfer to Laminar Flow in a Round Tube or Flat Conduit - The Graetz Problem Extended," Trans. ASME, 78(2), 441-448 (1956)

Siegel, R., E. M. Sparrow, and T. M. Hallman, "Steady Laminar Heat Transfer in a Circular Tube with Prescribed Wall Heat Flux," Appl. Sci. Res. Sect. A, 7, 386-392 (1958)

Siegel, R., and J. R. Howell, Thermal Radiation Heat Transfer, p. 794, McGraw-Hill, New York (1972)

Smith, W. O., P. D. Foote, and P. F. Busang, "Packing of Homogeneous Spheres," Phys. Rev., 34(5), 1271-1274 (1929)

Specchia, V., G. Baldi, and S. Sicardi, "Heat Transfer in Packed Bed Reactors with One Phase Flow," Chem. Eng. Commun., 4(2-3), 361-380 (1980)

Specchia, V., and S. Sicardi, "Modified Correlation for the Conductive Contribution of Thermal Conductivity in Packed Bed Reactors," Chem. Eng. Commun., 6(1-3), 131-139 (1980)

Sullivan, W. N., and R. H. Sabersky, "Heat Transfer to Flowing Granular Media," Int. J. Heat Mass Trns., 18(1), 97-107 (1975)

Touloukian, Y. S., R. W. Powell, C. Y. Ho, and P. G. Klemens (Eds.), Thermophysical Properties of Matter, 2, 510-512, IFI/Plenum, New York-Washington (1970)

Touloukian, Y. S., P. E. Liley, and S. C. Saxena (Eds.), Thermophysical Properties of Matter, 3, 512-514, IFI/Plenum, New York-Washington (1970)

Touloukian, Y. S., and E. H. Buyco (Eds.), Thermophysical Properties of Matter, 5, 1240-1242, IFI/Plenum, New York-Washington (1970)

Touloukian, Y. S., and T. Makita (Eds.), Thermophysical Properties of Matter, 6, 293-294, IFI/Plenum, New York-Washington (1970)

Touloukian, Y. S., S. C. Saxena, and P. Hestermans (Eds.), Thermophysical Properties of Matter, 11, 611, IFI/Plenum, New York-Washington (1975)

Touloukian, Y. S., R. K. Kirby, R. E. Taylor, and P. D. Desai (Eds.), Thermophysical Properties of Matter, 12, 149-151, IFI/Plenum, New York-Washington (1975)

Verschoor, H., and G. C. A. Schuitt, "Heat Transfer to Fluids Flowing Through a Bed of Granular Solids," App. Sci. Res. Sect. A, 2, 97-119 (1951)

Votruba, J., V. Hlavacek, and M. Marek, "Packed Bed Axial Thermal Conductivity," Chem. Eng. Sci., 27(10), 1845-1851 (1972)

Wakao, N., and K. Kato, "Effective Thermal Conductivity of Packed Beds," J. Chem. Eng. Japan, 2(1), 24-33 (1969)

Wakao, N., and D. Vortmeyer, "Pressure Dependency of Effective Thermal Conductivity of Packed Beds," Chem. Eng. Sci., 26(10), 1753-1765 (1971)

Wakao, N., "Effect of Radiating Gas on Effective Thermal Conductivity of Packed Beds," Chem. Eng. Sci., 28(4), 1117-1118 (1973)

Weast, R. C. (Ed.), Handbook of Chemistry and Physics, p. F-11, CRC Press, Cleveland (1971)

Wilhelm, R. H., W. C. Johnson, R. Wynkoop, and D. W. Collier, "Reaction Rate, Heat Transfer, and Temperature Distribution in Fixed-Bed Catalytic Converters," Chem. Eng. Prog., 44(2), 105-116 (1948)

Willhite, G. P., D. Kunii, and J. M. Smith, "Heat Transfer in Beds of Fine Particles (Heat Transfer Perpendicular to Flow)," AIChE J., 8(3), 340-345 (1962)

Yagi, S., and D. Kunii, "Studies on Effective Thermal Conductivities in Packed Beds," AIChE J., 3(3), 373-381 (1957)

Yagi, S., and N. Wakao, "Heat and Mass Transfer from Wall to Fluid in Packed Beds," AIChE J., 5(1), 79-85 (1959)

Yagi, S., and D. Kunii, "Studies on Heat Transfer Near Wall Surface in Packed Beds," AIChE J., 6(1), 97-104 (1960)

Yagi, S., D. Kunii, and N. Wakao, "Studies on Axial Effective Thermal Conductivities in Packed Beds," AIChE J., 6(4), 543-546 (1960)

Yagi, S., D. Kunii, and N. Wakao, "Radially Effective Thermal Conductivities in Packed Beds," Int. Dev. Ht. Trns., 4, 742-749 (1961)

Yagi, S., and D. Kunii, "Studies on Heat Transfer in Packed Beds," Int. Dev. Ht. Trns., 4, 750-759 (1961)

DISCLAIMER